Addressing Limitations in Gas-Phase Hydrogen/Deuterium Exchange Mass Spectrometry

Alesi Escobedo

A dissertation

submitted in partial fulfillment of the

requirements for the degree of

Doctor of Philosophy

University of Washington

2026

Reading Committee:

Miklos Guttman, Chair

Matthew F. Bush

Nicholas M. Riley

Program Authorized to Offer Degree:

Medicinal Chemistry

University of Washington

Abstract

Addressing Limitations in Gas-Phase Hydrogen/Deuterium Exchange Mass Spectrometry

Alesi Renee Escobedo

Chair of the Supervisory Committee:

Miklos Guttman

Department of Medicinal Chemistry

Gas-phase hydrogen/deuterium exchange (gHDX) is a structural mass spectrometry approach that provides information about molecular structure through differences in deuterium incorporation; however, its broader implementation is limited by incomplete understanding of negative-ion exchange behavior, experimental variability, and challenges in measurement comparability. This dissertation addresses these limitations by developing negative-mode gHDX, exchange reporters for standardization, and investigating post-ionization deuterium loss. Evaluation of a chemically diverse panel of anionic compounds demonstrated that exchange behavior is governed by multiple molecular features rather than charge-bearing functional groups alone and enabled identification of reporters spanning slow, intermediate, fast, and broad exchange behaviors. These reporters were used to develop a standardization strategy that successfully corrected changes in gHDX measurements on the Waters Synapt G2-Si; however,

different behavior on the Thermo LTQ suggested that an additional component of the exchange environment influenced deuterium incorporation. Investigation of this observation demonstrated that post-ionization deuterium loss occurs across multiple mass spectrometry instruments and in both positive- and negative-ion modes. Targeted humidity control and replacement of vacuum O-rings reduced deuterium loss. The work presented here advances negative-mode gHDX while demonstrating the importance of controlling both the exchange environment and post-ionization preservation of deuterium labeling to improve the reproducibility and reliability of HDX measurements.

Table of Contents

Chapter 1: Introduction

1.1 Gas-Phase Hydrogen Deuterium Exchange

Gas-Phase Hydrogen/Deuterium Exchange (gHDX) is a structural approach that monitors the exchange of labile hydrogens in analyte ions with deuterated neutral reagents (e.g., deuterated ammonia (ND_3), deuterium oxide (D_2O), or deuterated methanol (MeOD)). HDX occurs entirely in the gas phase following electrospray ionization (ESI) and occurs in mass spectrometry regions such as ion traps, ion guides, mobility cells, or transfer regions while maintaining stable instrument pressure and ion transmission[1-5]. For example, deuterated reagents can be introduced directly into selected post-ionization regions of the mass spectrometer, allowing the location and duration of the exchange reaction to be controlled through the instrumental configuration (Figure 1.1)[5]. Deuterium incorporation is measured from the change in mass of the analyte following exposure to the deuterating reagent. Replacing a hydrogen (^1H) with deuterium (^2H) increases the ion mass by approximately 1 Da per exchange, producing a corresponding shift in its isotopic distribution. The resulting deuterium uptake can be monitored as a function of reaction time to generate a deuterium uptake profile, allowing evaluation of both the rate and extent of exchange[2-4, 6]. Depending on the instrument platform and experimental conditions, gHDX measurements can span timescales from microseconds to hours, affecting both the extent of exchange and the structural information obtained. The structural information obtained from gHDX has enabled determination of the number of labile hydrogens, differentiation of isomeric species, characterization of structural features, and determination of thermochemical properties of exchange[1, 2, 6-10].

1.2 Objective of the Chapter

This chapter provides a foundational overview of gHDX, discussing the mechanistic principles, methodological development, and structural applications that have shaped the technique. The chapter explains fundamental aspects of gHDX to establish how ion–reagent interactions, molecular structure, reagent properties, and reaction energetics contribute to observed exchange behavior. We then present the evolution of gHDX across FT-ICR, ion-trap, and ion-mobility-based instrumentation to show how advances in mass spectrometry have expanded the accessible exchange timescales and experimental capabilities of the technique. We highlight applications of the technique to demonstrate how gHDX is used to investigate structural differences across a range of biomolecules. Finally, we discuss the experimental challenges that currently limit the reproducibility and comparability of gHDX measurements. The topics discussed in this chapter establish the current foundation of gHDX and highlight areas that need further development. The subsequent chapters build on this by addressing gHDX limitations through the development of negative-mode approaches, investigation of measurement standardization, and identification of underreported experimental factors that can affect deuterium labeling.

1.3 Fundamental Principles of gHDX

1.3.1 Mechanism of gHDX

Gas-phase HDX occurs through ion-molecule reactions between the analyte ion and a neutral deuterated reagent. Although incorporation of deuterium is experimentally observed as a mass shift to higher m/z values, successful exchange requires more than a collision between the

ion and reagent. The interaction must facilitate a stable ion-neutral intermediate complex in which hydrogen and deuterium transfer can occur[1, 11-13]. The main mechanistic model used to describe gHDX is the relay mechanism. Campbell et al. investigated the exchange behavior of protonated glycine oligomers with several deuterating reagents. They showed that exchange behavior depends on both the reagent and the environment of the exchange site [11]. The work contributed to the mechanistic model by showing that exchange doesn't occur directly (i.e., by a single direct collision that donates deuterium) but instead occurs through a transient hydrogen-bonded ion-molecule complex that provides a pathway for hydrogen and deuterium transfer between sites on the analyte [11]. Wyttenbach et al. further developed this mechanism as an interaction involving a hydrogen-bonded network between 1) the deuterated reagent, 2) a charge-bearing site, and 3) an exchangeable site[13]. They described the reagent first interacting with the protonated site through hydrogen bonding while simultaneously interacting with an exchangeable hydrogen elsewhere on the molecule, resulting in a relay exchange between the two analyte sites through the deuterated reagent and leaving the analyte with deuterium in place of the hydrogen. The deuterating reagent serves as an intermediary in this process, and successful exchange therefore depends on whether the participating sites can adopt a favorable spatial arrangement to form a stable ion-reagent intermediate complex, highlighting an important connection between molecular structure and experimentally observed exchange behavior. Arrington et al. provide computational detail on what must physically happen for the relay mechanism to proceed by combining experimental gHDX measurements of protonated lysine and three shorter homologs with density functional theory calculations. Their calculations described relay-mediated amine exchange as a pathway in which D_2O interacts between the protonated and neighboring amine

sites, allowing proton transfer between the two nitrogen groups through the reagent molecule (Figure 1.2). The reagent must first access this arrangement, which may require disrupting an existing intramolecular hydrogen bond [14]. The study therefore showed that forming an ion-reagent complex alone does not guarantee efficient exchange; the reagent must also access the exchangeable site and stabilize the transition states required for transfer. Although the relay mechanism has been extensively described for positively charged ions[2, 3, 6, 7, 11, 13-16], the mechanistic basis of negative-mode gHDX remains less well defined. Early studies established that negatively charged ions undergo gHDX and showed that exchange behavior depends on interactions between the anion and the deuterated reagent [12, 17-20]. However, these studies have not established a universal mechanism for negative-ion exchange comparable with the described relay mechanism for protonated ions. Instead, proposed exchange pathways vary across anion-reagent studies, leaving questions about the role of the charge site, whether exchange occurs through direct transfer or intermediate complexes, and how the deuterating reagent facilitates exchange within these pathways. Despite the lack of an established exchange pathway, these studies provide mechanistic insight into negative-mode gHDX in the context of the specific factors they investigated, as discussed in the following sections.

1.3.2 Structural Accessibility of Exchangeable Hydrogens

The presence of exchangeable hydrogens alone does not determine if deuterium incorporation can occur[1]. Instead, exchange depends on whether these hydrogens can be accessed and participate in interactions with the deuterating reagent[1]. Studies of protein conformations and charge-state differences have highlighted the relationship between structural

accessibility and gHDX. Suckau et al. observed that lower % deuterium uptake correlated with compact structures, and that higher charge states, associated with more elongated conformations, were associated with higher % deuterium uptake [21]. This suggests that hydrogens that are inaccessible or protected within a compact protein structure can become more accessible for exchange when the same protein adopts more extended conformations. However, Freitas et al.'s studies of ubiquitin argued that a higher charge state and a more elongated conformer have a lower % deuterium uptake [2]. Wyttenbach and Bowers provided a mechanistic explanation that reconciled these opposing observations. Their model emphasized that successful exchange requires not only accessibility of the participating sites but also a favorable spatial relationship between the charge-bearing site and the exchange site. Structural elongation/unfolding can expose previously protected hydrogens, increasing exchange as observed for cytochrome *c*; however, extensive elongation can also increase the distance between sites required to establish the relay mechanism, thereby decreasing the formation of the ion–reagent complex[13]. Therefore, compact structures reduce access to potential exchange sites, whereas highly extended structures can disrupt the spatial arrangement; both can restrict exchange, but for different reasons. Solution conditions during sample preparation can also influence deuterium incorporation of charge states. Beeston et al. demonstrated this by examining ubiquitin and β-lactoglobulin prepared in the absence and presence of 15% trifluoroethanol (TFE), a solvent used to stabilize protein secondary structure. Adding TFE reduced deuterium incorporation in both proteins across multiple charge states, indicating that stabilizing protein structure decreases conformational flexibility and limits ND_3 accessibility to labile hydrogens (Figure 1.3)[16].

Beyond changes in overall conformation, more localized differences in molecular structure can also alter the accessibility of exchangeable hydrogens. Arrington et al. illustrate the importance of local molecular structure by comparing protonated lysine with three homologs. Although all four compounds contained six exchangeable hydrogens and ultimately underwent six exchanges, their exchange rates differed substantially, following the order $DapaH^+$ > $LysH^+$ > $DabaH^+$ > $OrnH^+$ (Figure 1.4) [14]. These differences were associated with changes in intramolecular hydrogen bonding driven by side-chain length, showing that the local structural environment around the exchange site can strongly influence whether the hydrogen is readily accessible to gHDX. The influence of local molecular structure on exchange accessibility is not limited to peptides or amino acids. Local differences in functional-group arrangement can similarly alter exchange behavior in smaller ions. Studies of structurally related anions have shown that positional changes within a molecule can alter interactions between exchangeable sites and the deuterating reagent[1, 19, 20]. Kato et al., for example, observed different exchange behavior among substituted fluorophenyl anions depending on the position of substituents within the aromatic structure.[13] Similarly, Chipuk and Brodbelt demonstrated distinct exchange behavior among aromatic dicarboxylic acid anions, indicating that the relative arrangement of functional groups influences whether potential exchange sites can participate effectively in the ion–reagent interaction.[14] These observations extend the concept of structural accessibility beyond protein folding and demonstrate that even relatively small differences in local molecular geometry can alter gHDX behavior.

1.3.3 Influence of Deuterated Reagent Gas

The choice of deuterated reagent gas plays a central role in gHDX; commonly used reagent gases include ND_3, D_2O, and MeOD, each possessing distinct physicochemical properties that influence ion-neutral interactions and alter the rate and extent of exchange. One of the earliest investigations into reagent effects on exchange was conducted by Campbell et al., who examined protonated glycine oligomers using D_2O, MeOD, CD_3CO_2D, and ND_3 as deuterating reagents. Their work showed that reagent gas type influences exchange kinetics and the underlying exchange mechanism through differences in proton affinity, leading to a comparison of the relationship between reagent type and analyte energetics [11]. The study showed that changing the reagent can alter not only exchange favorability, but also the available exchange pathway. Green-Church et al. further supported this by showing that reagent type can influence both the extent of deuterium incorporation and the exchange sites accessible during gHDX. Positively charged mononucleotides were reacted with ND_3, D_2O, and D_2S, producing substantially different exchange behavior depending on the deuterating reagent. This reagent dependence is illustrated for deoxyguanosine-3'-monophosphate (dGp) in Figure 1.5, where reaction with D_2S produced only limited deuterium incorporation, D_2O resulted in greater exchange, and ND_3 produced the most extensive exchange of the three reagent types[7]. Their analysis showed that exchange with ND_3 occurred at multiple exchangeable hydrogen sites on the nucleotide, whereas D_2O and D_2S favored exchange primarily at phosphate and sugar hydrogens but not the nucleobases[7]. DePuy et al. first demonstrated gas-phase H/D exchange between carbanions and deuterated alcohols, establishing that exchange could occur for negatively charged ions through interactions with a neutral deuterating reagent.[2] Subsequent studies by Squires et al. extended these observations to reactions of vinyl and aryl carbanions with D_2O, demonstrating that exchange efficiency varied

among anions and depended on the environment of the exchangeable hydrogen.[3] Kato et al. examined reagent-dependent behavior in negative-mode gHDX in greater depth, where fluorophenyl anions exhibited different exchange behavior with D_2O and MeOD[19]. By conducting energetic calculations of the intermediate species along the exchange pathway, the authors attributed differences to the relative stability and energetic accessibility of the ion–reagent complexes formed with each reagent [13]. Thus, changing the deuterating reagent altered the energetic landscape through which exchange could proceed. Similarly, Chipuk and Brodbelt reported reagent influence on exchange of aromatic dicarboxylic acids, showing that some compounds exchanged more readily with D_2O, whereas others exchanged more readily with MeOD[20]. Importantly, the preferred reagent was therefore not constant across a single general class of structurally related compounds. Instead, reagent effectiveness depended on the molecular structure and the interactions that could be established between the analyte and reagent[20]. These findings demonstrate that a reagent that produces efficient exchange for one analyte cannot necessarily be assumed to provide equivalent exchange behavior for a structurally related species. Studies examining the same protein under different experimental conditions further illustrate the importance of reagent selection. Rand et al. used ND_3 as the reagent gas in their study of ubiquitin and found that deuterium uptake increased with charge state [4]. However, Evans et al., who also studied ubiquitin interactions using MeOD, observed that lower charge states exhibited increased deuterium incorporation relative to higher charge states[3]. This emphasizes how the choice of deuterated reagent gas influences the observed exchange behavior and the structural information obtained from gHDX measurements. These studies in both positive- and negative-mode reveal that no single reagent is universally optimal for gHDX. Instead,

exchange behavior depends on reagent properties and how the reagent gas interacts with the analyte to form stable ion-reagent complexes, influencing both the magnitude of deuterium incorporation and the structural information obtained from the exchange.

1.3.4 Energetics & Thermodynamics

Although the relay mechanism provides the mechanistic understanding of gHDX, the success of the reaction also depends on the thermodynamic and energetic favorability of the ion-neutral reaction. Deuterium incorporation requires that the ion-neutral interaction form stable intermediate complexes that can facilitate successful proton transfer. Many of the earliest gHDX investigations focused on understanding how proton affinity and other thermochemical properties influence exchange behavior. Ausloos and Lias established an energetic basis for understanding gHDX by identifying a relationship between cation isotope exchange and reaction energetics. They observed that when the proton-transfer reaction was endothermic by approximately 20-25 kcal/mol, H/D exchange was no longer observed [22]. The work suggested that a large energetic difference in the intermediate ion-reagent complex becomes unfavorable for exchange. Gard et al. showed that exchange can occur outside the simple energetic relationships proposed by Ausloos and Lias. By measuring the proton affinities of the ion-molecule complex between simple amino acids and MeOD, Gard et al. demonstrated that deuterium exchange can occur despite a large difference in proton affinity (30-40 kcal/mol)[15]. This suggests that multiple interacting functional groups could provide alternative exchange pathways. Campbell et al. further developed this concept by investigating the H/D behavior of protonated glycine oligomers with different deuterating reagents (e.g., D_2O, MeOD, and ND_3). They found that when proton affinities of the

exchange reagent and analyte are similar or differ by less than 20 kcal/mol, exchange could proceed through relatively direct hydrogen-bonded interactions, suggesting direct exchange. However, when the differences in proton affinities of the exchange reagent and analyte are greater than 20 kcal/mol, exchange occurs via the relay mechanism if a favorable long-lived ion-molecule complex can form[11]. The study by Campbell et al. shifts the notion from proton affinity alone predicting gHDX behavior to differences in proton affinity between the analyte and reagent influencing the exchange mechanism. The study showed that the formation of a favorable, long-lived ion-molecule complex (i.e., the relay mechanism) becomes increasingly important as the difference in proton affinity between the analyte and reagent increases. Green-Church et al. supported this by comparing the proton affinities of mononucleotide exchange sites with those of ND_3, D_2O, and D_2S. Green-Church et al. found that relatively small proton affinity differences between ND_3 and the mononucleotides were consistent with direct exchange. For D_2O and D_2S, only the phosphate and sugar hydrogens on all the mononucleotides had small differences in proton affinity and underwent direct exchange, but the large proton affinity differences observed for D_2O and D_2S at the nucleobase exchange sites suggested that exchange required the formation of a long-lived ion-molecule complex for proton transfer[7]. Arrington et al. further demonstrated that the energetics governing gHDX extend beyond proton affinity alone when examining lysine and its homologs. Protonated lysine and ornithine have similar proton affinities, yet $OrnH^+$ exhibited an HDX rate lower than $LysH^+$. Density functional theory calculations provided an energetic explanation for this difference: $OrnH^+$ contained a particularly strong intramolecular hydrogen bond that had to be disrupted before D_2O could insert and initiate the relay mechanism. The calculated barrier for D_2O insertion in $OrnH^+$ was 50.8 kJ/mol, compared to the calculated

barrier for $LysH^+$ of 38.3 kJ/mol[14]. These findings show that proton affinity alone cannot fully predict gHDX behavior; the energetic cost of disrupting existing intramolecular interactions, forming a productive ion–reagent complex, and proceeding through the proton-transfer pathway must also be considered. While these studies established energetic considerations in positive-mode gHDX, Kato et al. showed the importance of the ion-reagent complex's energetic landscape for negatively charged ions, using fluorophenyl anions and D_2O and MeOD as reagent gases. Kato et al. combined experimental gHDX measurements with energetic calculations to examine the intermediate species involved in the exchange pathway[19]. They attributed differences in deuterium incorporation among the fluorophenyl anions to differences in the relative energies of intermediate species formed within the ion-reagent complex. This work provided direct evidence that the energetic landscape of the intermediate ion–reagent complex can govern negative-ion gHDX behavior. Regardless of ion polarity, exchange depends on the energetic favorability and stability of the intermediate ion-reagent complexes and the accessibility of the pathways required for exchange.

1.4 Instrumentation Developments in gHDX

gHDX was initially used to investigate ion-molecule reaction mechanisms and the structures of simple gas ions[1, 12, 17, 18, 23, 24]. As mass spectrometry instrumentation developed. gHDX expanded to characterize increasingly complex biological molecules, including peptides and proteins[2, 6, 21]. This expansion was closely linked to the development of instrument platforms capable of controlling ion-reagent interactions over different reaction timescales. The evolution of gHDX instrumentation progressively expanded the experimentally

accessible exchange timescale, from reactions occurring over seconds to hours, then microseconds to milliseconds.

Fourier transform ion cyclotron resonance (FT-ICR) mass spectrometry provided one of the earliest major instruments for gHDX measurements. As described by Freitas et al., “FT-ICR combines the ability to trap and react gaseous ions for extended periods of time and to perform high-resolution detection of the masses of their reaction product ions, making it well suited for gas-phase H/D exchange”[2]. Reaction times ranging from seconds to hours resulted in longer trapping times, allowing detailed examination of exchange kinetics, isotopic distributions, and slowly exchanging ion populations[2, 6, 7, 11, 21]. Early FT-ICR studies commonly employed deuterating reagents such as D_2O and MeOD, establishing many of the mechanistic principles discussed in Section 1.3, including the importance of ion–reagent complex formation, molecular conformation, and reaction energetics [2, 6, 11, 13, 15]. However, the long reaction periods characteristic of many FT-ICR experiments also limited experimental throughput, and the specialized instrumentation restricted broader implementation of the technique. These considerations motivated adapting gHDX to other mass spectrometry platforms that provide increasingly rapid measurements and greater accessibility for researchers.

Implementing gHDX in quadrupole ion traps marked an important transition toward shorter, more readily controlled exchange experiments. Ion traps confine ions using radiofrequency electric fields, allowing an isolated ion population to interact with a deuterating reagent for a defined period before mass analysis. Compared with the lower-pressure environment of FT-ICR cells, the higher operating pressures of ion traps allow gHDX measurements over shorter reaction periods, from milliseconds to seconds [3, 20]. Ion-trap implementation also broadened access to

gHDX for peptide and protein studies. Evans et al., for example, demonstrated gHDX of cytochrome *c* and ubiquitin using MeOD in a quadrupole ion trap and showed that conformational information previously obtained using FT-ICR could also be investigated on an ion-trap platform [3]. This represented an important methodological development because structural gHDX measurements were no longer restricted to the extended trapping conditions characteristic of FT-ICR. Ion traps additionally provided flexibility in reaction-time control while requiring relatively small amounts of analyte. However, because ions are accumulated and subsequently retained within the reaction region, differences in the time at which ions enter and experience the deuterating reagent can broaden the effective exchange-time distribution of the ion population. Because both FT-ICR and ion-trap approaches rely on holding ion populations undergoing exchange, this has led to a major shift in gHDX toward traveling-wave ion guide (TWIG)-based instruments.

Rather than holding ions for a defined reaction time, traveling-wave ion guides (TWIGs) continuously propel ions through a pressurized gas-filled region using a sequence of traveling voltage waves. Rand et al. demonstrated that a TWIG could therefore function as a controlled gHDX reaction region by introducing a deuterating reagent into the ion guide and manipulating the traveling-wave conditions to control the time available for exchange[4]. This approach reduced the accessible reaction window from the second-timescale measurements typical of many trapped-ion experiments to approximately the microsecond-to-millisecond timescale. The transition to traveling-wave instrumentation also coincided with an important development in reagent selection. Whereas D_2O and MeOD had been extensively used in earlier trapped-ion studies, Rand et al. demonstrated the implementation of ND_3 within a traveling-wave ion guide[15]. ND_3

supported measurable exchange within the substantially shorter residence times available in the TWIG, enabling deuterium uptake to be followed over approximately 0.1–10 ms[15]. The use of ND_3 therefore became particularly advantageous for rapid traveling-wave implementations of gHDX, where efficient exchange must occur during the brief period ions travel through the reaction region. Importantly, traveling-wave implementation also enabled integration of gHDX with ion mobility-based structural measurements. In traveling-wave ion mobility spectrometry (TWIMS), ions are separated according to differences in their mobility through a buffer gas, providing information related to ion size, shape, and collision cross section. Incorporating gHDX into the same instrumental workflow provided an additional structural measurement based on exchange behavior.

The historical development of gHDX instrumentation therefore reflects a progressive expansion of the reaction timescales available for gHDX. FT-ICR provided extended trapping periods that were particularly valuable for establishing fundamental exchange mechanisms and characterizing slower exchange processes[1,4–7]. Ion traps expanded access to gHDX and enabled exchange to be examined at higher reagent pressures and shorter reaction periods[11,14]. The subsequent implementation of ND_3 within traveling-wave ion guides extended gHDX into the microsecond-to-millisecond timescale and enabled integration with ion mobility measurements[15]. Importantly, these platforms provide broad gHDX measurements because differences in reagent pressure, ion residence time, reaction location, and reagent delivery can influence the portion of the exchange process that is experimentally observed. Instrumentation has therefore not only expanded the capabilities of gHDX but has also become an important

experimental variable to consider when comparing exchange measurements across platforms and the structural information obtained.

1.5 Applications of gHDX

gHDX's ability to detect differences in molecular structure has enabled the technique to develop from a method for investigating fundamental gas-phase ion chemistry into a structural tool applicable to a broad range of biological molecules. Because gHDX measures differences in exchange behavior rather than relying solely on precursor mass or fragmentation, it can provide structural information for species that possess similar or identical molecular masses. Applications have therefore included characterizing peptide and protein conformations, differentiating nucleotide structures, and distinguishing closely related carbohydrate and glycan isomers[2, 3, 6-10, 16, 21].

Early peptide applications showed that gHDX could distinguish structural differences among closely related molecular species. Freitas et al. investigated protonated bradykinin (RPPGFSPFR) and several bradykinin analogs using D_2O in an FT-ICR. Despite the structural similarity of these peptides, differences were observed in both the rate and extent of deuterium incorporation. In particular, the position and presence of the arginine residue strongly influenced the measured exchange behavior, with removal of arginine producing faster exchange relative to protonated bradykinin[6]. Figure 1.6 shows the differences in exchange behavior observed among bradykinin and its analogs. These results demonstrated that gHDX could distinguish related peptide structures through their exchange profiles and provided an example of using deuterium incorporation as a structural measurement. Beyond peptide applications, gHDX has also been

used to identify coexisting conformational populations within protein sample. Beeston et al. demonstrated this capability using calmodulin, where multiple populations with different levels of deuterium incorporation were observed [16]. Three conformational populations could be distinguished by their exchange behavior, demonstrating that protein conformations can differ sufficiently to produce distinct exchange behavior[16]. This application demonstrates the utility of gHDX for identifying conformational populations.

Moving towards nucleic acids, Robinson et al. investigated 5'-, 3'-, and cyclic mononucleotide anions using D_2O in FT-ICR and observed distinct exchange behavior among the nucleotide classes. The 3'-mononucleotides exchanged more rapidly than the corresponding 5'-mononucleotides, whereas the cyclic mononucleotides exhibited little to no exchange under the conditions examined[8]. Differences were also observed among nucleotides containing different nucleobases. Thus, gHDX can distinguish changes in both phosphate connectivity and nucleobase identity through their distinct exchange behavior[8]. This study demonstrated that relatively subtle structural differences among nucleotide species could generate distinct deuterium uptake. Green-Church et al. expanded the application of gHDX to positively charged mononucleotides and examined their exchange using multiple deuterating reagents (e.g., ND_3, D_2O, and MeOD). Distinct exchange behaviors were again observed among the nucleotide species, where changing the deuterating reagent altered both the rate of exchange and the extent of deuterium incorporation[7].

The ability to differentiate structurally related species is particularly valuable for carbohydrates and glycans, where structural diversity arises from differences in monosaccharide composition, glycosidic linkage, stereochemistry, branching, and chemical modification. Many

carbohydrate isomers have identical elemental compositions and molecular masses, making differentiation by precursor m/z alone challenging and sometimes impossible using mass spectrometry. Uppal et al. demonstrated the utility of gHDX for this analytical challenge by investigating a series of carbohydrate and glycoconjugate isomers. Distinct deuterium exchange behavior was observed for several structurally related species, demonstrating that carbohydrate isomers could be differentiated based on their exchange profiles[9]. Importantly, some species not effectively resolved by ion mobility could be differentiated by gHDX, showing that the two techniques can provide complementary structural information. This work expanded the application of gHDX to an analytically challenging class of biomolecules for which structural differences are frequently not reflected by molecular mass alone. The application of gHDX was extended to sulfated glycosaminoglycans, which present an additional analytical challenge. Alonge et al. investigated the monosulfated chondroitin sulfate disaccharide isomers 4S-CS and 6S-CS, which differ in sulfation position. Traveling-wave ion mobility provided limited separation of the two deprotonated isomers across the evaluated drift gases. Figure 1.7 shows the arrival-time distributions of 4S-CS and 6S-CS obtained using different drift gases, illustrating the limited separation achieved by ion mobility [10]. In contrast, gHDX produced distinct exchange behavior for the two CS positional isomers. The 6S-CS isomer consistently exchanged more rapidly than 4S-CS, regardless of the deuterating reagent type tested (e.g., ND_3, D_2O, and MeOD) [10]. The distinct deuterium uptake profiles of 4S-CS and 6S-CS obtained using ND_3 and D_2O are shown in Figure 1.8, with 6S-CS exhibiting more rapid exchange than 4S-CS. Thus, gHDX's ability to differentiate positional isomers that were poorly resolved by ion mobility demonstrated its utility for structural characterization of negatively charged, sulfated glycans.

These applications demonstrate the versatility of gHDX as a structural mass spectrometry technique across peptides, proteins, nucleotides, carbohydrates, and glycans. The technique has been used to distinguish closely related molecular structures, identify different conformational populations, and differentiate isomeric species. Rather than replacing existing mass spectrometry techniques, gHDX provides a complementary structural measurement based on differences in exchange behavior, enabling structural distinctions that may not be accessible from precursor mass, ion mobility, or other traditional MS approaches alone.

1.6 Limitations of gHDX

Despite its ability to distinguish structurally related species, several limitations have restricted the broader implementation of gHDX. A central challenge arises from the same characteristic that makes gHDX structurally informative: deuterium exchange is highly sensitive to the reaction environment. As demonstrated throughout the chapter, exchange behavior is affected by the type and concentration of the deuterating reagent, ion–reagent interactions, reaction time, and the energetic landscape. This becomes particularly important when considering experimental reproducibility. Uppal et al. demonstrated that gHDX kinetics can vary with laboratory temperature, instrumental conditions, and instrument platform, producing variability in exchange measurements even when the analyte itself remains unchanged[25]. Earlier work had already demonstrated the sensitivity of exchange to individual experimental parameters. Rand et al., for example, showed that changing ND_3 pressure within a traveling-wave ion guide altered the extent and rate of exchange, and that instrument parameters controlling ion residence time provided access to different portions of the exchange profile [4, 5]. Therefore, reagent concentration,

reaction time, pressure, temperature, and instrument operating conditions must be considered and controlled before differences in gHDX behavior can confidently be attributed to molecular structure. Different mass spectrometer platforms have different reaction environments, and accessible exchange timescales present an additional challenge. FT-ICR instruments permit ions to react over comparatively long periods, ion traps provide controlled trapping over intermediate timescales, and traveling-wave ion guides enable exchange on microsecond-to-millisecond timescales. Because of this, exchange rates or uptake profiles obtained using different instruments cannot necessarily be used for direct, comparable measurements. The development of internal exchange standards has provided one strategy for distinguishing genuine structural differences from experimental variability. Uppal et al. initially incorporated an internal exchange control (i.e., peptide angiotensin I) when differentiating carbohydrate linkage and stereoisomers, allowing consistency of labeling conditions to be evaluated alongside the analytes [9]. Uppal et al. later expanded this concept into a reporter-based standardization strategy in which a mixture of exchange standards (i.e., Tris Mix- containing Tris, bis-tris methane, and bis-tris-propane) was co-sampled with the analyte. The analyte exchange was corrected relative to the behavior of the standards collected under the same experimental conditions rather than the original timescale. This approach substantially improved the precision and reproducibility of gHDX measurements across several analytes and ND_3 flow conditions [25]. However, these experiments also revealed an important limitation of the standardization approach: an exchange reporter is not necessarily universal across deuterating reagents. When the approach was extended from ND_3 to D_2O and MeOD, some the compounds used for TrisMix exhibited little or no measurable exchange with the alternative reagents, preventing the same reporter standardization approach from being directly

applied to different reagent gases[25]. This observation is consistent with the broader mechanistic literature showing that reagent type influences ion–neutral complex formation and the ability of exchange to occur [7, 11, 19, 20]. Therefore, although internal standards can substantially improve reproducibility, they must exhibit exchange behavior under broad reaction conditions to be used. These limitations demonstrate that differences in reagent type and concentration, reaction pressure, temperature, residence time, and instrumental parameters can alter the measured exchange profile. Internal exchange standards provide an important means of accounting for variation, but their effectiveness can depend on the reagent and instrument conditions employed. As a result, direct comparison of gHDX measurements across experimental conditions and particularly across instrument platforms remains challenging. Establishing approaches that can identify, account for, and ultimately minimize these sources of variability is therefore necessary for gHDX to progress toward a more reproducible and broadly adaptable structural mass spectrometry technique.

1.7 Conclusion

Over several decades, gas-phase hydrogen/deuterium exchange has progressed from fundamental studies of ion–molecule reactions to an analytical approach for examining molecular structure in the gas phase. The literature reviewed in this chapter shows that this progression was driven by an increasing understanding of what determines whether exchange occurs and what information can be obtained from the resulting deuterium incorporation. This chapter demonstrates that deuterium incorporation is not governed simply by the number of exchangeable hydrogens present within an analyte. Rather, the observed exchange behavior

reflects the combined influence of ion–reagent complex formation, structural accessibility, deuterating reagent, and the energetic favorability of the exchange pathway. Advances in mass spectrometry expanded how these exchange processes could be observed. Moving from long-duration trapping experiments to increasingly rapid reactions broadened the timescale range accessible by gHDX and allowed the technique to be incorporated into different workflows. These instrument developments were accompanied by an expansion in the types of biomolecules examined, progressing from relatively simple ions to peptides, proteins, nucleotides, carbohydrates, and glycans. Exchange differences have been used to distinguish conformations, closely related structures, and isomeric species, including cases in which conventional mass spectrometry approaches or ion mobility provided limited differentiation. The field's development has also revealed an important reproducibility challenge. The introduction of internal controls and exchange standards represents an important effort to address this problem. Still, existing studies also demonstrate that the behavior of these standards can depend on the reagent and experimental conditions under which they are used. The current state of gHDX reflects both the technique's strength and its challenge: its sensitivity to the molecular environment provides valuable structural information. In contrast, its sensitivity to the experimental environment can complicate interpretation and comparison. The literature reviewed in this chapter establishes the fundamental framework needed to distinguish these two contributions. It provides the basis for continued development of gHDX as a reproducible structural mass spectrometry approach.

1.8 Chapter Figures

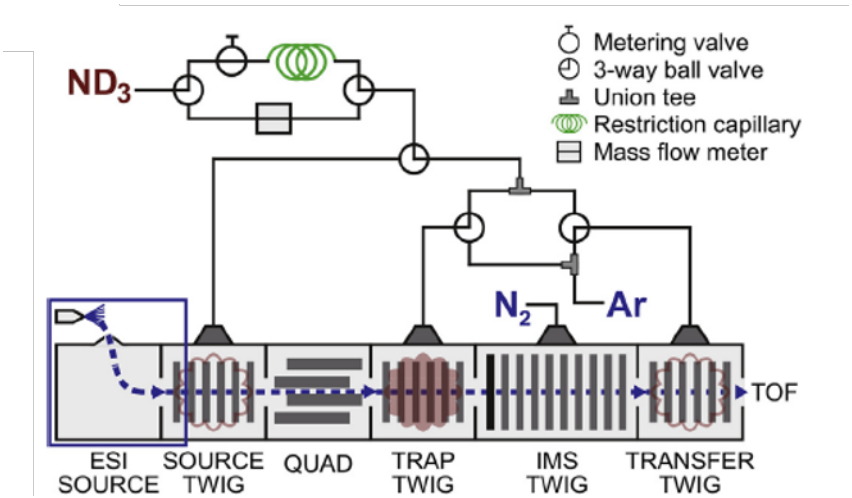

Figure1.1: Example instrumental configuration for gHDX. Schematic of a modified Synapt G2 hybrid Q-TOF mass spectrometer enabling the introduction of deuterated ammonia (ND_3) into the source, trap, or transfer traveling-wave ion guides (TWIGs). The configuration allows selection of the exchange region through external valves while maintaining the appropriate gas environment within the remaining instrument regions. The configuration shown depicts ND_3 introduction into the trap TWIG.

Adapted from Mistarz, Ulrik H, and Kasper D Rand. "Installation, validation, and application examples of two instrumental setups for gas-phase HDX-MS analysis of peptides and proteins." *Methods (San Diego, Calif.)* vol. 144 (2018): 113-124. doi:10.1016/j.ymeth.2018.05.002

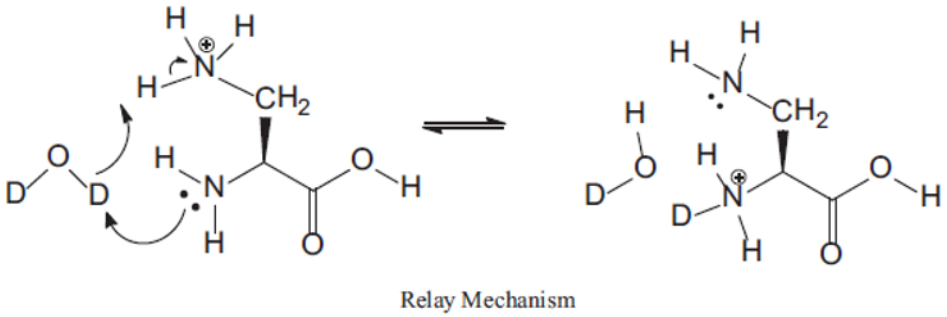

Figure 1.2: Relay mechanism for protonated gHDX. Exchange is initiated by formation of a hydrogen-bonded ion–reagent complex between the analyte ion and the deuterating reagent. A hydrogen-bonding network facilitates relay, resulting in deuterium incorporation into the analyte.

Adapted from Arrington, Justine V., et al. “Gas-Phase Hydrogen Deuterium Exchange Behavior of Lysine and Its Homologs.” *International Journal of Mass Spectrometry*, vols. 330–332, 2012, pp. 200–206. https://doi.org/10.1016/j.ijms.2012.07.018

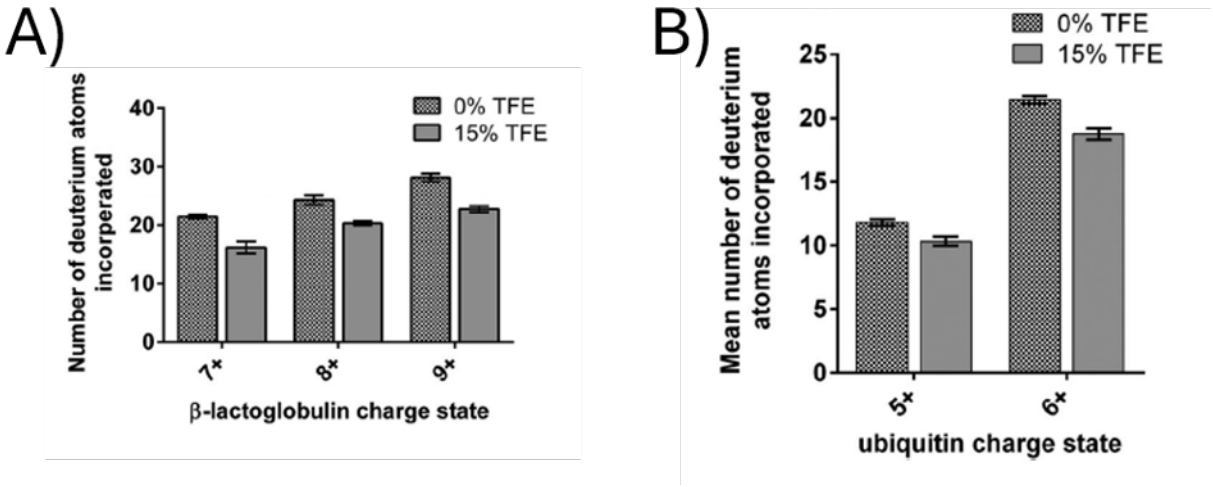

Figure 1.3: Effect of TFE on deuterium incorporation of β-lactoglobulin and ubiquitin. Number of deuterium atoms incorporated following gas-phase HDX of A) β-lactoglobulin charge states 7+, 8+, and 9+ and B) ubiquitin charge states 5+ and 6+ in the absence (0% TFE) and presence of 15% 2,2,2-trifluoroethanol (TFE). Adding 15% TFE decreased deuterium incorporation across the examined charge states of both proteins.

Adapted from Beeston, Helen S., et al. "Changes in Protein Structure Monitored by Use of Gas-Phase Hydrogen/Deuterium Exchange." *Proteomics*, vol. 15, no. 16, 2015, pp. 2842–2850. https://doi.org/10.1002/pmic.201400440

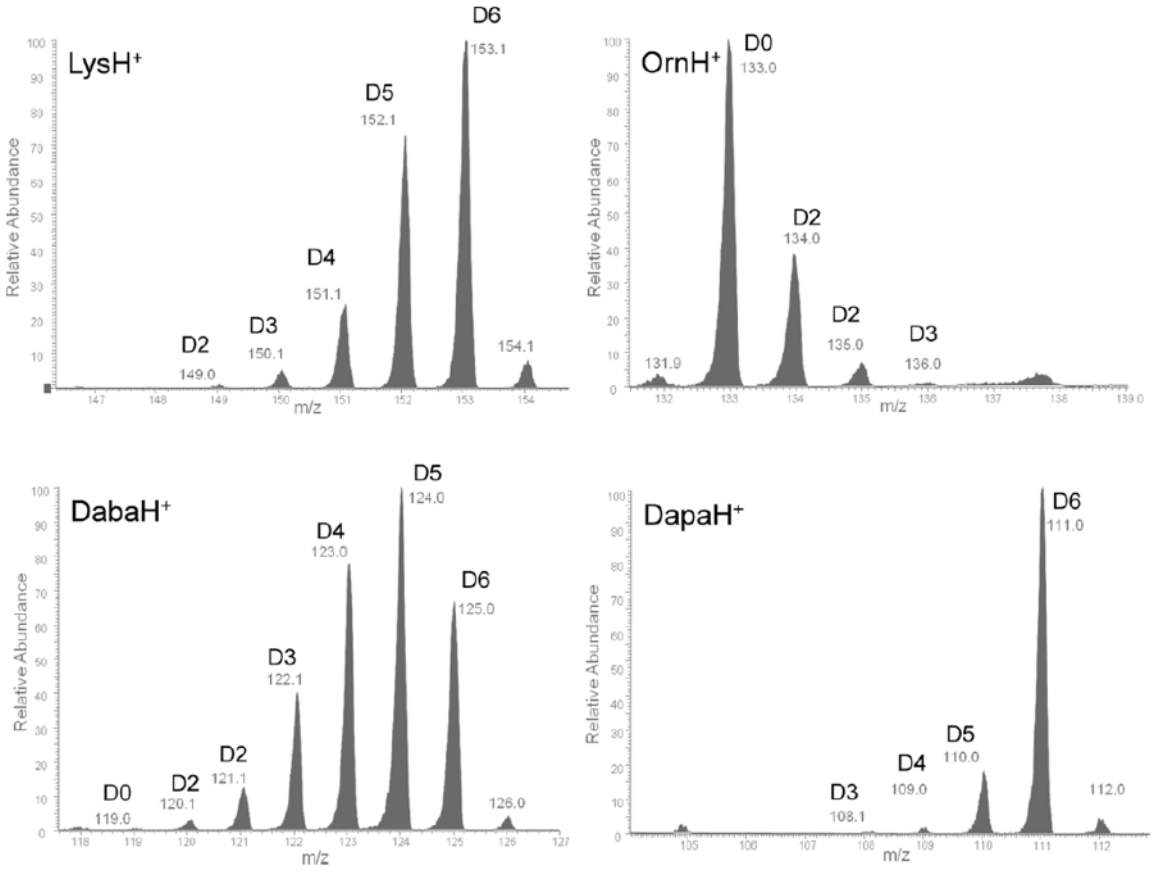

Figure 1.4: gHDX among protonated lysine homologs. Mass spectra showing the isotopic distributions of protonated lysine ($LysH^+$), ornithine ($OrnH^+$), 1,4-diaminobutanoic acid ($DabaH^+$), and 1,3-diaminopropanoic acid ($DapaH^+$) following reaction with D_2O for 250 ms at a pressure of approximately 1.7×10^{-6} Torr.

Reproduced from Arrington, Justine V., et al. "Gas-Phase Hydrogen Deuterium Exchange Behavior of Lysine and Its Homologs." *International Journal of Mass Spectrometry*, vols. 330–332, 2012, pp. 200–206. https://doi.org/10.1016/j.ijms.2012.07.018

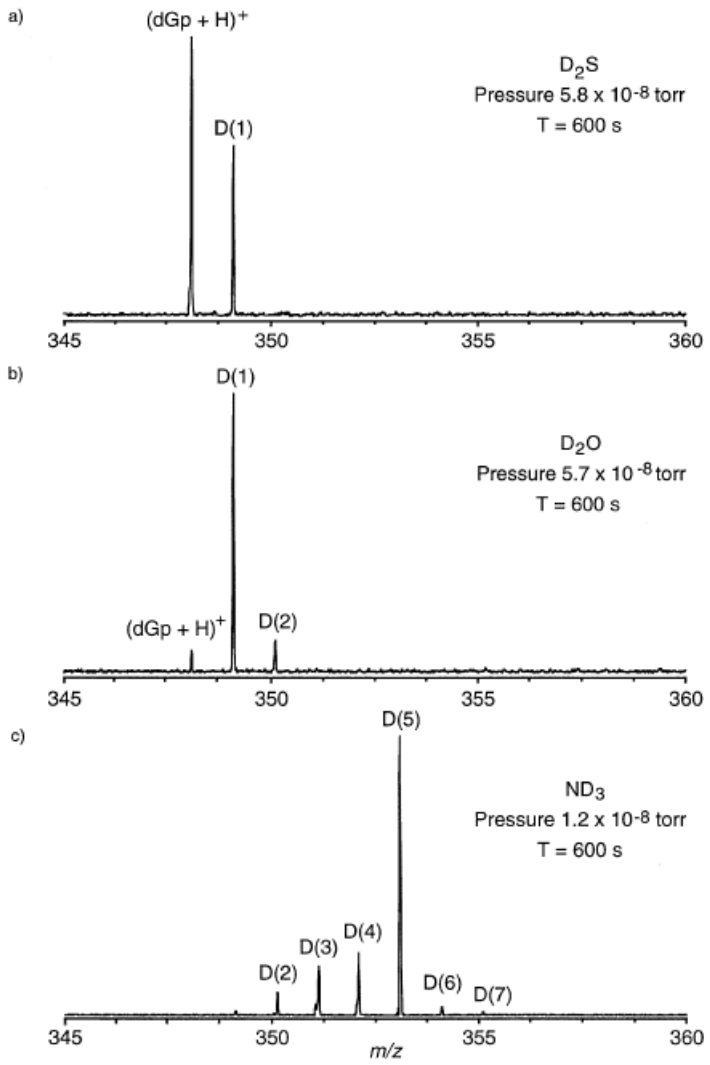

Figure 1.5: Influence of deuterating reagent on gHDX exchange. Spectra of protonated deoxyguanosine-3'-monophosphate (dGp) following 600 s of reaction with A) D_2S, B) D_2O, and C) ND_3. The spectra show differences in deuterium incorporation by reagent.

Reproduced from Green-Church, Kari B., Patrick A. Limbach, Michael A. Freitas, and Alan G. Marshall. "Gas-Phase Hydrogen/Deuterium Exchange of Positively Charged Mononucleotides by Use of Fourier-Transform Ion Cyclotron Resonance Mass Spectrometry." *Journal of the American Society for Mass Spectrometry*, vol. 12, no. 3, 2001, pp. 268–277.

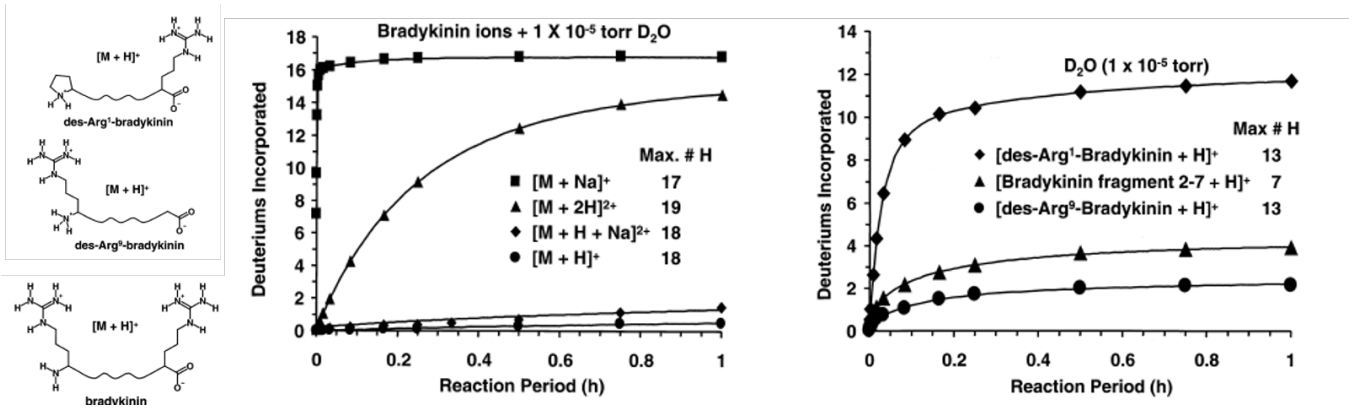

Figure 1.6:Impact of Arginine on the rate of exchange of Bradykinin and its analogs. The figure shows the three chemical structures of bradykinin and its two analogs, des-Arg-bradykinin, in which each analog has a single arginine at the 1 or 9 position of the peptide. The removal of both arginine groups forms the bradykinin fragment. The first deuterium uptake plot shows the low exchange rate of the protonated bradykinin [M+H]+, compared with the second uptake plot, which shows the increased exchange rate with the different analogs—outlining the role of arginine on the rate of exchange.

Adapted from Freitas, M. A., & Marshall, A. G. *International Journal of Mass Spectrometry* 182–183 (1999) 221–231. https://doi.org/10.1016/S1387-3806(98)14274-4.

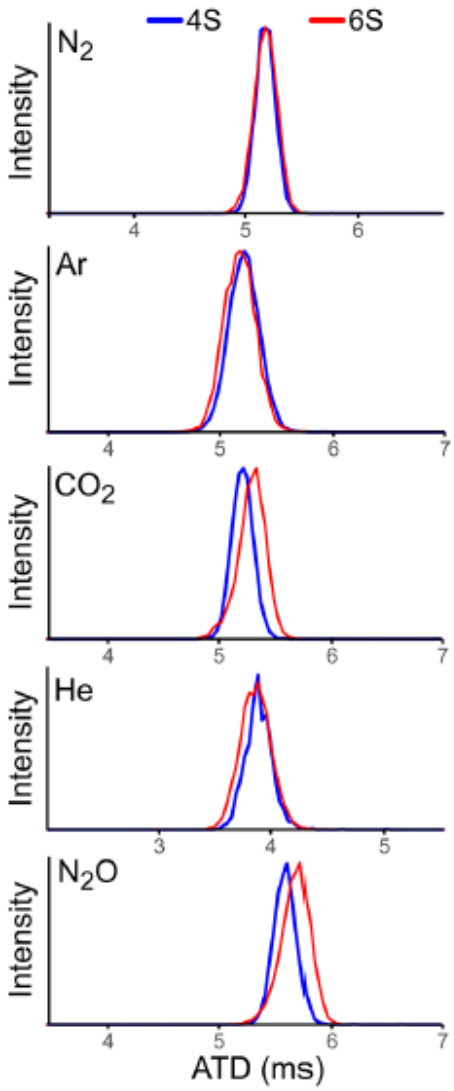

Figure 1.7: Ion mobility separation of monosulfated chondroitin sulfate isomers. Arrival-time distributions (ATDs) of 4S-CS (blue) and 6S-CS (red) measured using N_2, Ar, CO_2, He, and N_2O as drift gases. The two isomers exhibited overlapping ATDs across the gases examined. Although differences in arrival time were observed using CO_2 and N_2O, separation remained limited.

Reproduced from Alonge, Kimberly M et al. "Rapid Differentiation of Chondroitin Sulfate Isomers by Gas-phase Hydrogen-deuterium Exchange." *Current Molecular Medicine* vol. 20,10 (2020): 821-827. doi:10.2174/1566524020666200915110707

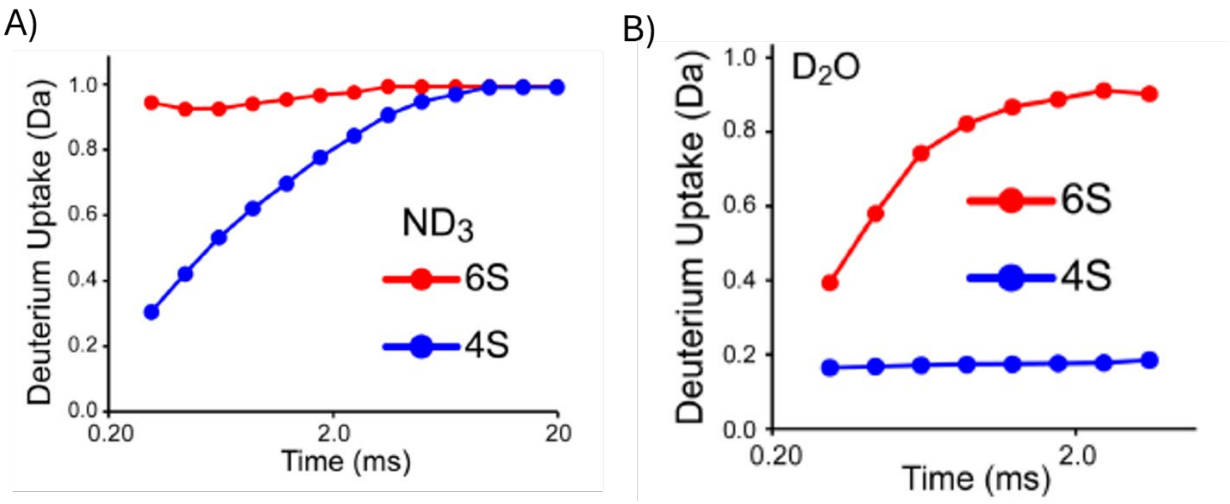

Figure1.9: gHDX differentiates monosulfated CS isomers. Deuterium uptake profiles of 4S-CS (blue) and 6S-CS (red) using A) ND_3 and B) D_2O as the deuterating reagent gas.

Adapted from Alonge, Kimberly M et al. "Rapid Differentiation of Chondroitin Sulfate Isomers by Gas-phase Hydrogen-deuterium Exchange." *Current Molecular Medicine* vol. 20,10 (2020): 821-827. doi:10.2174/1566524020666200915110707

1.9 References

1. B.S Freiser, R.L.W., and J.L Beauchamp, *Sequential deuterium exchange reactions of protonated benzenes with water-D2 in the gas phase by ion cyclotron resonance spectroscopy.* Journal of the American Chemical Society, 1975. **97**(23): p. 6893–6894.
2. Freitas, M.A., et al., *Gas-phase bovine ubiquitin cation conformations resolved by gas-phase hydrogen/deuterium exchange rate and extent.* International Journal of Mass Spectrometry, 1999. **185-187**: p. 565–575.
3. Evans, S.E., N. Lueck, and E.M. Marzluff, *Gas phase hydrogen/deuterium exchange of proteins in an ion trap mass spectrometer.* International Journal of Mass Spectrometry, 2003. **222**(1): p. 175–187.
4. Rand, K.D., et al., *Gas-phase hydrogen/deuterium exchange in a traveling wave ion guide for the examination of protein conformations.* Anal Chem, 2009. **81**(24): p. 10019–28.
5. Mistarz, U.H. and K.D. Rand, *Installation, validation, and application examples of two instrumental setups for gas-phase HDX-MS analysis of peptides and proteins.* Methods, 2018. **144**: p. 113–124.

6. Freitas, M. and A. Marshall, *Rate and extent of gas-phase hydrogen/deuterium exchange of bradykinins: evidence for peptide zwitterions in the gas phase*. International Journal of Mass Spectrometry, 1999. **182-183**: p. 221–231.
7. Green-Church, K.B., et al., *Gas-phase hydrogen/deuterium exchange of positively charged mononucleotides by use of Fourier-transform ion cyclotron resonance mass spectrometry*. J Am Soc Mass Spectrom, 2001. **12**(3): p. 268–77.
8. Robinson, J.M., et al., *Hydrogen/deuterium exchange of nucleotides in the gas phase*. Anal Chem, 1998. **70**(17): p. 3566–71.
9. Uppal, S.S., et al., *Gas-Phase Hydrogen/Deuterium Exchange for Distinguishing Isomeric Carbohydrate Ions*. Anal Chem, 2017. **89**(8): p. 4737–4742.
10. Alonge, K.M., R. Harkewicz, and M. Guttman, *Rapid Differentiation of Chondroitin Sulfate Isomers by Gas-phase Hydrogen-deuterium Exchange*. Curr Mol Med, 2020. **20**(10): p. 821–827.
11. Campbell, S., et al., *Deuterium exchange reactions as a probe of biomolecule structure. Fundamental studies of cas phase H/D exchange reactions of protonated glycine oligomers with D2O, CD3OD, CD3CO2D, and ND3*. Journal of the American Chemical Society, 1995. **117**(51): p. 12840–12854.
12. Grabowski, J.J., C.H. DePuy, and V.M. Bierbaum, *Gas-phase hydrogen-deuterium exchange reactions of anions: kinetics and detailed mechanism*. Journal of the American Chemical Society, 1985. **107**(25): p. 7384–7389.
13. Wyttenbach, T. and M.T. Bowers, *Gas phase conformations of biological molecules: the hydrogen/deuterium exchange mechanism*. Journal of the American Society for Mass Spectrometry, 1999. **10**(1): p. 9–14.
14. Arrington, J.V., et al., *Gas-phase hydrogen deuterium exchange behavior of lysine and its homologs*. International Journal of Mass Spectrometry, 2012. **330**: p. 200–206.
15. Gard, E., et al., *Gas-phase hydrogen/deuterium exchange as a molecular probe for the interaction of methanol and protonated peptides*. J Am Soc Mass Spectrom, 1994. **5**(7): p. 623–31.
16. Beeston, H.S., et al., *Changes in protein structure monitored by use of gas-phase hydrogen/deuterium exchange*. Proteomics, 2015. **15**(16): p. 2842–50.
17. DePuy, C.H., et al., *Hydrogen-deuterium exchange reactions of carbanions with deuterated alcohols in the gas phase*. Journal of the American Chemical Society, 1978. **100**(9): p. 2921–2922.
18. Squires, R.R., C.H. DePuy, and V.M. Bierbaum, *Gas phase hydrogen-deuterium exchange reactions in carbanions: exchange of vinyl and aryl protons by water-d2*. Journal of the American Chemical Society, 1981. **103**(14): p. 4256–4258.
19. Kato, S., et al., *Gas phase hydrogen/deuterium exchange reactions of fluorophenyl anions*. Journal of the American Society for Mass Spectrometry, 1999. **10**(9): p. 840–847.
20. Chipuk, J.E. and J.S. Brodbelt, *Investigation of the gas-phase hydrogen/deuterium exchange behavior of aromatic dicarboxylic acids in a quadrupole ion trap*. International Journal of Mass Spectrometry, 2007. **267**(1): p. 98–108.
21. Suckau, D., et al., *Coexisting stable conformations of gaseous protein ions*. Proceedings of the National Academy of Sciences, 1993. **90**(3): p. 790–793.

22. Ausloos, P. and S.G. Lias, *Thermoneutral isotope-exchange reactions of cations in the gas phase*. Journal of the American Chemical Society, 1981. **103**(13): p. 3641–3647.
23. Grabowski, J.J., C.H. DePuy, and V.M. Bierbaum, *Gas-phase hydrogen-deuterium exchange reactions of hydroxide and hydroxide-d ions with weakly acidic neutrals*. Journal of the American Chemical Society, 1983. **105**(9): p. 2565–2571.
24. Stewart, J.H., et al., *Hydrogen-deuterium exchange reactions of carbanions with water-d2 in the gas phase*. Journal of the American Chemical Society, 1977. **99**(23): p. 7650–7653.
25. Uppal, S.S., et al., *High-Precision, Gas-Phase Hydrogen/Deuterium-Exchange Kinetics by Mass Spectrometry Enabled by Exchange Standards*. Anal Chem, 2020. **92**(11): p. 7725–7732.

Chapter 2: Development of Negative Mode gHDX

2.1 Introduction

Gas-phase hydrogen/deuterium exchange (gHDX) has been applied to a wide range of molecules to obtain structural information, yet its development has predominantly centered on positively charged ions. Studies of protonated peptides, proteins, carbohydrates, and other biomolecules have established that deuterium incorporation can provide information complementary to conventional mass spectrometry and ion mobility measurements[1-6]. In comparison, the application of gHDX to negatively charged ions remains less developed. Expanding gHDX in negative-ion mode is particularly important because many biologically relevant molecules contain acidic functional groups and are readily analyzed as deprotonated ions, including nucleic acids, phosphorylated metabolites, phospholipids, and sulfated glycans such as glycosaminoglycans. The development of negative-mode gHDX provides an opportunity to extend gHDX structural analysis to molecular classes that may be difficult to characterize effectively in positive-ion mode.

Negative-ion analysis may also provide structural information that is complementary to that obtained from positive ions. Ion polarity changes the location and nature of the charge-bearing sites within a molecule and, therefore, the local environment through which the deuterating reagent interacts with the ion. This distinction matters for gHDX because exchange behavior depends on forming favorable interactions between the ion and reagent and on the accessibility of exchangeable hydrogens. Studies comparing protonated and deprotonated biomolecular ions have demonstrated that the two polarities can probe different regions of

molecular structure. For example, Khakinejad et al. used ion mobility spectrometry coupled with gHDX to examine bovine insulin in both polarities and demonstrated differences in deuterium accessibility between protonated and deprotonated ions. Thus, rather than serving simply as an alternative ionization condition, negative-mode gHDX can provide an additional perspective on molecular structure[7].

Although previous studies have established that negatively charged ions can undergo gas-phase H/D exchange and have demonstrated its utility, the literature focuses on specific analyte classes or individual mechanistic questions [7-21]. As a result, a broader understanding of how chemically diverse anions behave under a common set of gHDX conditions remains lacking. In particular, it is unclear whether general exchange trends can be identified across different charge-bearing functional groups and molecular structures. A comparison across a chemically diverse compound set is therefore needed to understand the range of negative-mode exchange behaviors better and identify molecular characteristics associated with different kinetic responses.

A second challenge is the absence of an established set of internal exchange reporters for negative-mode gHDX. Previous work by Uppal et al. demonstrated that internal exchange standards can improve the precision and comparability of positive-mode gHDX measurements by providing a reference response to the experimental exchange environment[6]. Such reporters are particularly valuable when measurements are collected under different instrumental conditions, where variation in reagent exposure, ion residence time, pressure, or ion transport may influence the observed exchange profile. However, implementation of a standardization strategy in negative mode requires compounds that exhibit reproducible and distinguishable exchange behavior.

This chapter aimed to broaden negative-mode gHDX. We first developed a negative-mode gHDX workflow on two instrument platforms with complementary reaction environments and accessible timescales. We then evaluated a chemically diverse panel of anionic compounds to characterize the range of exchange behaviors observed across different charge-bearing functional groups and molecular structures. Cross-platform measurements assessed whether these behaviors were maintained under different experimental conditions, while comparisons across the compound library provided a basis for examining molecular features associated with negative-ion exchange. Finally, compounds with distinct and reproducible exchange behavior were identified as internal exchange reporters, laying the foundation for subsequent studies aimed at improving the standardization and comparability of negative-mode gHDX measurements.

2.2 Results & Discussion

2.2.1 Development & Optimization of the Negative Mode gHDX Workflow

To broaden the use of gHDX for studying negative ions, it is first necessary to design an experimental workflow for both the Thermo LTQ and the Waters Synapt G2-Si. Both platforms were modified to control the introduction of ND_3, which served as the exchange reagent for all subsequent studies because it promotes rapid exchange reactions while maintaining stable instrument pressures [5, 6, 22, 23]. For the Thermo LTQ, exchange occurs in the linear ion trap, where a needle valve controls the ND_3 flow, which then mixes with helium before entering. For the Waters Synapt G2-Si, exchange occurs in the transfer cell, right before entry into the time-of-flight; a mass flow controller controls ND_3 flow. The two instrument platforms allow distinct timescale capabilities: the LTQ enables extended timescales ranging from milliseconds to seconds; in

contrast, the Synapt G2-Si enables exchange on microsecond to millisecond timescales. Implementing gHDX across both instruments enabled characterization of exchange behavior over a broad timescale and observation of the impact of the exchange environment (i.e., buffer gas, operating pressure, and ion holding/propulsion) on exchange, thereby distinguishing intrinsic molecular behavior from instrument-dependent effects.

The LTQ development and optimization consisted of 1) sample preparation by adjusting the working concentration to prevent suppression or oversaturation of the ion signal, 2) establishing holding times to control the duration of the exchange, and 3) testing different ND_3 flow rates to optimize ionization efficiency and control reaction kinetics. To achieve this, we first used a well-characterized positive-mode standard, Tris(hydroxymethyl)aminomethane (Tris), for which our lab had previously conducted extensive studies to develop internal exchange standards and standardization approaches for positive-mode gHDX, thereby identifying its exchange kinetics and the number of exchangeable hydrogens [6]. Tris provided a reliable benchmark for optimizing the experimental setup before transferring to negative-mode experiments. Evaluation of multiple dilutions established a working concentration of approximately 5- 10 µM, which produced a stable signal throughout the exchange experiments. We chose exchange times using a twofold logarithmic progression (1 ms to 32 s), with each time point twice the previous one. This time-point selection approach allowed us to sample early reaction times, when deuterium incorporation occurs rapidly, and longer times to capture slower deuterium incorporation, maintaining sufficient coverage to determine the overall kinetic profile for the analytes of interest. To assess the ND_3 flow rate, we set the holding time to 128 ms, which is the midpoint of the 16 total time points. Tris has six exchangeable hydrogens, and we wanted to reach a six-peak isotopic

envelope at 128 ms by incrementally increasing the ND_3 flow to ensure sufficient reagent infusion for complete exchange. Once this was complete, we examined the ND_3 concentration across the full 16-point timescale range. We observed the entire exchange process from the undeuterated precursor to the single-peak exchange product with a ~6 Da shift, creating an experimental setup on the LTQ.

After establishing the experimental setup, we transferred it to negative-ion mode using 5-sulfosalicylic acid, based on preliminary tests, which was identified as a deprotonated compound producing a stable negative-ion signal at a working concentration of 10 µM, prepared in a 50:50 MeOH: H_2O buffer. We investigated its ability to exchange with ND_3 and captured exchange of one labile hydrogen, resulting in a ~1 Da shift. We also tested 5-sulfosalicylic acid prepared in 90:10 ACN:H_2O; both solvents produced similar exchange profiles. The sample prepared in 90:10 exhibited kinetics slower than that prepared in 50:50 (Figure 2.1A), demonstrating how sample preparation influences exchange. Others have reported effects of sample preparation on gHDX behavior; for example, Beeston et al. showed that changes in sample preparation, including the addition of TFE, influenced the gHDX behavior of ubiquitin and resulted in reduced deuterium incorporation [24]. We selected 50:50 as the standard solvent for all subsequent experiments because it improved analyte solubility across the compounds tested.

To begin establishing an experimental setup on the Synapt G2-Si, we continued using 5-sulfosalicylic acid. We selected both exchange times and ND_3 flow settings based on our lab's previous work developing internal exchange standards and standardization approaches for positive-mode gHDX [6]. On the Synapt G2-Si, ions are transported through the TWIG by a traveling voltage wave generated by sequentially pulsing the ring electrodes. Because wave height controls

the amplitude of this traveling wave (TW) and may influence ion transport, wave heights of 2, 6, and 10 V were selected to represent low, intermediate, and high amplitudes, allowing the effect of traveling wave height on gHDX measurements to be evaluated with helium as the collision gas. Initial experiments revealed an unexpected decrease in deuterium incorporation near TW velocities, corresponding to a 200 ms exchange time across all three wave heights, indicating that the effect doesn't come from a shift in exchange kinetics. Still, the magnitude of the "deuterium loss" artifact increases with wave height (Figure 2.1B). This artifact was not reported in previous gHDX studies on the earlier generation of the Synapt platform[6]. To evaluate this artifact, we considered how to minimize it and examined whether alternative collision gases could "remove" it, since this is an easily adjustable parameter. We conducted the same experiment using Nitrogen, although the artifact was still present; a wave height of 6 minimized it more than 2 or 10, but did not fully resolve it (Figure 2.1C). We then used Argon: a wave height of 2 contained the artifact, a wave height of 6 resolved the artifact, and a wave height of 10 altered the exchange kinetics of 5-sulfosalicylic acid, resulting in a slower exchange rate (Figure 2.1D). In Figure 2.1E, a comparison of Helium, Nitrogen, and Argon collision gases at a wave height of 6 V shows that the effects likely arise from differences in gas properties, including mass and polarizability [25-27]. Despite changes in wave height and collision gas type, the overall kinetic exchange profiles of 5-sulfosalicylic acid remained relatively consistent across all experimental studies. We selected Argon as the collision gas and set the wave height to 6 V for all subsequent experiments on the Synapt G2-Si.

2.2.2 Negative-Mode gHDX Across Anionic Functional Groups

To advance an understanding of hydrogen-deuterium exchange in negative mode, a panel of 30 anionic compounds containing charge-bearing functional groups of phosphonate, sulfonate, and carboxylate was evaluated. As summarized in Figure 2.2, compounds were grouped according to their charge-bearing functional group; additional functional groups on each compound are identified as potential sites of exchange, with labile hydrogens identified in blue.

Initial studies were performed on the LTQ using the experimental setup developed in section 2.2.1. Deuterium uptake was monitored over the reaction timescale, and each compound was classified based on its exchange kinetics. Compounds that were not detected at their expected m/z were categorized as **not classified**. Four distinct exchange kinetic categories emerged: **no exchange**, in which no measurable deuterium incorporation was observed within the experimental timescale; **slow exchange**, in which exchange began but did not reach completion within the experimental timescale; **intermediate** exchange, in which the complete exchange profile was observed over the experimental timescale; and **fast exchange,** in which maximum deuterium incorporation was achieved at the shortest measurable reaction time point. Figure 2.3 summarizes the distribution of compounds among these exchange categories on the LTQ.

Assessment of exchange behavior across charge-bearing functional group classes revealed differences in deuterium uptake. Phosphonate-containing compounds generally exhibited increasing deuterium incorporation as phosphonate content increased. 4-Phosphonobenzoic acid exhibited slow exchange (Figure 2.4A), whereas 1,4-phenylenediphosphonic acid underwent intermediate exchanges with multiple deuterium incorporations (Figure 2.4B), and phytic acid displayed the highest deuterium incorporation

among all compounds examined, regardless of charge-bearing functional group (Figure 2.4C). This suggests that increasing the number of phosphonate groups increases the number of potential exchangeable sites and promotes greater overall deuterium uptake. Sulfonate-containing compounds exhibited the broadest range of exchange behavior, spanning every exchange category (Figure 2.4D-G). Despite sharing the same charge-bearing functional group, the location and type of additional functional groups as potential exchange sites led to distinct exchange behaviors. For example, benzene-1,2-disulfonic acid, whose second sulfonate is in the ortho position, exhibited slow exchange, whereas benzene-1,3-disulfonic acid, whose second sulfonate is in the meta position, exhibited fast exchange. Although the compounds possess similar functional groups, steric hindrance around the exchange site may contribute to their distinct exchange kinetics (Figure 2.2 and Figure2.4 E and G). The 2-, 3-, and 4-sulfobenzoic acid isomers exhibited no detectable exchange, regardless of the position of the carboxylic acid in relation to the charge-bearing sulfonate (Figure 2.2 and Figure 2.4A). Carboxylate-containing compounds showed no detectable exchange on experimental timescales, except for HEDTA and EDTA, which exhibited slow exchange (Figure 2.4H).

These observations demonstrate that a charge-bearing functional group alone does not determine exchange behavior; consideration of the entire compound, including the presence, type, and positioning of functional groups, influences exchange capability.

2.2.3 Cross-Platform Comparison of Negative-Mode gHDX Behavior

Having two instruments, with external modifications for gHDX, allowed us to investigate the effect of an exchange environment on kinetics and assess whether kinetics were conserved

across instruments. The Thermo LTQ and Waters Synapt G2-Si exchange environments differ in several aspects, including location of exchange (i.e., ion trap vs. traveling wave ion guide), reagent gas pressure (i.e., G2-Si operating pressure is higher in comparison to LTQ), ion residence time (i.e., trap times range from milliseconds to seconds versus transient ions affected by traveling wave velocity and traveling wave height, resulting in microseconds to milliseconds), and collision gas (i.e., Helium in the LTQ versus Argon in the Synapt G2-Si). Although ND_3 served as the reagent gas on both platforms, the Synapt G2-Si used a mass flow controller and the LTQ used a needle valve, resulting in different ND_3 concentrations/flow rates. Figure 2.5 summarizes the exchange behavior observed for all 30 compounds across both platforms.

Despite overall agreement in exchange classifications, we observed several important instrument-dependent differences in the deuterium uptake profiles. The Synapt G2-Si reaction time accessibility allowed us to capture a portion of the deuterium uptake profile before complete deuterium incorporation for fast-exchanging compounds such as 4,5-dihydroxybenzene-1,3-disulfonate (Figure 2.6A) and benzene-1,3-disulfonic acid (Figure 2.6 B), which was not observed on LTQ, where these compounds had complete deuterium incorporation at the earliest accessible time points. The higher pressure and concentration of ND_3 infused into the Synapt G2-Si revealed additional deuterium incorporation for 1,4-phenylenediphosphonic acid (Figure 2.6C) and phytic acid(Figure 2.6D); on the LTQ, 1,4-phenylenediphosphonic acid incorporated a total of two deuteriums, and on the Synapt G2-Si, a total of three deuteriums were incorporated. Phytic acid showed the largest overall uptake on the LTQ, incorporating up to five deuteriums; on the Synapt G2-Si, it incorporated eight deuteriums. Lastly, although slow exchanges never reach deuterium incorporation to completion, the later-timescale accessibility on the LTQ allowed us to observe

more progression of the deuterium uptake profile than on the Synapt G2-Si, as in the case of EDTA (Figure 2.6E)

The results demonstrated that exchange environments influence both the observable extent of deuterium incorporation and the kinetic window accessible for observation. The Synapt G2-Si revealed additional deuterium uptake and earlier stages of the exchange process due to its shorter exchange timescales, whereas the Thermo LTQ captured later stages of the slow reaction. Despite these platform-dependent differences, the exchange behavior of the 30 compounds was largely conserved, with compounds classified as slow-, intermediate-, or fast-exchanging maintaining their kinetic exchange rate profile across both instruments.

2.2.4 Mechanistic Framework for Negative-Mode gHDX

Evaluation of the thirty anionic compounds demonstrated broad trends emerging across the three classes of charge-bearing functional groups: phosphonate-containing compounds showed the greatest deuterium incorporation, sulfonates displayed exchange behaviors ranging from no exchange to fast exchange, and carboxylate-containing compounds showed no or slow exchange. These observations suggest that charge-bearing functional groups may set the overall exchange potential but are insufficient to explain the diverse exchange behavior across the compound panel. The study enabled us to propose that negative-mode gHDX is not governed by a single molecular property but by an interplay of hydrogen-bonding interactions, molecular geometry, and the accessibility of exchangeable hydrogens. To illustrate this, we designed representative ion-ND_3 interaction models from the experimental observations (Figure 2.7), which provide a conceptual framework for understanding the exchange process in negative-mode gHDX.

The first model is represented by 3-sulfobenzoic acid, which exhibited no exchange (Figure 2.7A). Although the compound contains both a charge-bearing sulfonate group and an exchangeable carboxylic acid hydrogen, the exchangeable hydrogen is isolated and lacks neighboring functional groups to support a productive hydrogen-bonding network with ND_3. This was also observed for compounds containing isolated hydroxyl or carboxylic acid functional groups, including salicylic acid, 5-nitrosalicylic acid, and phenolsulfonic acid, all of which showed no exchange. These observations illustrate that exchangeable hydrogens alone are insufficient to initiate exchange and promote gHDX. Consistent with previous studies of aromatic carboxylates, which demonstrated that successful gas-phase H/D exchange depends not simply on the presence of labile hydrogens but on their ability to participate in favorable ion-reagent interactions and accessible exchange pathways[12]. The importance of hydrogen-bonding interactions is further illustrated by EDTA (Figure 2.7B). Unlike 3-sulfobenzoic acid, EDTA contains multiple carboxylic acid groups interacting with ND_3. The proposed model depicts a more favorable ion-reagent interaction than with 3-sulfobenzoic acid, suggesting that multiple acidic groups form a stable ion-ND_3 complex and provide a pathway for exchange. Despite a stable ion-ND_3 complex, EDTA exhibited a slow exchange. This observation highlights that increasing the number of exchangeable hydrogens or potential hydrogen-bonding interactions alone does not necessarily produce complete exchange. Instead, the local arrangement of these interactions and the positioning of exchangeable hydrogens relative to the reagent gas may be equally important determinants of exchange. For example, when comparing EDTA and 5-sulfosalicylic acid, both compounds form stable ion-ND_3 complexes that enable exchange. However, the hydroxyl group in 5-sulfosalicylic acid is proposed to create a more favorable hydrogen-bonding interaction, resulting in an intermediate exchange

(Figure 2.7C). Although the preceding comparisons (i.e., EDTA and 5-sulfosalicylic acid) demonstrated the importance of hydrogen-bonding interactions in forming an ion-ND_3 complex, they also involved different functional group compositions. To consider the influence of structural organization from functional group identity, the positional isomers benzene-1,2-disulfonic acid and benzene-1,3-disulfonic acid were examined. Both compounds possess identical elemental composition and the same charge-bearing functional group; however, benzene-1,2-disulfonic acid exhibited slow exchange, and benzene-1,3-disulfonic acid exhibited fast exchange. Because the two isomers differ only in the relative positions of the sulfonate groups, the observed differences cannot be attributed to functional group identity. Instead, the proposed models show that the relative positioning of functional groups alters the accessibility of exchangeable hydrogens and ND_3's ability to form stable ion-reagent complexes (Figure 2.7D). Similar positional effects have previously been reported for aromatic dicarboxylic acids, where subtle changes in functional group arrangement altered gHDX behavior[12]. The clearest example of a highly favorable interplay between hydrogen-bonding networks, functional group arrangement, and exchangeable hydrogen accessibility is seen with phytic acid and 1,4-phenylenediphosphonic acid (Figure 2.7E). These phosphonate-containing compounds exhibited the greatest extent of deuterium incorporation observed across all 30 compounds surveyed, and rather than the phosphonate functional group alone governing efficient exchange, these compounds provided a favorable exchange environment with the combined multiple acidic functional groups, extensive hydrogen-bonding networks, and favorable structural organization, allowing numerous accessible relay pathways for multiple exchanges to occur. These conceptual models presented in Figure 2.7 demonstrate how

hydrogen-bonding interactions, functional group arrangement, and the accessibility of exchangeable hydrogens collectively govern negative-mode gHDX.

2.2.5 Identification of Negative-Mode gHDX Exchange Reporters

The evaluation of negative-ion gHDX behavior in thirty anionic compounds yielded a practical outcome beyond mechanistic insight: the identification of compounds with reproducible, distinct exchange kinetics suitable for use as exchange reporters. The three reporters introduced in this chapter represent the three categories of exchange behaviors: slow, intermediate, and fast (Figure 2.8). Although they capture the kinetic range observed during the compound survey, they undergo only limited deuterium incorporation (typically ~1 Da). To address this limitation, we included a broad exchange reporter (Figure 2.8). Using a broad-exchange reporter that undergoes multiple deuterium incorporations yields an expanded isotopic distribution, which can be used to calculate the maximum deuterium content (%Dmax) achieved under the experimental conditions. For example, consider two gHDX experiments performed on different days. Under both conditions, a fast-exchange reporter may exhibit complete deuterium incorporation (1 Da), suggesting that the experiments produce equivalent exchange behavior. Similarly, the intermediate-exchange reporter may reach its maximum deuterium-incorporation profile over the timescales in both conditions, with only subtle differences in exchange rates. In comparison, a broad exchange reporter may incorporate 3 deuteriums in one experiment and 7 deuteriums in the other, clearly demonstrating that the second experiment supported greater deuterium incorporation. The ability to determine the maximum deuterium content (%Dmax) achieved under each set of experimental conditions becomes valuable for assessing experimental

reproducibility, monitoring instrument performance, and comparing exchange conditions across data sets.

Here we report our four exchange reporters. Ethylenediaminetetraacetic acid (EDTA) exhibited minimal deuterium incorporation over the experimental timescales on both platforms and thus serves as the slow-exchange reporter. 5-Sulfosalicylic acid exhibited intermediate exchange kinetics, completing exchange across the accessible timescale on each platform while maintaining consistent uptake behavior across instrument types and during experimental workflow optimization and development in section 2.2.1. Benzene-1,3-disulfonic acid exchanged rapidly, reaching maximum deuterium incorporation on the shortest accessible timescales. However, the shorter reaction times available on the Synapt G2-Si allowed observation of part of its uptake kinetics before complete deuterium incorporation. Phytic acid incorporated up to eight deuteriums, providing the broadest range of mass shifts observed among all compounds examined and becoming our broad exchange reporter. Together, the exchange reporters spanning diverse kinetic behaviors enable evaluation of experimental reproducibility, data standardization, and assessment of analyte reaction behavior and differences under varying gHDX conditions.

2.3 Materials & Methods

2.3.1 Materials

Deuterated Ammonia (ND_3) (99%) was purchased from Cambridge Isotopes Laboratories (Tewksbury, MA, USA). Potassium Benzene-1,2-disulfonate, 4-Hydroxyisophthalic Acid, N-(2-Hydroxyethyl)ethylenediamine-N, N', N'-triacetic Acid (HEDTA), 2-Hydroxy-5-nitrobenzoic Acid, Salicylic Acid, phenolsulfonic Acid, Hydroquinone sulfonic acid potassium salt, 4,5-Dihydroxy-

1,3-benzenedisulfonic Acid disodium salt monohydrate, Sodium benzene-1,3-disulfonate, (1,4-Phenylenebis(methylene))diphosphonic Acid, Iminodiacetic Acid, Nitrilotriacetic Acid, Sulfosuccinic Acid solution, 4-Sulfophthalic Acid trisodium salt, 5-Sulfoisophthalic Acid sodium salt, Sulfoacetic Acid, 4-Carboxyphenylboronic Acid, Methylmalonic Acid, HEPES buffer, 5-sulfosalicylic acid dihydrate, phytic acid, and Tris-EDTA buffer solution were purchased from Sigma-Aldrich (St. Louis, MO, USA). 2-Sulfobenzoic Acid hydrate and Acetate buffer solution were purchased from Fisher Scientific (San Diego, CA, USA). 3-Sulfobenzoic Acid monosodium salt, 4-Sulfobenzoic Acid monopotassium salt, PIPES buffer solution, ACES buffer, 4,5-Dihydroxynaphthalene-2,7-disulfonic Acid disodium salt dihydrate, and TCEP-HCl were purchased from Thermo Fisher Scientific (St. Louis, MO, USA). Methanol, formic acid, and Optima LC/MS-grade water were purchased from Fisher Scientific (Somerville, New Jersey).

2.3.2 Sample Preparation

Individual compounds used were prepared as stock solutions in Optima LC/MS-grade water and subsequently diluted in 50% Methanol and 0.1% formic acid to a working concentration of 1-10 µM.

2.3.3 Mass Spectrometry

All experiments were conducted on a Waters Synapt G2-Si (Waters Corp., Milford, MA, USA) or a Thermo Fisher Scientific LTQ (San Jose, CA, USA) in negative-ion mode. Each instrument was equipped with external instrument modifications to enable ND_3 infusion. We purchased steel gas lines, valves, and unions from Swagelok (Solon, OH, USA), with corrosion-resistant components and seals made of either polytetrafluoroethylene (PTFE) or nylon.

2.3.4 Gas-Phase Hydrogen/Deuterium Exchange

We have modified the gas inlets of the commercially available Thermo LTQ and Waters Synapt G2-Si to enable gHDX. We performed gas-phase HDX on both instrument platforms by introducing ND_3 into the respective ion-storage or ion-transport region. On the Thermo LTQ, exchange occurred during controlled ion storage within the linear ion trap. On the Waters Synapt G2-Si, exchange occurred during ion transport through the transfer traveling-wave ion guide (TWIG). The different ion-handling architectures provided complementary experimental exchange periods ranging from milliseconds to seconds on the LTQ and from microseconds to milliseconds on the Synapt G2-Si. All lines are thoroughly flushed with N_2, He, or Ar before and after use. All compounds were infused directly into the mass spectrometer via a nano-ESI needle or a fused silica capillary using a syringe pump (Harvard Apparatus, Holliston, MA, USA) at flow rates of 5 or 10 µM/min. Between each compound infusion, we flushed the lines and system with ESI buffer (50% Methanol, 0.1% formic acid) to prevent crossover between compounds with similar m/z values. All samples were collected in triplicate unless otherwise stated.

Waters Synapt G2-Si

To evaluate the influence of traveling-wave conditions on negative-mode gHDX, 5-sulfosalicylic acid was analyzed using transfer TWIG wave heights of 2, 6, and 10 V. Helium, nitrogen, and argon were independently evaluated as collision gases under otherwise comparable acquisition conditions. A transfer TWIG wave height of 6 V and argon collision gas were selected for subsequent Synapt G2-Si gHDX measurements.

The Synapt G2-Si infusion of deuterated ammonia (ND_3) is achieved using mixtures of Argon (Ar) and ND_3, with two mass flow controllers (Aalborg, Orangeburg, NY) mixing the gases just before the gas inlet to the transfer cell TWIG[4].

Operated with a capillary voltage of 2 kV, Source Temp 70 °C, sampling cone 20 V, and source offset 20 V. Acquisition mass range 50- 600 *m/z*, Scan time per collection 2 sec. The trap and transfer collision energies were set to 4 V. For deuterated labeling, the T-wave velocity of the transfer TWIG was ramped from 8 to 1300 m/s to achieve labeling times of 0.1 to 12 ms.

Thermo LTQ

The Thermo LTQ was outfitted with a custom needle valve to control the amount of deuterated ammonia (ND_3) mixed with the Helium collision gas infused into the ion trap.

Thermo LTQ: each analyte was isolated and held for a set period to allow exchange with ND_3. The peak *m/z* was isolated with an isolation width of at least 10 Th (centered within the isotopic distribution) to cover the full exchange window in the spectra. We sampled a wide range of exchange times (16), from 1 millisecond to 30 seconds. The exchange times were defined within the instrument method as extended collision-induced dissociation (CID) experiments with zero collision energy, allowing ions to be held in the collision cell for controlled reaction times without fragmentation. Mass spectra were acquired in enhanced scan mode for resolution setting. The Ion Source parameters were set as follows: NanoESI capillary Temp 210°, source voltage 2.30 kV, Source Current 100 uA, Capillary Voltage -9.00 V, Tube Lens -65.0 V, Lens 1 Voltage 39.00 V, Front Lens 14.0 V.

Anionic Compound Screening

Each compound was analyzed independently in negative-ion mode on both the Thermo LTQ and Waters Synapt G2-Si using the instrument-specific gHDX conditions described above. Following precursor ion selection, ions were exposed to ND_3 across the experimental exchange-time range accessible on each platform. Mass spectra were collected at each exchange time, and deuterium incorporation was determined from the resulting shift in the isotopic distribution relative to the undeuterated ion. Deuterium uptake profiles were generated by plotting the measured deuterium incorporation as a function of experimental exchange time. Compounds were then categorized according to their observed exchange behavior as no exchange, slow, intermediate, fast, or broad exchange. Classification was based on the relative timescale and extent of deuterium incorporation across the experimental exchange window.

2.3.5 Data Analysis

Spectra for each time point were manually extracted from MassLynx and Thermo Xcalibur Qual Browser. Compound spectra were processed and analyzed using HX-Express.[28]. The experimental error in measured deuterium values was estimated from the standard deviation of triplicate measurements (n=3), unless stated otherwise.

2.4 Chapter Summary

This chapter established an experimental workflow for negative-mode gHDX on the Thermo LTQ and Waters Synapt G2-Si, providing complementary exchange timescales and experimental environments. Using these platforms, a chemically diverse panel of 30 anionic compounds was evaluated to characterize negative-mode exchange behavior across phosphonate-, sulfonate-, and carboxylate-containing species. The resulting exchange profiles of the 30 compounds

spanned no, slow, intermediate, and fast exchange behavior, demonstrating that the charge-bearing functional group alone was insufficient to predict gHDX behavior. Instead, the experimental observations supported a model in which hydrogen-bonding interactions, functional-group arrangement, and accessibility of exchangeable hydrogens influence exchange. From this evaluation, EDTA, 5-sulfosalicylic acid, benzene-1,3-disulfonic acid, and phytic acid were selected to represent slow, intermediate, fast, and broad exchange and be used as negative-mode exchange reporters.

2.5 Acknowledgements

The research reported was supported by the National Institute of General Medical Sciences (NIGMS) of the National Institutes of Health (NIH) under Award Number T32GM008268. National Institutes of Health grants funded this work: R01GM127579 (M.G.) and the National Science Foundation Award: 2304707 (M.G.).

2.6 Chapter Figures

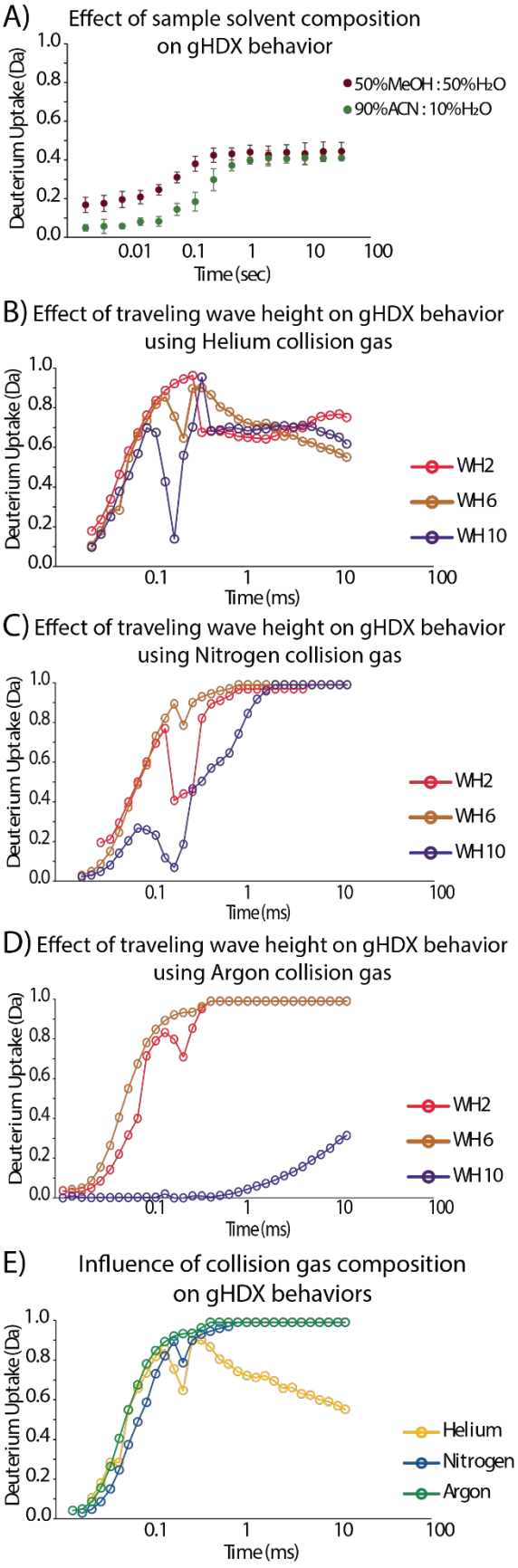
A)
Effect of sample solvent composition
on gHDX behavior
Deuterium Uptake (Da)
1.0
0.8
0.6
0.4
0.2
0.0
50%MeOH : 50%H2O
90%ACN : 10%H2O
0.01
0.1
1
10
100
Time (sec)
B) Effect of traveling wave height on gHDX behavior
using Helium collision gas
Deuterium Uptake (Da)
WH2
WH6
WH10
0.1
1
10
100
Time (ms)
C) Effect of traveling wave height on gHDX behavior
using Nitrogen collision gas
Deuterium Uptake (Da)
WH2
WH6
WH10
0.1
1
10
100
Time (ms)
D) Effect of traveling wave height on gHDX behavior
using Argon collision gas
Deuterium Uptake (Da)
WH2
WH6
WH10
0.1
1
10
100
Time (ms)
E)
Influence of collision gas composition
on gHDX behaviors
Deuterium Uptake (Da)
Helium
Nitrogen
Argon
0.1
1
10
100
Time (ms)

Figure 2.1: Evaluation of sample preparation and instrumental parameters for development of the negative-mode gHDX workflow. Experimental parameters affecting deuterium uptake behavior were evaluated using 5-sulfosalicylic acid. A) Effect of sample solvent composition on gHDX behavior measured on the LTQ, comparing 50:50 methanol/water and 90:10 acetonitrile/water buffers. B-D) Effect of traveling wave height: 2 (red), 6 (brown), and 10 (purple) on deuterium uptake measured on the Waters Synapt G2-Si using B) helium, C) nitrogen, and D)argon as the collision gas. E) Direct comparison of helium, nitrogen, and argon at a traveling wave height of 6V.

Phosphonates

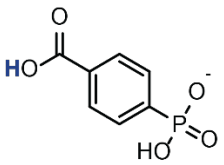

4-Phosphonobenzoic Acid

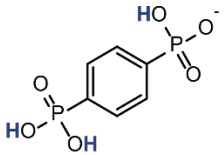

1,4-Phenylenediphosphonic Acid

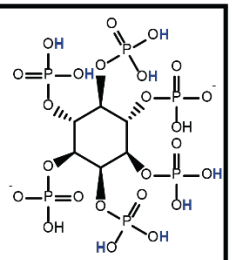

Phytic Acid

Carboxylates

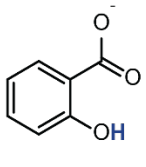

Salicyclic Acid

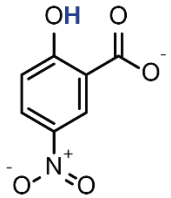

5-Nitrosalicyclic Acid

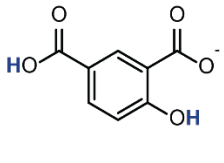

4-Hydroxyisophthalic Acid

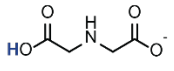

Iminodiacetic Acid

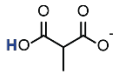

Methylmalonic Acid

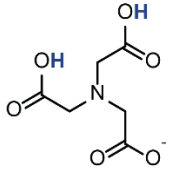

Nitrilotriacetic Acid

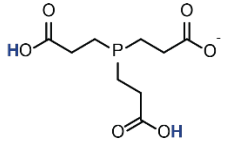

TCEP

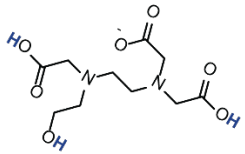

Hydroxyethylethylenediaminetriacetic Acid (HEDTA)

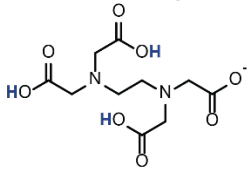

Ethylenediaminetetraacetic Acid (EDTA)

Sulfonates

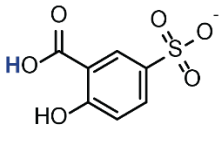

5-Sulfosalicylic Acid

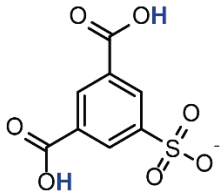

5-Sulfoisophthalic Acid

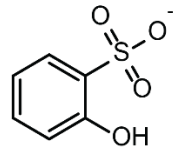

Phenolsulfonic Acid

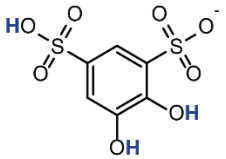

4,5-Dihydroxybenzene-1,3-Disulfonate

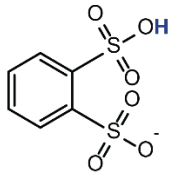

Benzene-1,2-Disulfonic Acid

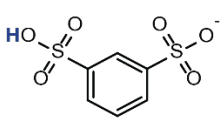

Benzene-1,3-Disulfonic Acid

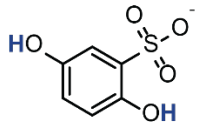

Hydroquinone Sulfonic Acid

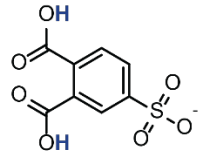

4-Sulfophthalic Acid

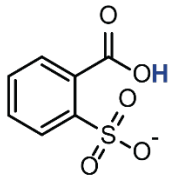

2-Sulfobenzoic Acid

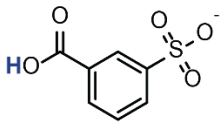

3-Sulfobenzoic Acid

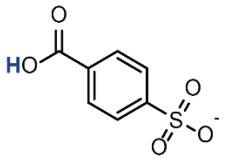

4-Sulfobenzoic Acid

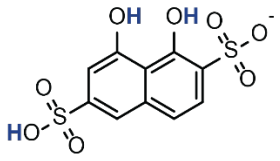

4,5-Dihydroxynaphthalene-2,7-Disulfonic Acid

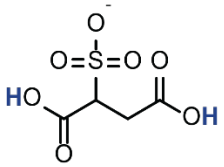

Sulfosuccinic Acid

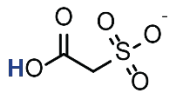

Sulfoacetic Acid

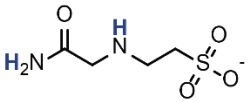

ACES

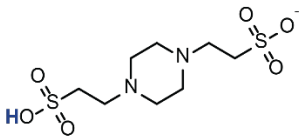

PIPES

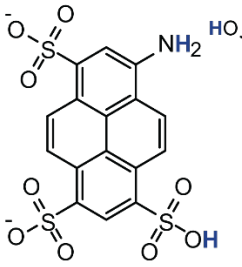

APTS

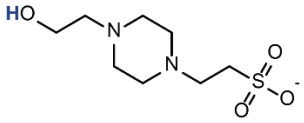

HEPES

Figure 2.2: Structural classification of analytes evaluated for negative-mode gHDX. Thirty analytes were selected and organized by their charge-bearing functional group: phosphonate, sulfonate, or carboxylate. Molecular structures and names are shown for each analyte. Functional groups containing blue-highlighted hydrogens indicate sites that may participate in hydrogen/deuterium exchange.

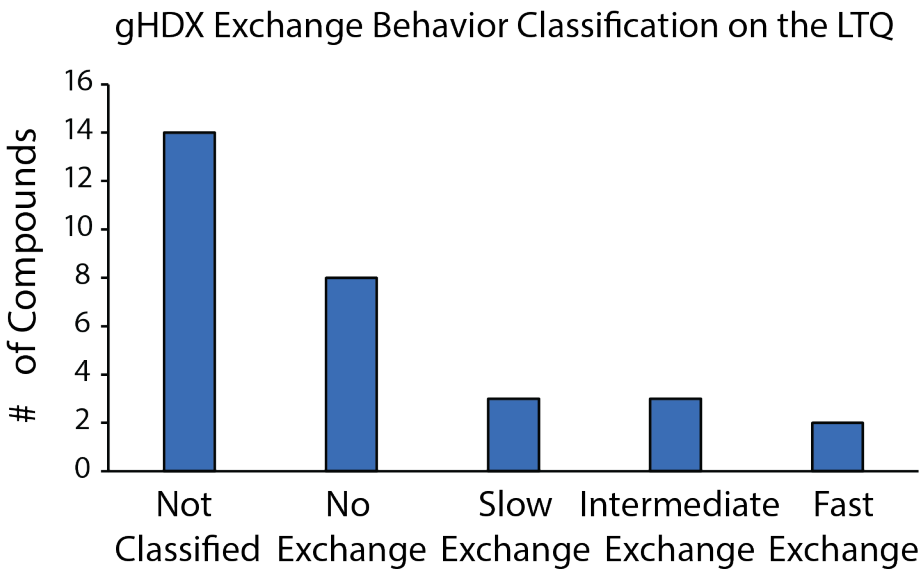

Figure 2.3: Classification of negative-mode gHDX behavior on the Thermo LTQ. Thirty compounds were evaluated on the Thermo LTQ and categorized according to their observed exchange behavior. Compounds were classified as no exchange, slow exchange, intermediate exchange, or fast exchange. Compounds that were not at their expected m/z value were not classified. Of the 30 compounds, 14 were not classified, 8 exhibited no exchange, 3 exhibited slow exchange, 3 exhibited intermediate exchange, and 2 exhibited fast exchange.

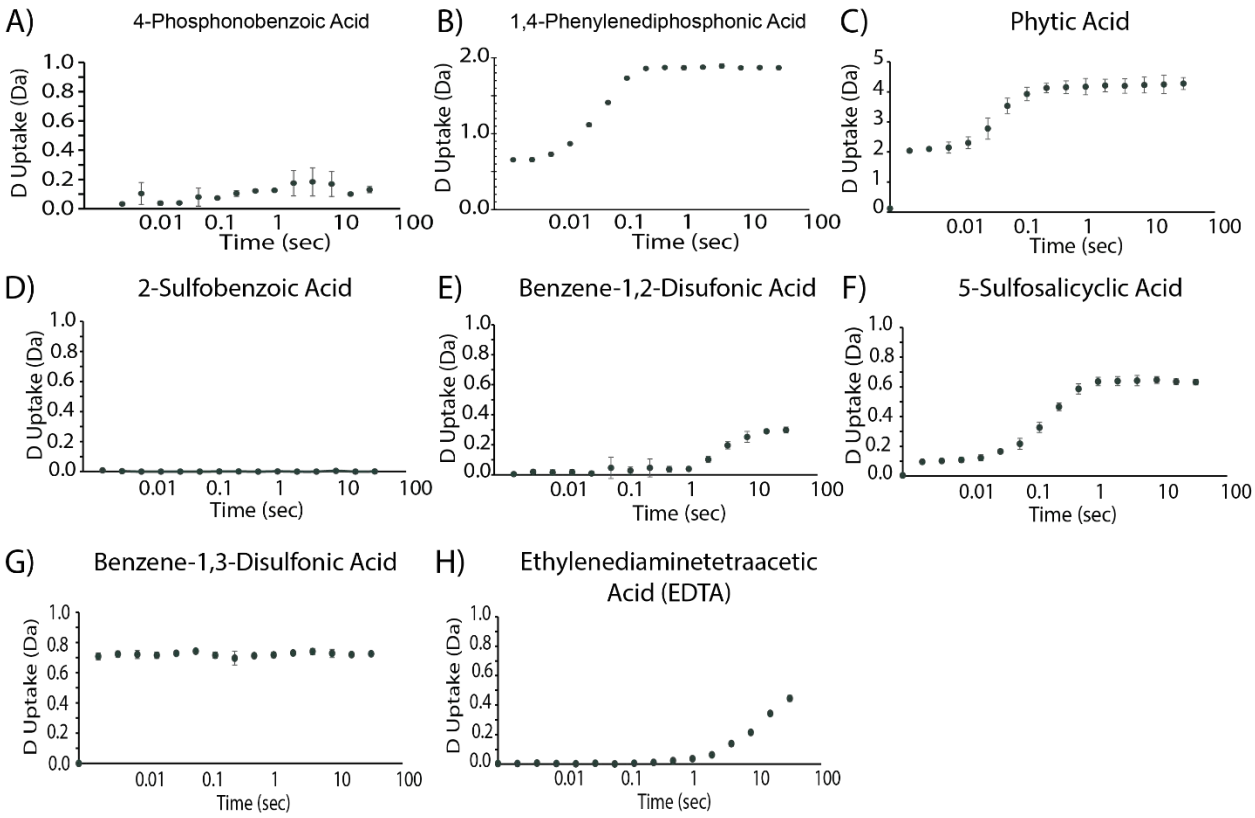

Figure 2.4: Charge-bearing functional group trends observed on Thermo LTQ. Deuterium uptake profiles of selected compounds grouped according to their charge-bearing functional group. A-C) Phosphate-containing compounds exhibited increasing deuterium incorporation with increasing phosphate functional groups. D-G) Sulfonate-containing compounds exhibited the greatest diversity in exchange behavior, displaying no exchange, slow exchange, intermediate exchange, and fast exchange. H) EDTA, a selected carboxylate-containing compound, exhibited slow exchange. Error bars represent the standard deviation of triplicate measurements (n = 3), where shown.

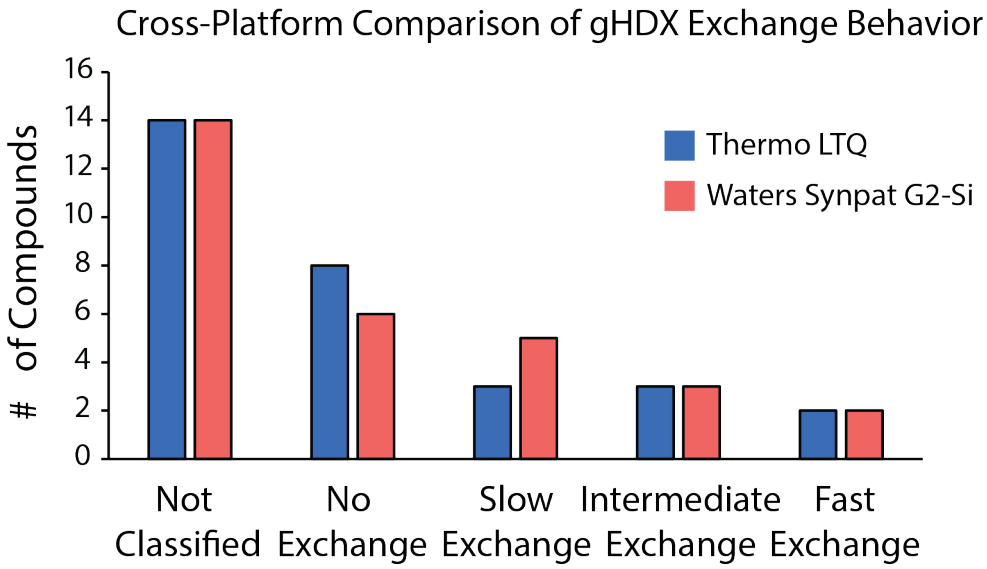

Figure 2.5: Cross-platform comparison of negative-mode gHDX behavior on the Thermo LTQ and Waters Synapt G2-Si. The same 30 compounds were evaluated on both Thermo LTQ (blue) and Waters Synapt G2-Si (red) and categorized according to observed exchange behavior. Compounds were classified as: not classified, no exchange, slow exchange, intermediate exchange, and fast exchange. The number of compounds classified in each category was consistent, except for 3 compounds whose behavior was reclassified on Synapt G2-Si.

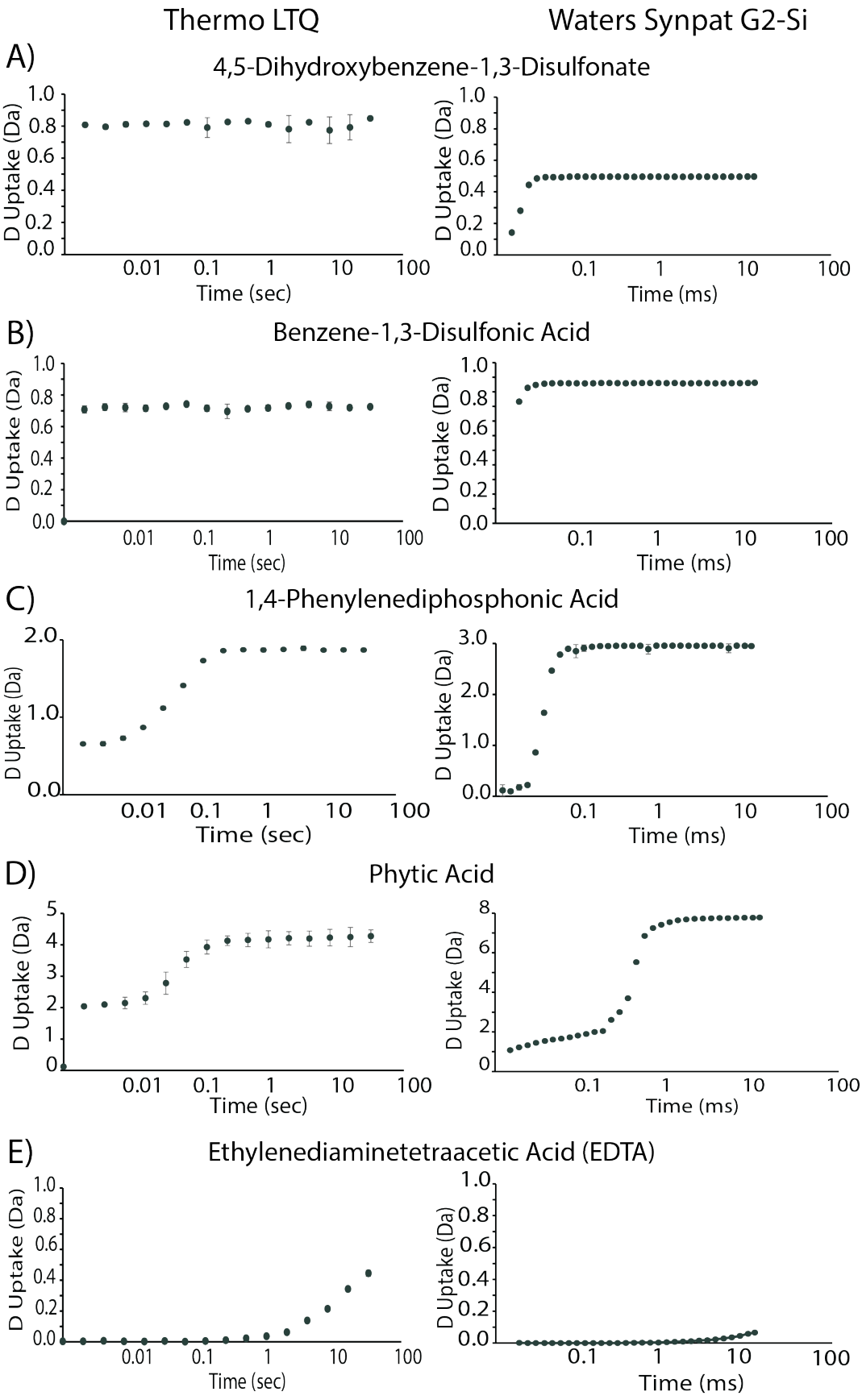
Thermo LTQ
Waters Synpat G2-Si
A)
4,5-Dihydroxybenzene-1,3-Disulfonate
B)
Benzene-1,3-Disulfonic Acid
C)
1,4-Phenylenediphosphonic Acid
D)
Phytic Acid
E)
Ethylenediaminetetraacetic Acid (EDTA)
D Uptake (Da)
Time (sec)
Time (ms)

Figure 2.6: Cross-platform comparison of selected compounds' gHDX uptake profiles on the Thermo LTQ and Waters Synapt G2-Si. Deuterium uptake profiles are shown for selected analytes: A) 4,5-dihydroxybenzene-1,3-disulfonate, B) benzene-1,3-disulfonic acid, C) 1,4-phenlenediphosphonic acid, D) phytic acid, and E) EDTA on the Thermo LTQ (left panels) and the Waters Synapt G2-Si (right panels), allowing direct comparison of exchange behavior across both instruments. Error bars represent the standard deviation of triplicate measurements (n = 3), where shown.

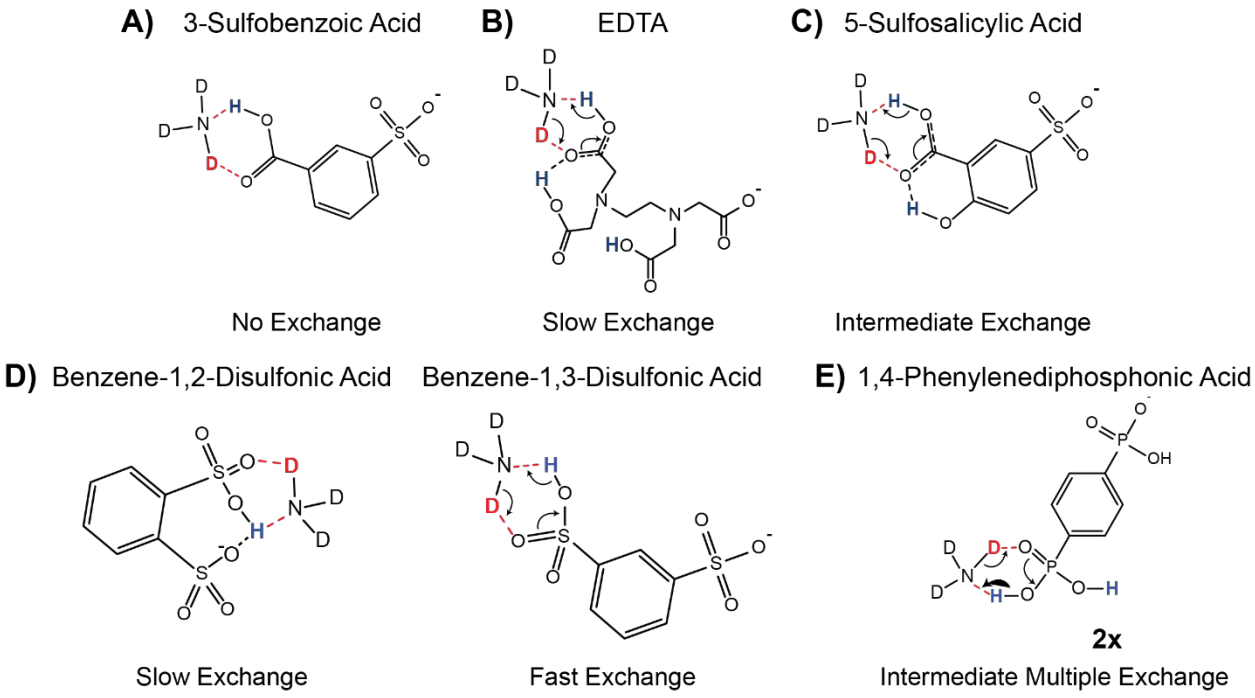

Figure 2.7: Proposed ion-ND_3 conceptual models. Representative models illustrating ion-ND_3 interactions based on experimentally observed exchange behavior. Red dashed lines indicate potential hydrogen-bond interactions between ND3 and the compound that may facilitate H/D exchange. A) Isolated exchangeable hydrogen on 3-sulfobenzoic acid lacks favorable interactions that limit exchange. B) Multiple acidic or exchangeable sites in EDTA support an extended hydrogen-bonding network capable of stabilizing the ion-ND_3 complex and facilitating exchange. C) 5-sulfosalicylic acid shows that the identity and positioning of neighboring functional groups may alter the local interaction environment surrounding the exchange hydrogens and influence its ability to interact more favorably with ND_3. D) Differences in the spatial arrangement of benzene-1,2-disulfonic acid and benzene-1,3-disulfonic acid alter the accessibility of exchangeable hydrogens, reflecting differences in exchange behavior. E) Phosphonate-containing compounds like 1,4-phenylenediphosphonic acid provide multiple exchangeable hydrogens capable of participating in ion-ND3 highly favorable interactions.

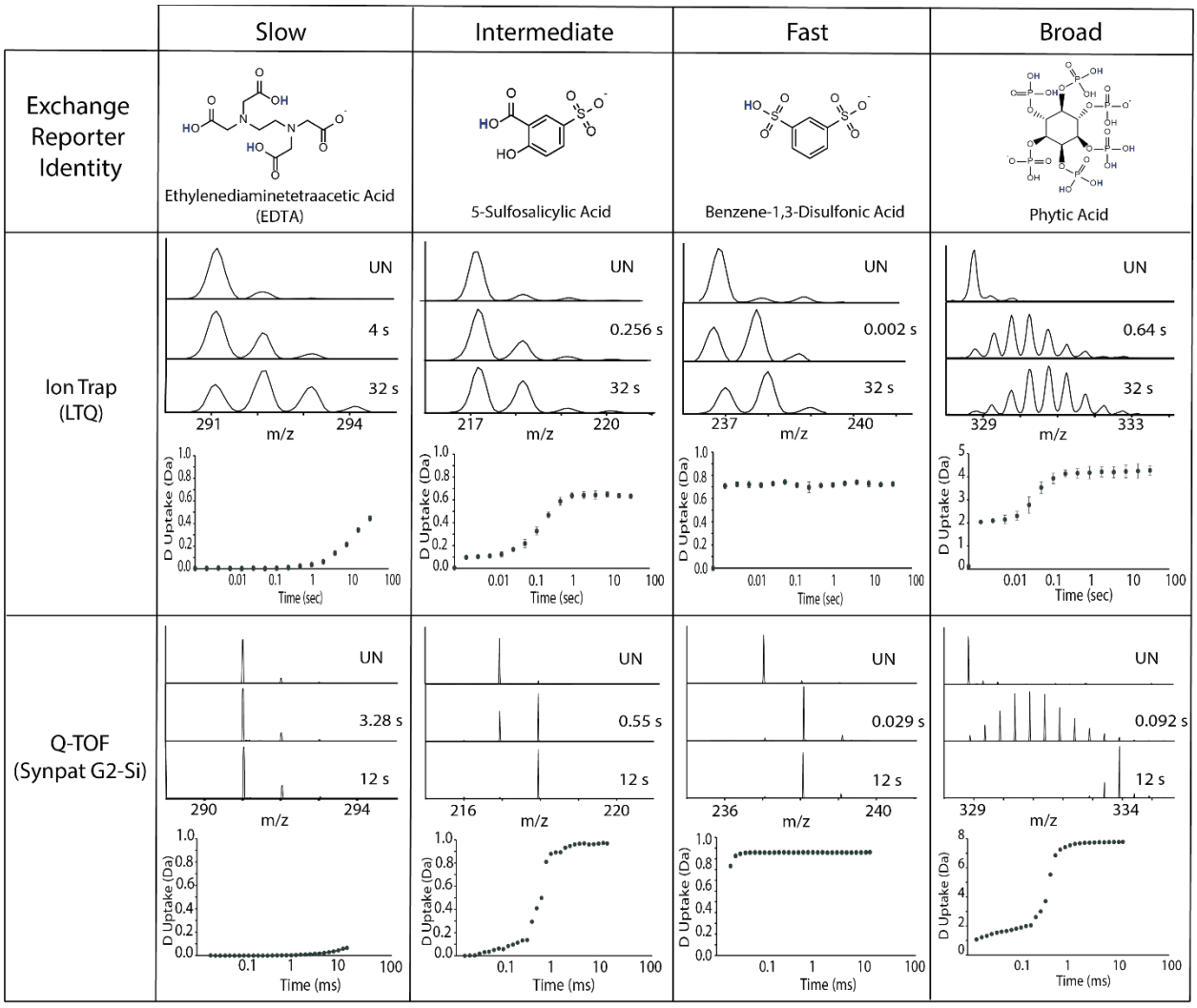

Figure 2.8: Kinetic classification and cross-platform comparison of negative-mode gHDX reporters. Four exchange reporters were selected: ethylenediaminetetraacetic acid (EDTA), slow exchanger; 5-sulfosalicylic acid, intermediate exchanger; benzene-1,3-disulfonic acid, fast exchanger; and phytic acid, broad exchanger. The top row shows the molecular structure of each reporter. The second row presents mass spectra collected at selected exchange times and the deuterium uptake profiles obtained on the Thermo LTQ. The third row presents spectra and deuterium uptake profiles on the Waters Synapt G2-Si. Error bars represent the standard deviation of triplicate measurements (n=3).

2.7 References

1. Freitas, M. and A. Marshall, *Rate and extent of gas-phase hydrogen/deuterium exchange of bradykinins: evidence for peptide zwitterions in the gas phase.* International Journal of Mass Spectrometry, 1999. **182-183**: p. 221–231.
2. Freitas, M.A., et al., *Gas-phase bovine ubiquitin cation conformations resolved by gas-phase hydrogen/deuterium exchange rate and extent.* International Journal of Mass Spectrometry, 1999. **185-187**: p. 565–575.
3. Evans, S.E., N. Lueck, and E.M. Marzluff, *Gas phase hydrogen/deuterium exchange of proteins in an ion trap mass spectrometer.* International Journal of Mass Spectrometry, 2003. **222**(1): p. 175–187.
4. Rand, K.D., et al., *Gas-phase hydrogen/deuterium exchange in a traveling wave ion guide for the examination of protein conformations.* Anal Chem, 2009. **81**(24): p. 10019–28.
5. Uppal, S.S., et al., *Gas-Phase Hydrogen/Deuterium Exchange for Distinguishing Isomeric Carbohydrate Ions.* Anal Chem, 2017. **89**(8): p. 4737–4742.
6. Uppal, S.S., et al., *High-Precision, Gas-Phase Hydrogen/Deuterium-Exchange Kinetics by Mass Spectrometry Enabled by Exchange Standards.* Anal Chem, 2020. **92**(11): p. 7725–7732.
7. Khakinejad, M., et al., *Ion Mobility Spectrometry-Hydrogen Deuterium Exchange Mass Spectrometry of Anions: Part 3. Estimating Surface Area Exposure by Deuterium Uptake.* J Am Soc Mass Spectrom, 2016. **27**(3): p. 462–73.
8. Attygalle, A.B., et al., *An unexpected ion-molecule adduct in negative-ion collision-induced decomposition ion-trap mass spectra of halogenated benzoic acids.* Rapid Commun Mass Spectrom, 2006. **20**(15): p. 2265–70.
9. Liu, D., T. Wyttenbach, and M.T. Bowers, *Hydration of mononucleotides.* J Am Chem Soc, 2006. **128**(47): p. 15155–63.
10. Robinson, J.M., et al., *Hydrogen/deuterium exchange of nucleotides in the gas phase.* Anal Chem, 1998. **70**(17): p. 3566–71.
11. Chipuk, J.E. and J.S. Brodbelt, *Gas-phase hydrogen/deuterium exchange of 5'- and 3'-mononucleotides in a quadrupole ion trap: exploring the role of conformation and system energy.* J Am Soc Mass Spectrom, 2007. **18**(4): p. 724–36.
12. Chipuk, J.E. and J.S. Brodbelt, *Investigation of the gas-phase hydrogen/deuterium exchange behavior of aromatic dicarboxylic acids in a quadrupole ion trap.* International Journal of Mass Spectrometry, 2007. **267**(1): p. 98–108.
13. Crestoni, M.E. and S. Fornarini, *Gas-phase hydrogen/deuterium exchange of adenine nucleotides.* J Mass Spectrom, 2003. **38**(8): p. 854–61.
14. DePuy, C.H., et al., *Hydrogen-deuterium exchange reactions of carbanions with deuterated alcohols in the gas phase.* Journal of the American Chemical Society, 1978. **100**(9): p. 2921–2922.
15. Grabowski, J.J., C.H. DePuy, and V.M. Bierbaum, *Gas-phase hydrogen-deuterium exchange reactions of anions: kinetics and detailed mechanism.* Journal of the American Chemical Society, 1985. **107**(25): p. 7384–7389.

16. Grabowski, J.J., C.H. DePuy, and V.M. Bierbaum, *Gas-phase hydrogen-deuterium exchange reactions of hydroxide and hydroxide-d ions with weakly acidic neutrals*. Journal of the American Chemical Society, 1983. **105**(9): p. 2565–2571.
17. Kato, S., et al., *Gas phase hydrogen/deuterium exchange reactions of fluorophenyl anions*. Journal of the American Society for Mass Spectrometry, 1999. **10**(9): p. 840–847.
18. Mo, J. and K. Hakansson, *Oligonucleotide gas-phase hydrogen/deuterium exchange with D2S in the collision cell of a quadrupole-Fourier transform ion cyclotron resonance mass spectrometer.* Anal Chem, 2007. **79**(20): p. 7893–8.
19. Mo, J., G.C. Todd, and K. Håkansson, *Characterization of nucleic acid higher order structure by gas-phase H/D exchange in a quadrupole-FT-ICR mass spectrometer.* Biopolymers, 2009. **91**(4): p. 256–264.
20. Squires, R.R., C.H. DePuy, and V.M. Bierbaum, *Gas phase hydrogen-deuterium exchange reactions in carbanions: exchange of vinyl and aryl protons by water-d2*. Journal of the American Chemical Society, 1981. **103**(14): p. 4256–4258.
21. Stewart, J.H., et al., *Hydrogen-deuterium exchange reactions of carbanions with water-d2 in the gas phase*. Journal of the American Chemical Society, 1977. **99**(23): p. 7650–7653.
22. Alonge, K.M., R. Harkewicz, and M. Guttman, *Rapid Differentiation of Chondroitin Sulfate Isomers by Gas-phase Hydrogen-deuterium Exchange.* Curr Mol Med, 2020. **20**(10): p. 821–827.
23. Mookherjee, A., et al., *Linkage Memory in Underivatized Protonated Carbohydrates*. J Am Soc Mass Spectrom, 2021. **32**(2): p. 581–589.
24. Beeston, H.S., et al., *Changes in protein structure monitored by use of gas-phase hydrogen/deuterium exchange.* Proteomics, 2015. **15**(16): p. 2842–50.
25. Asbury, G.R. and H.H. Hill, Jr., *Using different drift gases to change separation factors (alpha) in ion mobility spectrometry.* Anal Chem, 2000. **72**(3): p. 580–4.
26. Matz, L.M., et al., *Investigation of drift gas selectivity in high resolution ion mobility spectrometry with mass spectrometry detection*. J Am Soc Mass Spectrom, 2002. **13**(4): p. 300–7.
27. Jurneczko, E., et al., *Effects of drift gas on collision cross sections of a protein standard in linear drift tube and traveling wave ion mobility mass spectrometry.* Anal Chem, 2012. **84**(20): p. 8524–31.
28. Guttman, M., et al., *Analysis of overlapped and noisy hydrogen/deuterium exchange mass spectra*. J Am Soc Mass Spectrom, 2013. **24**(12): p. 1906–12.

Chapter 3: Development and Evaluation of Reporter-Based Standardization of Negative-Mode gHDX

3.1 Introduction

Reproducibility remains a major challenge in gHDX; variables such as reagent gas delivery, pressure, temperature, reaction time, and instrument type can influence the observed kinetics or extent of deuterium incorporation. Differences between gHDX measurements may arise from changes in experimental conditions rather than structural differences between analytes, complicating comparisons between datasets and limiting the broader application of gHDX as a structural analysis technique. One strategy for addressing experimental variability is the use of internal exchange reporters. Previous work from our laboratory established exchange standards for positive-ion gHDX[1]. By providing a measurable response to changes in the exchange environment, these standards enabled correction of the differences between experimental conditions and improved the comparability of gHDX measurements. The development of negative-mode exchange reporters in Chapter 2 provided an opportunity to extend this strategy to negative-ion gHDX. However, establishing reporter compounds alone does not demonstrate that they can successfully standardize gHDX measurements. This chapter evaluates negative-mode exchange reporters as tools for improving the reproducibility and comparability of gHDX measurements. Experiments were designed to establish whether negative-mode exchange reporters can account for experimental variability within a platform and to assess the extent to which reporter-based standardization can be applied across instruments.

3.2 Results & Discussion

3.2.1 Differentiation of Chondroitin Sulfate Disaccharide Isomers by Negative-Mode gHDX

Chondroitin sulfate (CS) belongs to the broader family of glycosaminoglycans (GAGs), which includes chondroitin sulfate, dermatan sulfate, heparan sulfate, keratan sulfate, and hyaluronan. CS-GAGs are linear, negatively charged polysaccharides that participate in a wide range of biological processes, including cellular signaling, development, and aging, making structural characterization of CSs important for understanding their biological function [2]. The polysaccharide backbone of CS-GAGs is made up of repeating disaccharide units that contain different numbers and positions of sulfate substituents, resulting in positional isomers that possess identical elemental composition and molecular masses but differ in sulfate location on the disaccharide. For example, the monosulfated CS-A and CS-C isomers differ in sulfate location but have the same mass of approximately 458 m/z in mass spectrometry analysis, preventing differentiation by precursor mass alone [2]. Previous work from our lab, in collaboration with the Alonge lab, established the initial basis for applying gHDX to this analytical challenge. Alonge et al. investigated the monosulfated CS-A and CS-C positional isomers and demonstrated the difficulty of differentiating these species using ion mobility. The results showed similar arrival-time distributions (ATD) for the deprotonated isomers, with limited separation even with different drift gases[2]. However, when the isomers were investigated using gHDX and ND_3 as the reagent gas, CS-A and CS-C showed different gHDX kinetics. Despite having identical masses and being poorly differentiated by IMS, the two positional isomers could be distinguished by their deuterium uptake profiles. Building on the work of Alonge et al., the present study expanded the analysis to include

gHDX on five chondroitin sulfate disaccharides: CS-O, CS-A, CS-C, CS-D, and CS-E (Figure 3.1A). The expanded panel included the unsulfated (CS-O), two monosulfated isomers (CS-A and CS-C), and two disulfated isomers (CS-D and CS-E). This allowed negative-mode gHDX to be evaluated across differences in both the number and position of sulfate substituents. Despite their closely related structures, the five CS isomers showed distinct deuterium uptake behavior on both the LTQ (Figure 3.1B) and Synapt G2-Si (Figure 3.1C). Isomeric structures possessing identical masses remained distinguishable by their exchange behavior. The differentiation of CS-A and CS-C supported the observations reported by Alonge et al. At the same time, inclusion of CS-O, CS-D, and CS-E extends the application to a broader range of CS sulfation patterns. These results reveal that negative-mode gHDX can provide structural information for biologically relevant negatively charged biomolecules, revealing subtle structural differences that may not be distinguishable by conventional MS or IMS approaches alone. Although all of the isomers had distinguishable gHDX kinetics, CSA was selected as the representative analyte for the subsequent standardization studies primarily because sufficient sample was available to support the large number of experiments required during the standardization studies.

3.2.2 Exchange Reporter-Based Standardization Corrects ND_3 Variability on the Synapt G2-Si.

A current limitation of gHDX is reproducibility, which can be attributed to differences in laboratory temperature, instrumental conditions, and instrument platform [1]. Variability in the exchange environment can directly affect observed kinetics and the extent of deuterium incorporation, complicating comparisons of interday datasets. With suitable negative-mode

exchange reporters identified, we wanted to demonstrate their utility in data standardization. By monitoring reporter responses alongside a representative analyte, we selected the ND_3 flow rate as a controllable parameter to introduce variation into the datasets on the Waters Synapt G2-Si.

We selected chondroitin sulfate isomer A (CSA) as the analyte and co-infused it with the exchange reporters 5-sulfosalicylic acid and benzene-1,3-disulfonic acid. We varied ND_3 flow and used six flow rates (0.25, 0.50, 0.75, 1.0, 1.25, and 1.50 mL/min), with 1.0 mL/min as the reference condition. To determine how changes in ND_3 affect gHDX measurements, we evaluated both the kinetics and extent of deuterium incorporation of the exchange reporters. As ND_3 flow increased, uptake curves for both exchange reporters (Figure 3.2A-B) shifted left toward shorter reaction times, thereby increasing the exchange rate. For each ND_3 flow rate, we quantified exchange kinetics by fitting the data to a single-exponential uptake model to extract the exchange rate constants (k) and plateau deuterium uptake values (Figure3.2C-D). Dashed lines connecting the values across ND_3 flow settings are included only as visual guides and do not represent fitted trends or quantitative relationships. Although both reporters showed increased exchange rate constants with increasing ND_3 flow rates, as indicated by the upward progression of the dashed lines, benzene-1,3-disulfonic acid showed a large increase across the ND_3 flow rate range (Figure 3.2C). Recognizing that benzene-1,3-disulfonic acid exchanges rapidly, only a limited portion of the uptake curve was available for kinetic fitting at each ND_3 flow rate, reducing confidence in the extracted rate constants. Whereas 5-sulfosalicylic acid provided a measurable increase in exchange rate constants across the range of ND_3 flow rates (Figure 3.2A and C); therefore, it was selected as the exchange reporter for subsequent standardization. To determine whether changes in ND_3 flow altered the extent of the exchange, plateau deuterium incorporation was evaluated. In

Figure 3.2D, the constant plateau values observed across the flow-rate range for both exchange reporters, as indicated by a flat dashed line, illustrated that changes in the ND_3 flow rate did not change the extent of deuterium incorporation.

The results provided the basis for developing a reporter-based standardization strategy by correcting the exchange timescale. We performed the correction using exchange rate constants (k) determined for 5-sulfosalicylic acid. The scaling factor (R) was calculated as the ratio of the exchange rate at the flow rate to that of the reference flow rate of 1.0 mL/min ND_3, as shown in Figure 3.3A. We then applied the scaling factor to the experimental timescale for each time point acquired at a given flow rate, yielding a "corrected exchange time" for each data set. Section 3.3.5 describes the reporter-based standardization procedure, including the equations used to calculate the scaling factors. Before correction, 5-sulfosalicylic acid exhibited distinct flow-dependent shifts in its uptake curves, with increasing ND_3 flow producing faster exchange kinetics (Figure 3.3B). Applying the reporter-based scaling factors markedly improved the overlap of uptake profiles across datasets of 5-sulfosalicylic acid acquired under different ND_3 flow conditions (Figure 3.3C). We applied the scaling factors calculated from 5-sulfosalicylic acid directly to the CSA datasets collected under the same ND_3 flow conditions. Before correction, CSA exhibited a similar trend to exchange reporters, with a leftward shift in exchange kinetics as ND_3 flow increased (Figure 3.4A). Following correction, the six CSA uptake profiles collapsed into a single unified kinetic curve (Figure 3.4B). These results provide evidence that exchange reporters can account for variability and improve the reproducibility and comparability of gHDX measurements on the Waters Synapt G2-Si.

3.2.3 The LTQ Exhibits a Distinct Response to Changes in ND_3 Flow

A challenge in gHDX is the lack of a cross-platform approach to standardizing measurements across different mass spectrometry instruments. Differences in exchange environments can influence measured deuterium incorporation, making direct comparison of gHDX data between instruments difficult. Establishing a reporter-based standardization approach that accounts for platform-dependent differences in the exchange environment would represent an important step toward improving reproducibility and the broader application of gHDX. Access to two instruments allowed us to evaluate whether reporter-based standardization could be applied across platforms. Having demonstrated the success of standardized gHDX measurements acquired on the Waters Synapt G2-Si, we next explored whether the same strategy could be implemented for measurements acquired on the Thermo LTQ.

We repeated the experimental workflow established on the Waters Synapt G2-Si using chondroitin sulfate A (CSA) as the analyte and 5-sulfosalicylic acid, benzene-1,3-disulfonic acid, and phytic acid as the exchange reporters. As in the Synapt G2-Si study, ND_3 was systematically increased to assess the effect of reagent gas flow on gHDX exchange behavior. However, unlike the Waters Synapt G2-Si, which regulates ND_3 delivery via a mass flow controller with a numerical flow readout, the Thermo LTQ reagent gas introduction is controlled by a needle valve without a direct numerical flow readout. The needle valve was opened until a stable ND_3 flow was established, thereby defining the low-flow setting. The valve was then opened through four successive full rotations to generate a total of five relative ND_3 flow settings (i.e., low, low-medium,

medium, medium-high, and highest). At each flow-rate setting, the instrument ion gauge was monitored to verify that the pressure had stabilized before data acquisition.

On the Thermo LTQ, increasing ND_3 flow resulted in increased deuterium incorporation for both the exchange reporters and the analyte CSA, and the exchange rate of the deuterium uptake curves remained largely unchanged (Figure 3.5A-D). Because this was observed across all compounds, it indicated to us that the response reflected the exchange environment of the LTQ and was not unique to a single compound. This response contrasted with what was observed on the Waters Synapt G2-Si, where increasing ND_3 flow increased the exchange rate rather than deuterium incorporation, making the LTQ response unexpected. The deuterium uptake curves were fitted to a single exponential function to extract exchange rate constants (k) and plateau deuterium uptake values (Figure 3.6). Dashed lines connecting the values across ND_3 flow settings are included only as visual guides and do not represent fitted trends or quantitative relationships. Exchange rate constants remained relatively constant across all five ND_3 flow settings (Figure 3.6A), indicating that increasing ND_3 flow did not accelerate the rate of exchange. Among the exchange reporters, 5-sulfosalicylic acid exhibited the least change in the exchange rate constants across the tested flow range, as indicated by a flat dashed line. Although the exchange rate constants for benzene-1,3-disulfonic acid and phytic acid showed a downward progression along the dashed guidelines, isolated measurements at the low ND_3 flow for benzene-1,3-disulfonic acid and at the highest ND_3 flow for phytic acid explain this. Excluding those isolated measurements, the exchange rate constants remained relatively constant across the four remaining ND_3 flow rates. Evaluating plateau deuterium uptake, increasing ND_3 flow resulted in increased deuterium incorporation for all three exchange reporters and can be seen visually by the

dashed line for each one in Figure3.6B. Phytic acid exhibited the greatest increase in deuterium uptake across the tested flow range, while 5-sulfosalicylic acid and benzene-1,3-disulfonic acid, although minimal in comparison, exhibited increases in their plateau values. The analyte CSA responded similarly to the exchange reporters: increasing ND_3 flow increased deuterium uptake while leaving the exchange rate largely unchanged (Figure 3.5D).

Across both Waters Synapt G2-Si and Thermo LTQ, the response to increasing ND_3 flow setting differed substantially, as shown by a direct comparison of the exchange behavior of 5-sulfosalicylic acid on the two platforms (Figure 3.7). On the Waters Synapt G2-Si, increasing ND_3 accelerated the exchange, producing a leftward shift in the deuterium uptake curves, while the plateau deuterium uptake remained unchanged (Figure 3.7A, C-D). This enabled us to acquire exchange rate constants and apply reporter-derived scaling factors to standardize datasets collected under different experimental conditions. In contrast, on the Thermo LTQ, increasing ND_3 flow increased plateau deuterium uptake while the exchange remained largely unchanged across the tested flow settings (Figure 3.7B-D). Because the exchange rate constants remained unchanged and the reporter-derived scaling factors rely on changes in the exchange rate, the absence of measurable differences in the kinetic response prevented calculation of equivalent correction factors for the Thermo LTQ, thereby preventing standardization of datasets collected under different experimental conditions. The distinct behavior observed on the Thermo LTQ indicated that an additional factor contributes to the LTQ exchange environment. These findings suggest that successful cross-platform standardization will require identifying the additional factor governing exchange on the Thermo LTQ. Identifying this factor formed the basis of the following hypothesis and the subsequent investigations presented in Chapter 4.

3.2.4 Trace Water is Hypothesized to Contribute to the LTQ Exchange Environment

The reporter-based standardization strategy developed for the Synapt G2-Si could not be applied to the Thermo LTQ because it produced a fundamentally different response to increases in ND_3 flow. Rather than accelerating the exchange kinetics, increasing ND_3 flow shifted the deuterium incorporation plateau to higher values. This unexpected behavior suggested that the LTQ environment differs from that of the Synapt G2-Si and indicated that an additional factor contributes to the effective pool of exchangeable hydrogen/deuterium species, and that ND_3 alone is not the sole participant in the LTQ reaction exchange environment. ***We hypothesize that trace water or water vapor within the instrument is the unaccounted-for factor involved in the exchange environment, thereby altering the effective pool of exchangeable hydrogen/deuterium species.*** In this scenario, the total pool of exchangeable hydrogen/deuterium species consists of both ND_3 and trace water; increasing ND_3 flow would increase the relative abundance of deuterium available for exchange, resulting in greater overall deuterium incorporation while leaving the measured exchange kinetics largely unchanged.

Previous studies have demonstrated that the composition of the gas-phase reaction environment can influence ion chemistry, establishing a basis for considering trace water as an additional component of the LTQ exchange environment. Xia and Attygalle provided direct evidence that water influences post-ionization ion chemistry. In their study of protonated benzocaine, water vapor altered the protomer distribution after the ions entered the gas phase[3]. Attygalle et al. provided additional evidence that trace water within a mass spectrometer can

participate directly in ion chemistry. During CID experiments on halogenated benzoic acid anions, unexpected water-adducted ions were observed. The authors initially considered whether the water originated from the precursor or electrospray source. Isotopic-labeling experiments instead concluded that water involved in adduct formation originated from trace water introduced by the helium line of the damping and collision gas. The ability of background water within ion traps to participate in post-ionization ion–molecule reactions has also been demonstrated across several carbohydrate studies. Campbell, Chen, and Glish showed that lithiated hexoses and pentoses react with water while held within quadrupole ion traps, with the kinetics and extent of water adduction providing structural discrimination among isomers[4, 5]. This approach was subsequently extended to disaccharide product ions, where water-adduction behavior differentiated linkage position and anomeric configuration[6].

These studies establish that trace water, particularly in ion-trapping environments, can participate in post-ionization ion–molecule chemistry and measurably alter the observed ion population. The findings support our hypothesis that trace water or water vapor contributes to the LTQ exchange environment, and provide a plausible explanation for why the reporter-based standardization strategy developed on the Synapt G2-Si cannot be applied to the LTQ. This finding shifts the focus to whether the post-ionization environment itself alters the measured deuterium content. Building upon this hypothesis, Chapter 4 therefore investigates the underlying source(s) of trace water entry, evaluates its impact on HDX measurements, and ultimately considers mitigation strategies.

3.3 Materials & Methods

3.3.1 Materials

Deuterated Ammonia (ND_3) (99%) was purchased from Cambridge Isotope Laboratories (Tewksbury, MA, USA). Sodium benzene-1,3-disulfonate, 5-sulfosalicylic acid dihydrate, and phytic acid were purchased from Sigma-Aldrich (St. Louis, MO, USA). Chondroitin sulfate-derived disaccharide isomers were purchased from Biosynth-Carbosynth (Oakbrook Terrace, IL, USA). Methanol, formic acid, and Optima LC/MS-grade water were purchased from Fisher Scientific (Somerville, New Jersey)

3.3.2 Sample Preparation

Individual compounds used were prepared as stock solutions in Optima LC/MS-grade water and subsequently diluted in 50% Methanol and 0.1% formic acid to a working concentration of 1-10 μM.

Chondroitin Sulfate disaccharide isomers were separately resuspended in HPLC-grade Optima water and diluted to a working concentration of 5-10 μM in aqueous 0.1% formic acid.

On the Synapt, CSA was co-infused with 5-sulfosalicylic acid and benzene-1,3-disulfonic acid. On the LTQ, CSA was co-infused with a mixture of 5-sulfosalicylic acid, benzene-1,3-disulfonic acid, and phytic acid.

3.3.3 Mass Spectrometry

All experiments were conducted on a Waters Synapt G2-Si (Waters Corp., Milford, MA, USA) or a Thermo Fisher Scientific LTQ (San Jose, CA, USA) in negative-ion mode. Each is equipped with external instrument modifications to enable ND_3 infusion. Steel gas lines, valves, and unions were

purchased from Swagelok (Solon, OH, USA) with corrosion-resistant components and seals made of either polytetrafluoroethylene (PTFE) or nylon.

3.3.4 Gas-Phase Hydrogen Deuterium Exchange

All lines are thoroughly flushed with He or Ar before and after use. All compounds were infused directly into the mass spectrometer via a nano-ESI needle or a fused silica capillary using a syringe pump (Harvard Apparatus, Holliston, MA, USA) at flow rates of 5 or 10 µL/min.

Waters Synapt G2-Si

The Synapt G2-Si infusion of deuterated ammonia (ND_3) is achieved using mixtures of Argon (Ar) and ND_3, with two mass flow controllers (Aalborg, Orangeburg, NY) mixing the gases just before the gas inlet to the transfer cell TWIG[7]. The described external modifications did not result in a loss of sensitivity or changes in pressure at the instrument's various vacuum stages.

Operated with a capillary voltage of 2 kV, Source Temp 70 °C, sampling cone 20 V, and source offset 20 V. Acquisition mass range 50- 600 *m/z*, Scan time per collection 2 sec. The trap and transfer collision energies were set to 4 V. A transfer TWIG wave height of 6 V and argon collision gas were selected for subsequent Synapt G2-Si gHDX measurements. For deuterated labeling, the T-wave velocity of the transfer TWIG was ramped from 8 to 1300 m/s to achieve labeling times of 0.1 to 12 ms.

Thermo LTQ

The Thermo LTQ was outfitted with a custom needle valve to control the amount of deuterated ammonia (ND_3) mixed with the Helium collision gas infused into the ion trap. The described

external modifications did not result in a loss of sensitivity or changes in pressure at the instrument's various vacuum stages.

Each analyte was isolated and held for a set period to allow exchange with ND_3. The peak m/z was isolated with an isolation width of at least 10 Th (centered within the isotopic distribution) to cover the full exchange window in the spectra. We sampled a wide range of exchange times (16), from 0.001 to 32.768 s. The exchange times were defined within the instrument method as extended collision-induced dissociation (CID) experiments with zero collision energy, allowing ions to be held in the linear ion trap for controlled reaction times without fragmentation. Mass spectra were acquired in enhanced scan mode for resolution setting. The Ion Source parameters were set as follows: NanoESI capillary Temp 210°, source voltage 2.30 kV, Source Current 100 uA, Capillary Voltage -9.00 V, Tube Lens -65.0 V, Lens 1 Voltage 39.00 V, Front Lens 14.0 V.

Chondroitin Sulfate Isomer

Five chondroitin sulfate disaccharide isomers (CS-O, CS-A, CS-C, CS-D, and CS-E) were analyzed by negative-mode gHDX on both the Thermo LTQ and Waters Synapt G2-Si using the instrument-specific exchange conditions described above. We generated deuterium uptake profiles across the accessible experimental exchange times on each platform to compare isomer-specific exchange behavior.

Standardization Experiments

We evaluated the robustness of internal exchange reporters by varying the ND3 flow rate to assess its effects on the deuterium exchange rate and the standardization approach. Chondroitin Sulfate Isomer A (CSA), along with our internal exchange reporters' kinetic exchanges, was collected at six

ND_3 flow rates: 0.25, 0.50, 0.75, 1.00, 1.25, and 1.50 mL/min on a Waters Synapt G2-Si, and 1.0 mL/min was the reference condition. The needle valve was opened until a stable ND_3 flow was established. The valve was then opened through four successive full rotations to generate five relative ND_3 flow settings (i.e., low, low-medium, medium, medium-high, highest. Following each adjustment of the ND_3 needle valve, instrument pressure was monitored and allowed to stabilize before data acquisition. Unless otherwise stated, experiments were performed in triplicate (n = 3).

3.3.5 Data Analysis

Spectra for each time point were manually extracted from MassLynx and Thermo Xcalibur Qual Browsers. Compound spectra were processed and analyzed using HX-Express[8]. The experimental error of measured deuterium values was estimated from the standard deviation of triplicate measurements (n=3) unless stated otherwise. For each flow rate, we fitted the exchange behavior to a skewed exponential function. The slope of the best-fit curve is the exchange rate constant for that condition. A scaling factor was calculated as the ratio of the exchange rate at a given flow rate to that obtained at the reference flow rate. This scaling factor was then applied to the experimental time axis. Each time point acquired at a given flow rate was multiplied by its corresponding scaling factor, resulting in a shifted (corrected) time axis.

Using a reference condition, the scaling factor is defined as:

$$R = \frac{k_{ref}}{k_{ref,0}}$$

The corrected exchange time is then:

$$t_{corr=t \cdot R}$$

Let:

- t = experimental exchange time
- t_{corr} = corrected exchange time
- R = scaling factor derived from the internal exchange reporter
- k_{ref} = observed exchange rate of the internal exchange reporter
- $k_{ref,0}$ = exchange rate at the reference condition

3.4 Chapter Summary

This chapter evaluated the application of negative-mode exchange reporters for improving the reproducibility and comparability of gHDX measurements. Chondroitin sulfate disaccharides were first examined as biologically relevant molecules, demonstrating distinct deuterium uptake behavior among five isomers on both the Waters Synapt G2-Si and Thermo LTQ. CSA was subsequently selected as the representative analyte for standardization studies. On the Synapt G2-Si, increasing ND_3 flow accelerated exchange kinetics without changing plateau deuterium incorporation. Reporter-derived scaling factors were therefore used to correct the experimental exchange timescale, improving the agreement of both reporter and CSA uptake profiles collected under different ND_3 flow conditions. In contrast, increasing ND_3 flow on the LTQ increased plateau deuterium incorporation while exchange kinetics remained unchanged. Because the standardization approach relies on changes in reporter exchange kinetics, an equivalent correction could not be applied to the LTQ. The distinct response observed on the LTQ led to the

hypothesis that trace water or water vapor contributes to its exchange environment, providing the basis for the investigations presented in Chapter 4.

3.5 Acknowledgements

Research reported in this publication was supported by the National Institute of General Medical Sciences (NIGMS) of the National Institutes of Health (NIH) under Award Number T32GM008268. National Institutes of Health grants funded this work: R01GM127579 (M.G.) and the National Science Foundation Award: 2304707 (M.G.).

3.6 Chapter Figures

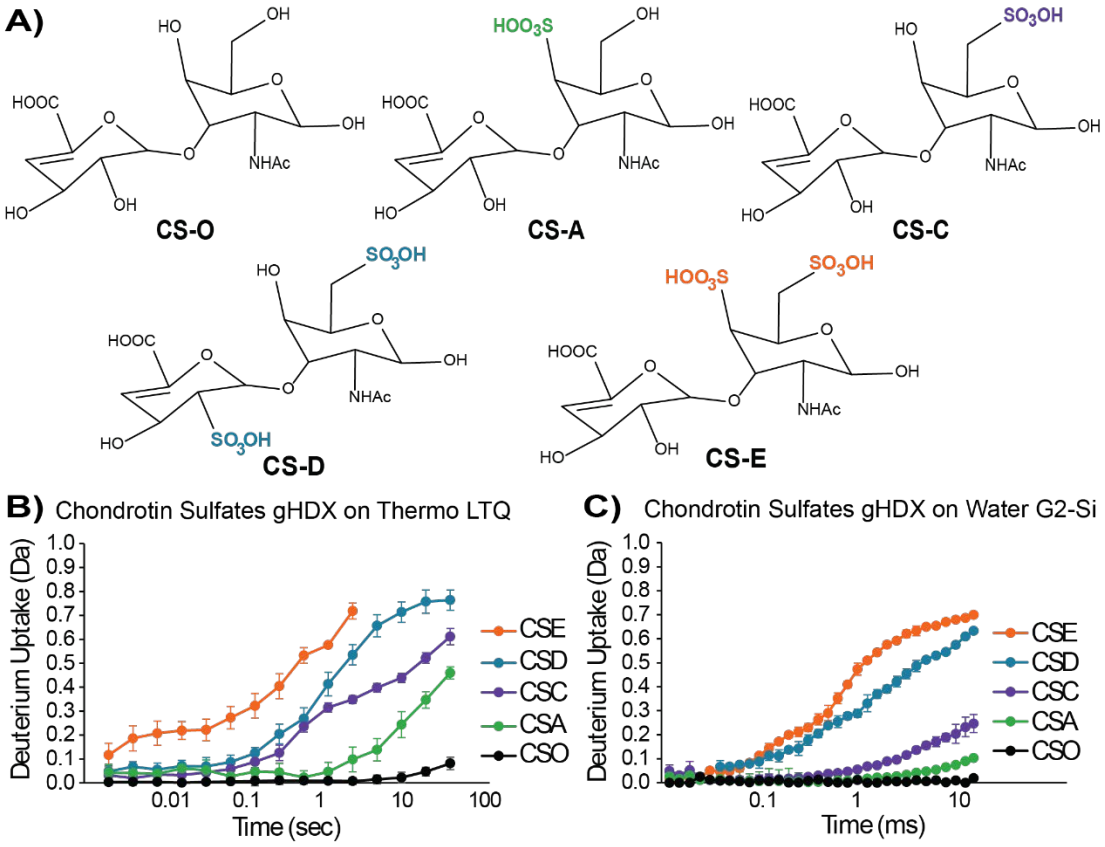

Figure 3.1: Negative-mode gHDX differentiates chondroitin sulfate disaccharide isomers across two instruments. A) Chemical structures of the five chondroitin sulfate (CS) disaccharide isomers, including the unsulfated CS-O, the monosulfated isomers CS-A and CS-C, and disulfated isomers CS-D and CS-E. Sulfation sites distinguishing the individual isomers are highlighted. Deuterium uptake profiles obtained on the B) Thermo LTQ and C) Waters Synapt G2-Si demonstrate distinct exchange behavior among the CS isomers.

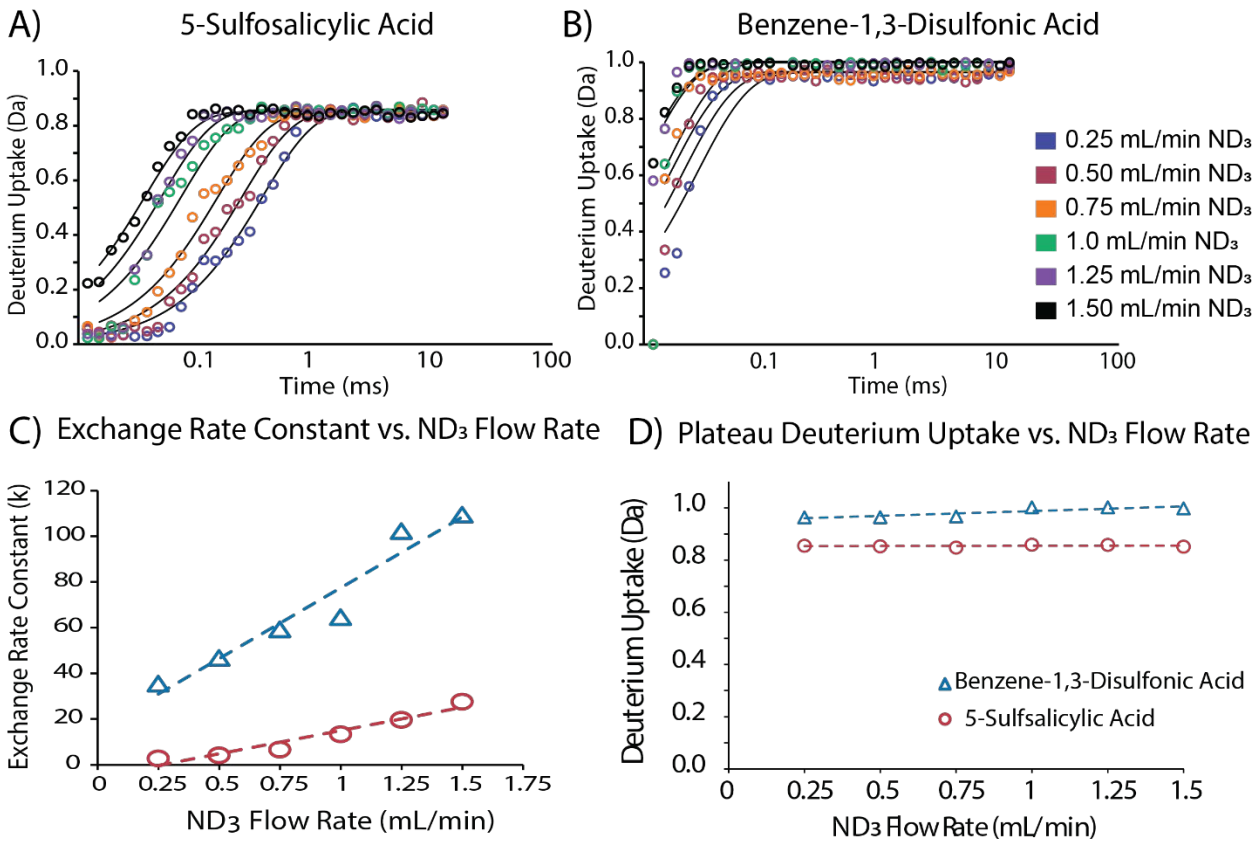

Figure 3.2: Effect of ND_3 flow on exchange reporter kinetics on the Waters Synapt G2-Si. gHDX measurements were acquired for exchange reporters 5-sulfosalicylic acid and benzene-1,3-disulfonic acid across six ND3 flow rates: 0.25 (blue), 0.50 (red), 0.75 (orange), 1.0 (green), 1.25 (purple), and 1.50 (black) mL/min. A) Deuterium uptake profiles of 5-sulfosalicylic acid shift toward shorter exchange times as ND_3 flow increases, while plateau deuterium incorporation remains constant. B) Benzene-1,3-disulfonic acid exhibits the same trend, shifting toward shorter exchange times with increasing ND_3 flow. C) Exchange rate constants derived from kinetic fitting are plotted as a function of ND_3 flow, producing a progressive increase in measured exchange rate constants. D) Plateau deuterium uptake remains relatively constant across the ND_3 flow conditions for both reporters. Dashed lines are included as visual guides and do not represent fitted relationships.

A)

Derived Scaling Factors

ND_3 Flow Rate (mL/min)	Exchange Rate Constant (k)	Scaling Factor (R)
0.25	2.79	0.21
0.5	4.17	0.31
0.75	6.72	0.50
1	13.41	1.00
1.25	19.73	1.47
1.5	27.64	2.06

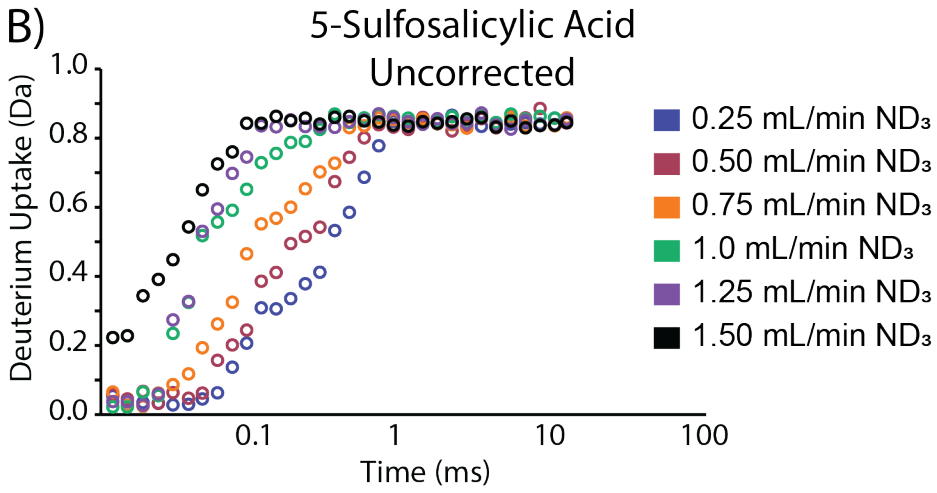

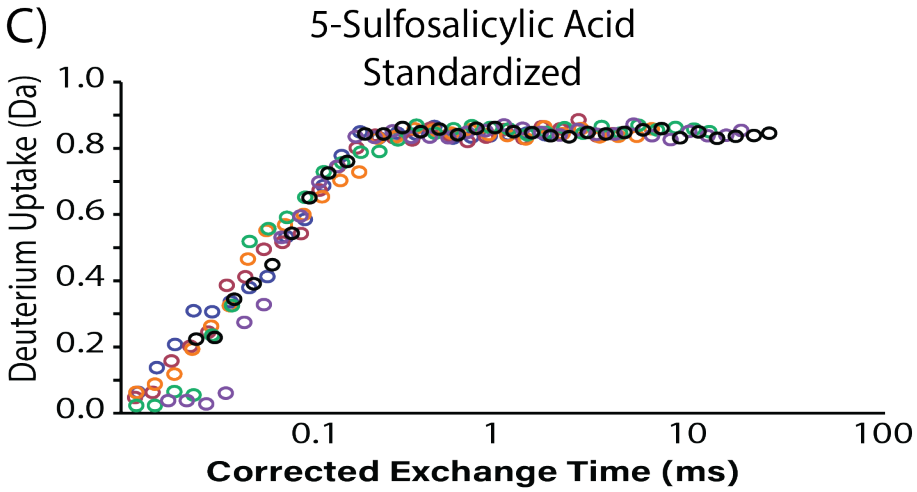

Figure 3.3: Reporter-based scaling factors correct ND_3 flow differences in gHDX measurements on the Waters Synapt G2-Si. Scaling factors were derived from exchange rate

constants of 5-sulfosalicylic acid across six ND_3 flow conditions(0.25, 0.50, 0.75, 1.00, 1.25, and 1.50 mL/min), with 1.0 mL/min designated as the reference condition. A)The table shows the measured exchange rate constant (k) and scaling factor (R) for each ND_3 flow condition. B) Uncorrected 5-sulfosalicylic acid deuterium uptake profiles exhibiting a shift in exchange kinetics, with increasing ND_3 flow. B) The report-based scaling factor for each flow condition was applied to the experimental exchange time results, resulting in convergence of uptake profiles into a common kinetic profile.

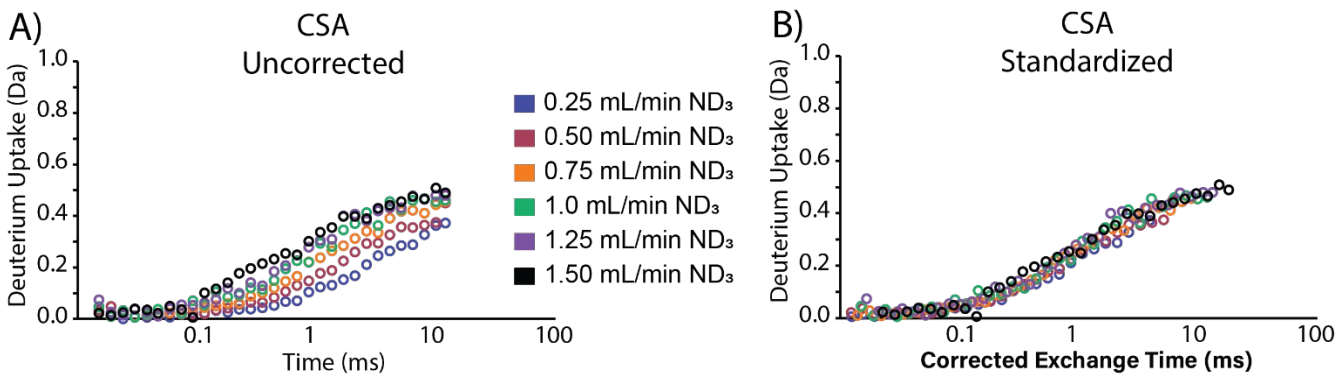

Figure 3.4: Application of reporter-based scaling factors standardizes CSA gHDX kinetics across ND_3 flow conditions on the Waters Synapt G2-Si. Chondroitin sulfate isomer A (CSA) was analyzed across six different ND3 flow conditions: 0.25, 0.50, 0.75, 1.00, 1.25, and 1.50 mL/min. A) Before correction, CSA exhibits a flow-dependent shift in deuterium uptake with increasing ND_3 flow. B) Scaling factors derived from the 5-sulfosalicylic acid exchange reporter at each ND_3 flow condition were applied to the CSA experimental times. Following correction, the CSA uptake profiles converge onto a common kinetic profile, demonstrating that exchange reporter-based standardization can account for changes in experimental conditions.

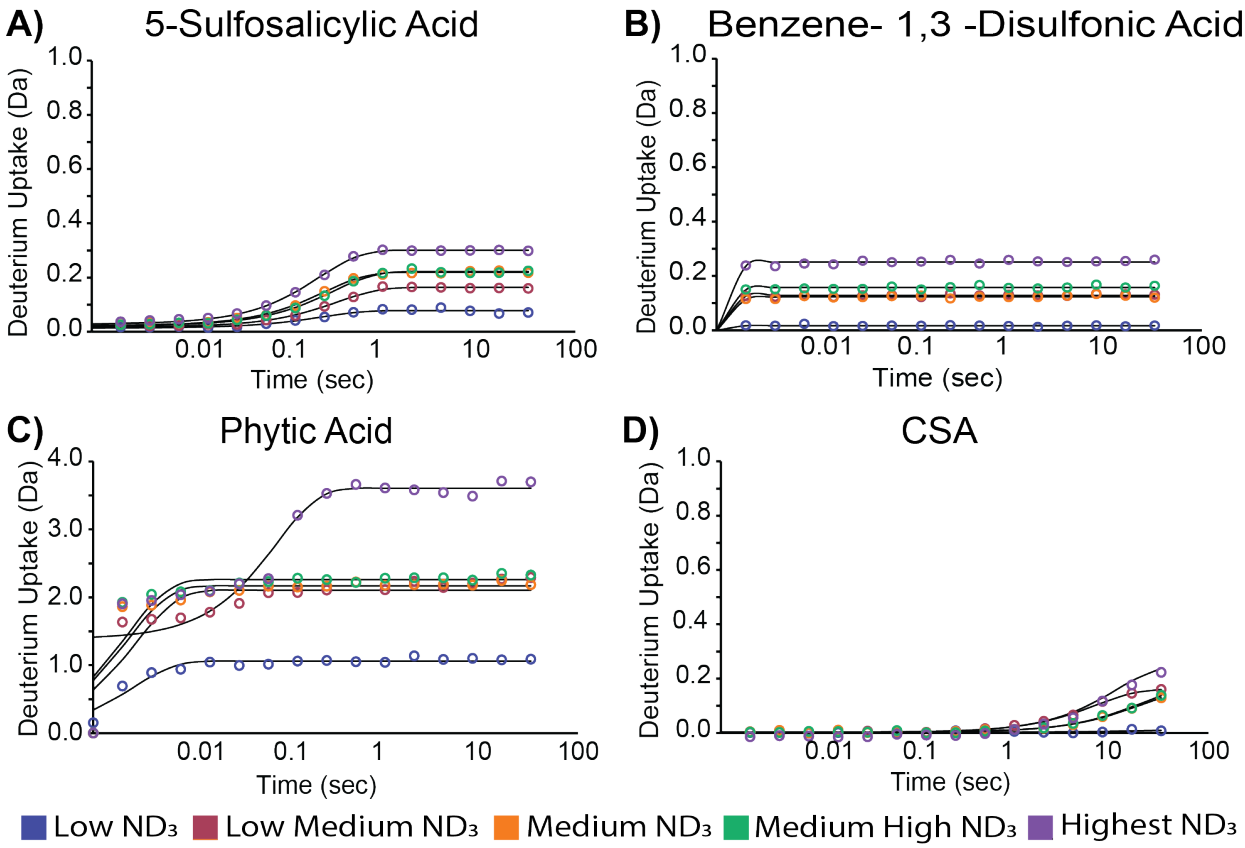

Figure 3.5: Increasing ND_3 flow increases the extent of deuterium incorporation without altering exchange kinetics on the Thermo LTQ. Deuterium uptake profiles are shown for A) 5-sulfosalicylic acid, B) benzene-1,3-disulfonic acid, C) phytic acid, and D) chondroitin sulfate isomer A (CSA), on the Thermo LTQ across five ND_3 flow conditions: low (blue), low-medium (red), medium (orange), medium-high (green), and highest (purple). Across all four compounds, increasing ND_3 flow increased deuterium incorporation, but the exchange rate remained similar, with no expected leftward shift as ND_3 flow increased.

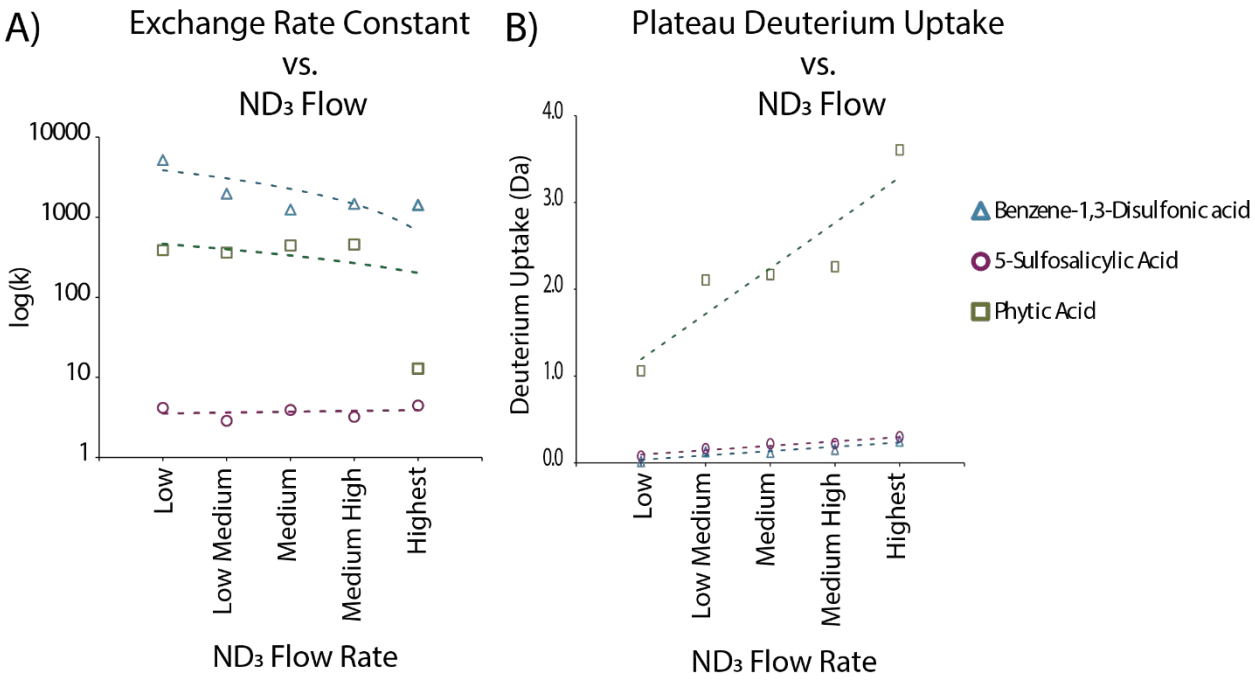

Figure 3.6: Exchange rate constants and plateau deuterium uptake responses to ND_3 flow on the Thermo LTQ. Exchange rate constants and plateau deuterium uptakes for 5-sulfosalicylic acid (purple circles), benzene-1,3-disulfonic acid (blue triangles), and phytic acid (green squares) are compared across five ND_3 flow conditions. A) Exchange rate constants did not increase as ND_3 flow increased. B) Plateau deuterium uptake increased with increasing ND_3 flow for all three reporters, with the largest observed for phytic acid. Dashed lines are included as visual guides and do not represent fitted relationships.

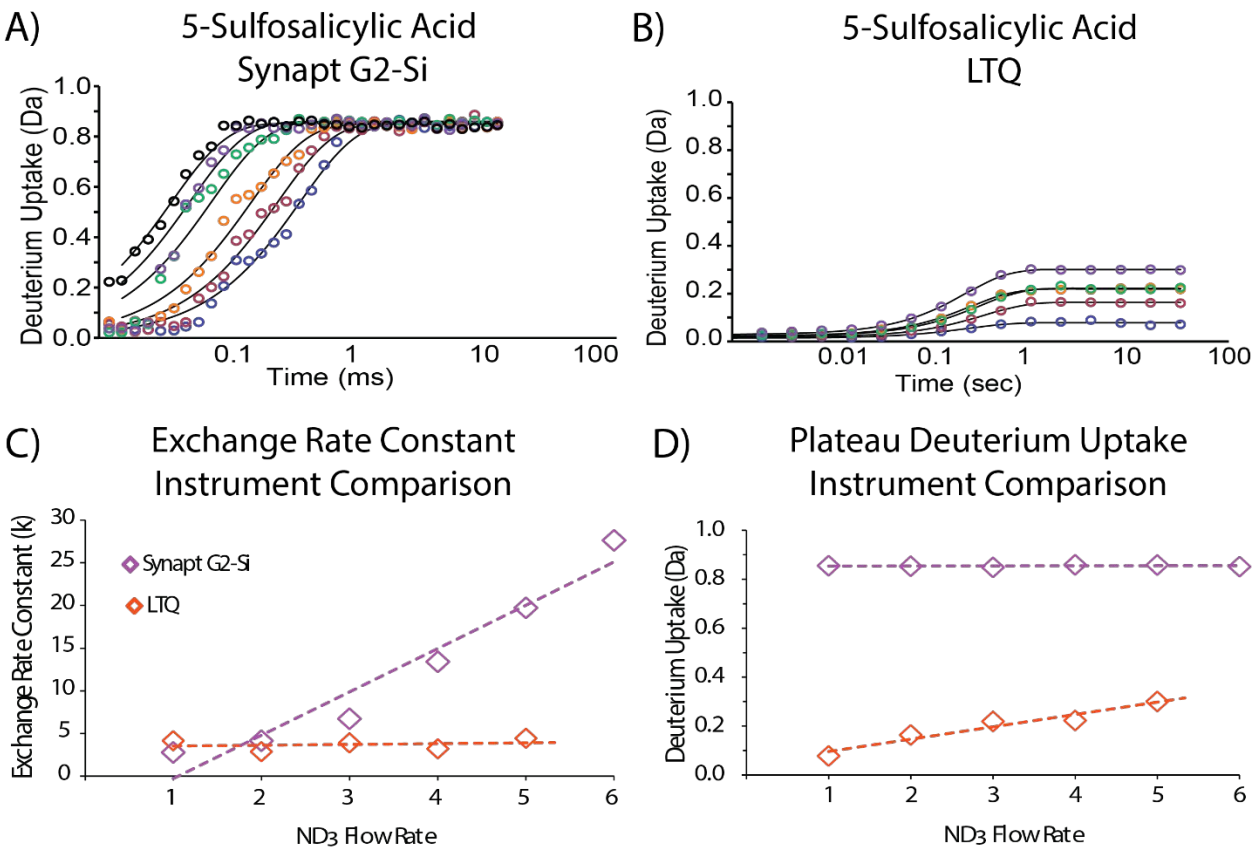

Figure 3.7:ND_3 flow produces different effects on gHDX kinetics and deuterium incorporation in the Synapt G2-Si and LTQ. The response of 5-sulfosalicylic acid to changes in ND_3 flow was compared between the Waters Synapt G2-Si and Thermo LTQ. A) On the Synapt G2-Si, increasing ND3 flow produces a shift in the deuterium uptake profiles toward shorter exchange times while maintaining a similar plateau in deuterium incorporation. B) On the LTQ, increasing ND_3 flow increases the plateau of deuterium uptake, while uptake profiles remain relatively the same along the experimental timescales. C) Comparison of exchange rate constants (k) further demonstrates the differences in ND_3 response on Synapt G2-Si (purple) and the LTQ (orange). D) Plateau deuterium differences in response to changes in ND_3 flow conditions on the Synapt G2-Si (purple) and LTQ (orange). Dashed lines are included as visual guides to illustrate the trends.

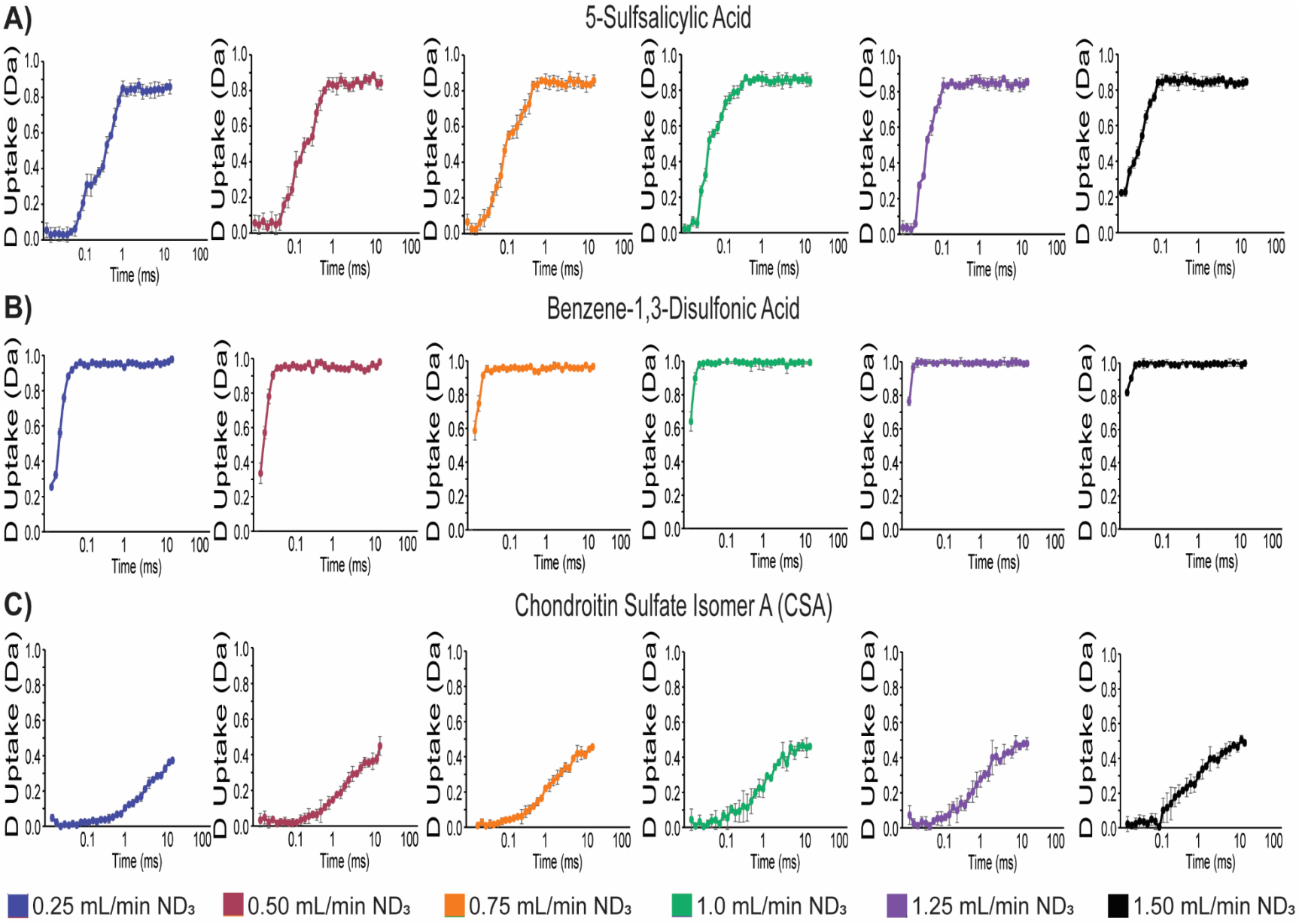
A)
5-Sulfsalicylic Acid
B)
Benzene-1,3-Disulfonic Acid
C)
Chondroitin Sulfate Isomer A (CSA)
D Uptake (Da)
Time (ms)
0.25 mL/min ND3
0.50 mL/min ND3
0.75 mL/min ND3
1.0 mL/min ND3
1.25 mL/min ND3
1.50 mL/min ND3

Supporting Figure 3.1: Deuterium uptake profiles of exchange reporters and CSA under varying ND3 flow conditions on the Waters Synapt G2-Si. gHDX measurements were acquired of a mixture containing the exchange reporters A) 5-sulfosalicylic acid, B) benzene-1,3-disulfonic acid, and C) the analyte CSA via direct infusion. Triplicate measurements were collected across six different flow rates: 0.25 (blue), 0.50 (red), 0.75 (orange), 1.0 (green), 1.25 (purple), and 1.50 (black) mL/min. Error bars represent the standard deviation of the triplicate measurements.

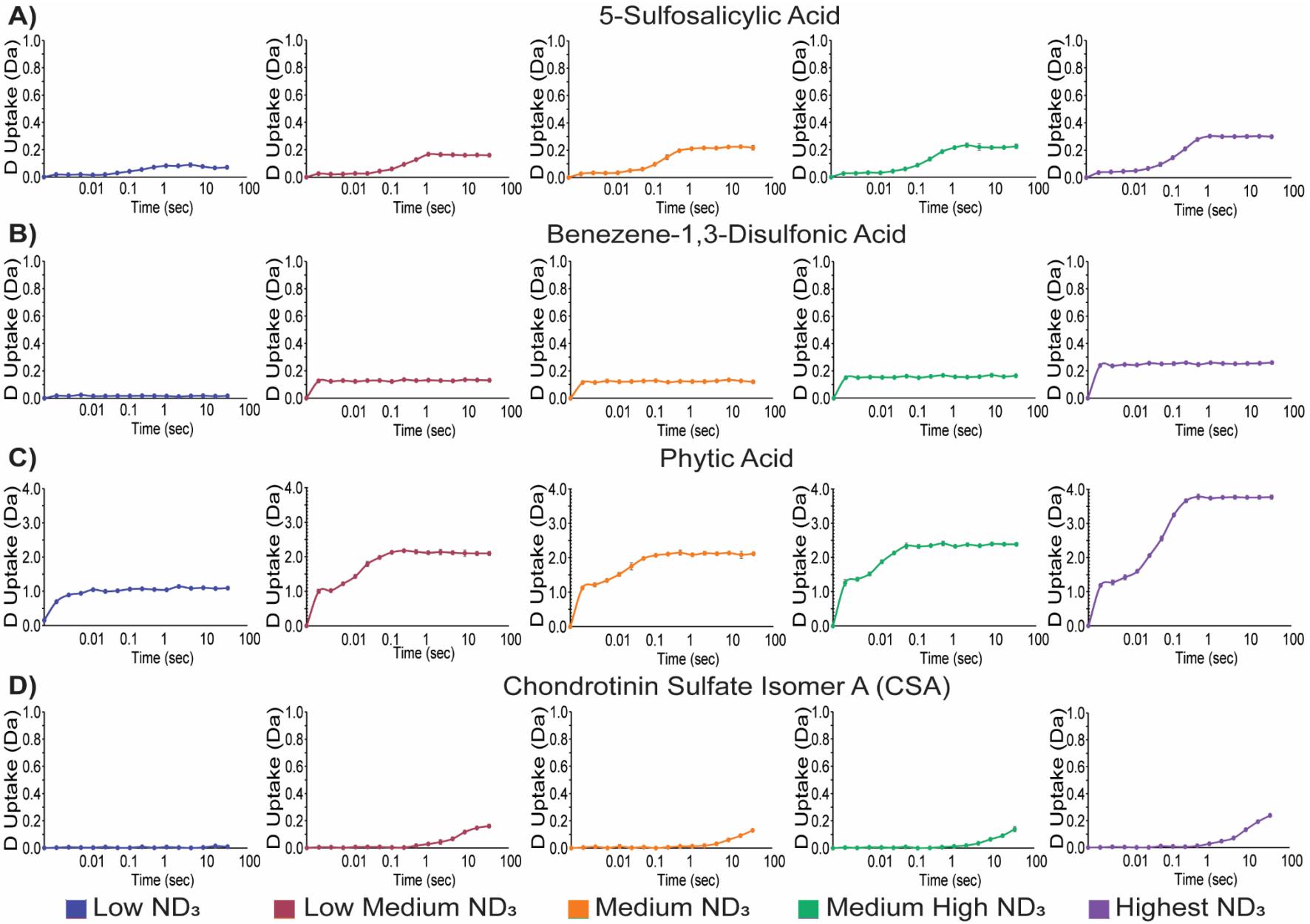
A)
5-Sulfosalicylic Acid
B)
Benezene-1,3-Disulfonic Acid
C)
Phytic Acid
D)
Chondrotinin Sulfate Isomer A (CSA)
D Uptake (Da)
Time (sec)
0.01
0.1
1
10
100
Low ND3
Low Medium ND3
Medium ND3
Medium High ND3
Highest ND3

Supporting Figure 3.2: Deuterium uptake profiles of exchange reporters and CSA under varying ND_3 flow conditions on Thermo LTQ. gHDX measurements were acquired of a mixture containing the exchange reporters A) 5-sulfosalicylic acid, B) benzene-1,3-disulfonic acid, C) phytic acid, and D) the analyte CSA via direct infusion. Triplicate measurements were collected across five ND_3 flow conditions: low (blue), low-medium (red), medium (orange), medium-high (green), and highest (purple). Error bars represent the standard deviation of the triplicate measurements.

3.7 References

1. Uppal, S.S., et al., *High-Precision, Gas-Phase Hydrogen/Deuterium-Exchange Kinetics by Mass Spectrometry Enabled by Exchange Standards.* Anal Chem, 2020. **92**(11): p. 7725–7732.
2. Alonge, K.M., R. Harkewicz, and M. Guttman, *Rapid Differentiation of Chondroitin Sulfate Isomers by Gas-phase Hydrogen-deuterium Exchange.* Curr Mol Med, 2020. **20**(10): p. 821–827.
3. Xia, H. and A.B. Attygalle, *Untrapping Kinetically Trapped Ions: The Role of Water Vapor and Ion-Source Activation Conditions on the Gas-Phase Protomer Ratio of Benzocaine Revealed by Ion-Mobility Mass Spectrometry.* J Am Soc Mass Spectrom, 2017. **28**(12): p. 2580–2587.
4. Campbell, M.T., D. Chen, and G.L. Glish, *Identifying the D-Pentoses Using Water Adduction to Lithium Cationized Molecule.* Journal of the American Society for Mass Spectrometry, 2017. **28**(7): p. 1420–1424.
5. Campbell, M.T., et al., *Distinguishing Biologically Relevant Hexoses by Water Adduction to the Lithium-Cationized Molecule.* Anal Chem, 2017. **89**(19): p. 10504–10510.
6. Campbell, M.T., D. Chen, and G.L. Glish, *Distinguishing Linkage Position and Anomeric Configuration of Glucose–Glucose Disaccharides by Water Adduction to Lithiated Molecules.* Analytical Chemistry, 2018. **90**(3): p. 2048–2054.
7. Rand, K.D., et al., *Gas-phase hydrogen/deuterium exchange in a traveling wave ion guide for the examination of protein conformations.* Anal Chem, 2009. **81**(24): p. 10019–28.
8. Guttman, M., et al., *Analysis of overlapped and noisy hydrogen/deuterium exchange mass spectra.* J Am Soc Mass Spectrom, 2013. **24**(12): p. 1906–12.

Chapter 4: Investigating Post-Ionization Back-Exchange (BEX) in Hydrogen/Deuterium Exchange

4.1 Introduction

The studies in the preceding chapters focused on advancing gHDX by developing negative-ion approaches and strategies to improve measurement reproducibility. During these investigations, however, an unexpected observation raised a broader question about deuterium labeling after ions enter the mass spectrometer. As discussed in Chapter 3, the Thermo LTQ's response to changes in ND_3 flow could not be explained by ND_3 alone and suggested that trace water or water vapor may contribute to the exchange environment. This observation prompted consideration of a process that has received little attention in HDX measurements: whether the measured deuterium content can continue to change after ionization and before detection. Regardless of whether deuterium labeling occurs in solution or in the gas phase, accurate HDX measurements ultimately depend on preservation of the isotopic label until analysis. Replacement of incorporated deuterium by hydrogen following labeling, commonly referred to as back-exchange (BEX), decreases the amount of deuterium ultimately measured and can obscure differences between populations, introduce experimental variability, and complicate quantitative interpretation.

Considerable effort within the HDX field has focused on minimizing deuterium loss. In solution-phase HDX-MS, these efforts have largely focused on the period before ionization through approaches such as rapid quenching, low-temperature sample handling, shortened chromatographic separations, and optimized sample processing with the development of HDX

robotic carts. In gHDX, experimental development has similarly emphasized control of the labeling reaction itself, including reagent type, instrument pressure, ion residence time, and instrument type. HDX measurements are generally interpreted with the expectation that, once the labeled ion population has entered the mass spectrometer, its deuterium content is preserved during analysis to represent the labeling state being measured. But what happens after ionization in these nominally “dry” vacuum systems? Residual water molecules may remain within vacuum regions and interact with ions as they travel through the instrument, continuing ion–molecule interactions that can replace incorporated deuterium with hydrogen. So the question is: are we introducing this water through sample ionization, or is it entering from alternative sources?

Mass spectrometers contain numerous sealing interfaces that separate atmospheric and vacuum regions, many of which use elastomeric O-rings. Viton, a fluoroelastomer commonly used in vacuum sealing applications, provides an effective mechanical vacuum seal but is not completely impermeable to atmospheric gases. Studies have demonstrated water-vapor permeation through Viton O-rings, and the magnitude of permeation can depend on factors including atmospheric exposure, humidity, and material properties [1-3]. This provides a physical pathway connecting the observations of Chapter 3 with the mass spectrometer's post-ionization environment. If atmospheric water vapor continuously permeates vacuum seals, hydrogen-containing molecules may be replenished within instrument regions. Ions carrying incorporated deuterium could therefore encounter trace water during transmission or storage, allowing exchange to continue after the intended labeling reaction. From this perspective, an apparently routine component of mass spectrometer construction (i.e., the vacuum seals) could influence the amount of isotopic labeling ultimately measured.

The objective of this chapter was therefore to investigate post-ionization back-exchange as a potential source of deuterium loss in HDX-MS. A reporter-based workflow was developed to monitor changes in deuterium content directly, and post-ionization BEX was evaluated across multiple mass spectrometry instruments and in both positive- and negative-ion modes. The role of the instrument environment was then investigated through engineering approaches designed to reduce exposure to atmospheric water vapor, followed by evaluation of alternative O-ring sealing materials.

4.2 Results & Discussion

4.2.1 Experimental Workflow for Measuring Post-Ionization Deuterium Loss

Hydrogen/deuterium exchange (HDX) experiments are generally interpreted under the assumption that isotopic labeling remains unchanged following ionization. Extensive method development has focused on minimizing deuterium loss before ionization by optimizing sample preparation, quenching conditions, chromatographic separation, and experimental workflows. For gHDX, where exchange occurs after ionization, it has similarly been assumed that deuterium incorporation remains unchanged during ion transmission through the mass spectrometer. As a result, the possibility that the extent of isotopic labeling may continue to change following ionization has received limited consideration within the HDX field. To investigate this possibility directly, we developed a reporter-based experimental workflow to quantify post-ionization deuterium loss, which forms the experimental foundation for all subsequent studies presented in this chapter.

First, we equilibrated the instrument by continuously infusing pure D_2O to replace readily exchangeable H_2O on the source and instrument surfaces before data collection. This equilibration minimized contributions from the ionization process, allowing any deuterium loss to be attributed primarily to interactions occurring after ionization within the mass spectrometer. After equilibration, we infused reporters prepared in D2O directly; we selected two reporters to monitor post-ionization BEX in positive- and negative-ion modes. Positive-ion mode experiments use the P1 peptide, originally developed to investigate amide hydrogen scrambling during HDX-MS[4]. A particularly useful feature of P1 is that each charge state (e.g., +5, +4, +3, and +2) exhibits a distinct rate of deuterium loss, providing multiple exchange reporters from a single peptide. This allows post-ionization BEX to be monitored across a broad kinetic range without requiring multiple compounds in positive-ion mode. Negative-ion mode experiments use EDTA together with its singly and doubly sodiated species. As demonstrated in previous chapters, EDTA exhibits slow exchange kinetics, making it well suited for monitoring gradual deuterium loss over extended ion residence times. During preliminary development of the experimental workflow, we also observed that singly and doubly sodiated EDTA ions incorporate deuterium and undergo measurable post-ionization deuterium loss. These observations prompted their inclusion as additional reporters for monitoring post-ionization deuterium loss in negative-ion mode. The overall experimental workflow was consistent across all instrument platforms; however, instrument-specific methods were designed to achieve the desired ion residence times (i.e., experimental time points). Detailed descriptions of the instrument-specific methods are provided in section 4.3.2 of the methods section. Mass spectra were acquired at a series of experimental time points, allowing monitoring of changes in deuterium abundance. The spectra were then

processed and converted into uptake profiles for each reporter and instrument tested to evaluate deuterium loss.

Representative isotope distributions and the corresponding deuterium uptake profiles are shown in Figure 4.1. The representative positive-ion spectra of the P1 peptide +5 charge state and the negative-ion spectra of EDTA show a progressive shift in the isotopic distribution toward lower m/z values as ion residence time increases, indicating post-ionization deuterium loss. Throughout this chapter, results are presented as deuterium uptake profiles to compare post-ionization deuterium loss. Supporting figures provide additional representative isotope distribution spectra for selected experiments and instrument platforms.

4.2.2 Magnitude of Post-ionization BEX Across Instruments

With the experimental workflow established to measure post-ionization deuterium loss, we then asked: if trace water or water vapor enters the mass spectrometer, does post-ionization BEX occur across different instruments and ion polarities? Access to multiple instruments gave us a unique opportunity to answer this question. Post-ionization deuterium loss was measured on the Bruker TIMS-TOF, Thermo Orbitrap Ascend, Thermo Orbitrap Eclipse, Waters Synapt G2-Si, and Thermo LTQ. Figure 4.2 shows a schematic overview of each instrument architecture. The regions used to control ion residence time included trapped ion mobility spectrometry (TIMS) on the Bruker TIMS-TOF, the ion trap and ion routing multipole on both the Thermo Orbitrap Ascend and Thermo Orbitrap Eclipse, the ion mobility (IMS) region of the traveling-wave ion guide (TWIG) on the Waters Synapt G2-Si, and the linear ion trap on the Thermo LTQ. Measurements were collected in both positive- and negative-ion modes to determine whether this is unique to a single

instrument or a general phenomenon across mass spectrometry instruments, regardless of polarity.

Positive-mode measurements were collected using P1 on the Bruker TIMS-TOF, Thermo Orbitrap, Waters Synapt G2-Si, and Thermo LTQ and summarized in Figure 4.3. Despite differences in instrument architecture and regions used to control ion residence times, a consistent pattern emerged. Across all instruments, deuterium loss occurred; these findings affirm that post-ionization BEX is not unique to a single instrument but is observed across all instruments tested. A second observation was that higher charge states exhibited greater deuterium loss than lower charge states across all instruments, with deuterium loss consistently following the trend +5 > +4 > +3 > +2. The +5 charge state of P1 showed the most significant deuterium loss over the experimental time scale, whereas the +2 charge state of P1 retained most of its initial deuterium labeling. On the Thermo Orbitrap Ascend, we performed measurements independently within the ion trap and the ion-routing multipole. We observed nearly identical deuterium loss profiles from both regions, revealing that post-ionization BEX occurred to a comparable extent despite differences in the trapping environment within a single instrument. Among the platforms tested, the Thermo LTQ exhibited the most noticeable deuterium loss. The LTQ showed the lowest initial deuterium content for every P1 charge state; at the earliest experimental time point, substantial deuterium had already been lost before controlled ion trapping began, and it continued to decrease throughout the experimental timescale. This observation suggests that some deuterium loss occurs early as ions travel through the LTQ before experimentally controlled ion-residence measurements begin.

Having established that post-ionization BEX occurs across all instruments in positive mode, we next investigated it in negative mode. We collected negative-mode measurements using EDTA and its sodium adducts on the Bruker TIMS-TOF, Thermo Orbitrap, Thermo Eclipse, Waters Synapt G2-Si, and Thermo LTQ, and summarized them in Figure 4.4. Every instrument exhibited deuterium loss; these findings highlight that post-ionization BEX occurs across all instruments tested regardless of ion polarity. A second observation showed that the location of ion storage within a single instrument did not significantly affect the extent of deuterium loss. Measurements were performed independently within the ion trap and ion-routing multipole of both the Thermo Orbitrap Ascend and the Thermo Orbitrap Eclipse. They revealed nearly identical deuterium loss profiles for EDTA and its sodium adducts despite differences in the trapping environment within a single instrument. The most significant observation was the substantial differences in initial deuterium content; each instrument exhibited a different initial deuterium content at the earliest experimental time point. Across EDTA and both sodium adducts, the instruments can be ranked by initial deuterium content from highest to lowest as follows: Thermo Orbitrap Ascend ≈ Waters Synapt G2-Si > Bruker TIMS-TOF ≈ Thermo Orbitrap Eclipse > Thermo LTQ. Although every platform exhibited deuterium loss over the experimental timescale, this ranking of initial deuterium content across all three ion species indicates that deuterium loss occurs as ions travel through instrument regions before controlled ion residence can begin, highlighting differences in each instrument's post-ionization environment.

The positive- and negative-mode studies established several conclusions. First, post-ionization deuterium loss was observed across every mass spectrometry instrument examined. Second, a comparison of different ion-storage regions within a single instrument showed nearly

identical deuterium-loss profiles. Lastly, although deuterium loss occurred over the experimental timescale regardless of instrument type, the initial deuterium content differed among instruments. These observations highlight that post-ionization can alter deuterium labeling following the exchange reaction and should be considered when interpreting H/D exchange measurements and comparing data sets across different instruments or experimental conditions.

4.2.3 Environmental Control to Reduce Post-Ionization BEX

Having observed post-ionization deuterium loss across multiple mass spectrometry instruments, the next objective was to determine whether environmental control strategies could reduce the contribution of atmospheric water vapor entering the instrument and thereby mitigate post-ionization BEX. Our hypothesis predicts that reducing the instrument exposure to ambient laboratory humidity should reduce deuterium loss. To test this hypothesis, we designed environmental enclosures and continuously monitored both temperature and relative humidity throughout these studies.

We selected the Thermo LTQ as the initial proof of concept because its relatively small size allowed us to fully enclose the instrument. We constructed a full environmental enclosure around the LTQ to reduce exposure to laboratory ambient humidity (Figure 4.5A). Three temperature and humidity sensors were installed to monitor conditions in 1) the laboratory, 2) within the enclosure, and 3) within the instrument itself over an approximately 5-month period. Throughout the study, changes in both temperature and relative humidity within the enclosure and within the instrument closely followed fluctuations measured in the laboratory (Figure B). This indicates that although the enclosure physically surrounded the LTQ, the internal environment remained strongly

influenced by laboratory-based changes, suggesting that the enclosure did not provide sufficient environmental isolation to reduce humidity. Although the LTQ enclosure did not achieve the intended reduction in ambient humidity, the experiment provided an important engineering insight: a physical enclosure alone is not equivalent to environmental isolation if it remains responsive to fluctuations in laboratory temperature and humidity.

Learning from this study, we shifted our focus to the Waters Synapt G2-Si and updated our engineering strategy. The first approach similarly involved an enclosure around the entire instrument, with dry air actively supplied to the enclosed environment to reduce atmospheric humidity (Figure 4.6A). The full-instrument Synapt enclosure initially appeared successful. EDTA and its sodium adducts showed reduced deuterium loss relative to baseline measurements, indicating reduced post-ionization BEX (Figure 4.6E). However, environmental monitoring data (i.e., temperature and humidity sensors installed inside the instrument and the laboratory) showed that the full enclosure substantially increased the instrument's temperature (Figure 4.6D). This suggests that the apparent reduction in post-ionization BEX was due to instrument heating rather than a true reduction in ambient humidity, stressing the importance of monitoring both temperature and humidity. If we had monitored relative humidity alone, we would have attributed the observed improvement in deuterium loss directly to reduced humidity, but monitoring temperature prevented that conclusion. Concerns about prolonged operation amid continued temperature rise posed a risk to the instrument electronics; we therefore terminated the experiment and designed a more targeted engineering strategy. The second approach focused specifically on the TriWave region, which contains the trap, helium, ion mobility, and transfer compartments, along with their associated sealing interfaces. A localized enclosure was

constructed around the external O-ring housing of the TriWave ion gauges (Figure 4.6 B-C), and dry air was continuously supplied through an inline moisture trap to minimize water vapor around these interfaces. The targeted TriWave enclosure reduced relative humidity, while temperature remained constant over the course of the study (Figure 4.6D). Unlike the full-instrument enclosure, the relative humidity therefore decreased without an increase in temperature, allowing changes in deuterium loss to be interpreted directly in relation to reduced atmospheric humidity, rather than as a consequence of heating. EDTA and both its sodium adducts all exhibited a reduction in deuterium loss relative to baseline measurement (Figure 4.6E). These results provide strong experimental support for our hypothesis that reducing exposure to ambient laboratory humidity reduces deuterium loss and provide evidence that water vapor from the surrounding environment contributes to post-ionization BEX.

4.2.4 The impact of Alternative Sealing Materials on Deuterium Loss

Having demonstrated that reducing exposure of the TriWave region to ambient laboratory humidity decreased post-ionization deuterium loss, we next investigated whether replacing the O-rings surrounding the TriWave vacuum compartments with alternative sealing materials could further limit water vapor entering the instrument and minimize deuterium loss. The O-rings of the ion gauges in the trap, helium, ion mobility, and transfer cells of the TriWave region were selected for evaluation (Figure 4.7A). We selected commercially available sealing materials. These included the original Waters-installed O-rings, replacement Viton from Edwards Vacuum, polytetrafluoroethylene (PTFE), EPDM-90 (ethylene propylene diene monomer), AFLAS (a copolymer of tetrafluoroethylene and propylene), and silicone (Figure 4.7B). Viton and AFLAS are

fluorinated elastomers commonly used for sealing applications, whereas EPDM-90 is an elastomer widely used in industrial applications because of its environmental resistance. PTFE is a rigid fluoropolymer rather than an elastomer and therefore provided a different sealing material for comparison. Silicone was used because of its relatively high water-vapor permeability. Together, this panel allowed us to determine whether changing the physical material influenced post-ionization deuterium loss. For each O-ring condition, we vented the instrument, installed the O-rings, pumped it down, and allowed it to equilibrate for approximately three days before measurements began. We then evaluated each material over approximately one month, collecting measurements throughout. This extended experimental design minimized the influence of short-term, day-to-day variability due to changes in lab temperature and humidity.

The original Waters-installed O-rings, which had been present on the instrument for at least six years, served as the experimental baseline (Figure 4.7C). Although the exact composition of these manufacturer-installed O-rings was unknown, they showed the greatest post-ionization deuterium loss among the sealing materials evaluated(Figure 4.7C). Replacement with Edwards Vacuum Viton O-rings produced a measurable reduction in deuterium loss relative to the original Waters-installed O-rings (Figure 4.7C). The TriWave O-rings were subsequently replaced with PTFE, EPDM-90, and AFLAS. PTFE reduced post-ionization deuterium loss relative to the original Waters-installed O-rings despite being considerably more difficult to install because of its rigidity(Figure 4.7C). EPDM-90 and AFLAS also reduced deuterium loss relative to the baseline. No significant difference was observed between EPDM-90 and AFLAS, indicating comparable performance despite their different material compositions and properties (Figure 4.7C). Silicone O-rings provided an informative comparison because silicone is known to exhibit relatively high

water-vapor permeability (Figure 4.7C). Although replacing the O-rings with silicone still reduced deuterium loss relative to the original Waters-installed O-rings, it produced the smallest improvement among the replacement materials evaluated. Silicone's comparatively poor performance is consistent with the proposed role of water-vapor entry through the instrument O-rings and further supports the relationship between the sealing environment and post-ionization deuterium loss. Overall, replacing the original O-rings with newly installed sealing materials consistently reduced deuterium loss compared to the baseline, indicating that seal material influenced the post-ionization environment within the TriWave region. These findings also demonstrate that post-ionization deuterium loss is not solely a consequence of ion residence within the mass spectrometer. Instead, its magnitude can change with the surrounding instrument environment and vacuum-sealing interfaces. Identifying these experimentally controllable factors provides a path to mitigate post-ionization BEX and improve the reliability of HDX measurements.

4.3 Methods

4.3.1 Reporter Compounds and Sample Preparation

Deuterated oxide (D_20) (99%) was purchased from Cambridge Isotope Laboratories (Tewksbury, MA, USA). Tris-EDTA buffer solution and peptide P1 (HHHHHHIIKIIK) were purchased from Sigma-Aldrich (St. Louis, MO, USA).

P1 peptide was diluted to a working concentration of 5 µg/mL with D_2O. EDTA was diluted to a working concentration of 10 µM with D_2O. Infusion flow rate ranged from 5 µL/min to 20 µL/min depending on the instrument platform. P1 was used for positive-mode experiments, and EDTA/EDTA sodium adducts were used for negative mode.

4.3.2 Instrument Platforms

Thermo LTQ: In negative mode, each analyte was isolated and held for a set period. The peak m/z was isolated with an isolation width of at least 10 Th (centered within the isotopic distribution) to cover the full exchange window in the spectra. We sampled a wide range of exchange times (16), from 1 millisecond to 30 seconds. The exchange times were defined within the instrument method as extended collision-induced dissociation (CID) experiments with zero collision energy, allowing ions to be held in the linear ion trap for controlled reaction times without fragmentation. Mass spectra were acquired in enhanced scan mode for resolution setting. The Ion Source parameters were set as follows: NanoESI capillary temperature 210 °C, source voltage 2.30 kV, Source Current 100 uA, Capillary Voltage -9.00 V, Tube Lens -65.0 V, Lens 1 Voltage 39.00 V, Front Lens 14.0 V. For positive ion mode, the spray voltage was set to 2.5 kV, with a capillary temperature of 275 °C. Data were acquired comprising 10 sequential scan events targeting a precursor ion for each P1 charge state, with a 20 m/z isolation window. Activation time was varied across the acquisition window from 1 ms to 1380 ms to evaluate time-dependent ion behavior.

Waters Synapt G2-Si: nanoESI source operated in negative ion mode. Data were acquired using MassLynx 4.2 over an *m/z* range of 150–4000 in continuum acquisition mode. Each acquisition consisted of a 2 min run time with a 0.50 s scan time. Instrument parameters: source temperature 80 °C; sampling cone voltages between 20–80 V depending on the mobility condition; capillary voltages were set between 1.25–1.50 kV. Reaction time was controlled by systematically varying traveling-wave ion mobility parameters to modulate ion residence time in the mobility region. Four mobility conditions were used: Short mobility conditions: IMS wave velocity 230 m s^{-1} and wave

height 25 V. Short–medium conditions: IMS wave velocity 325 m s^{-1} and wave height 21 V. Medium conditions: IMS wave velocity 475 m s^{-1} and wave height 19 V. Long conditions: IMS wave velocity 311 m s^{-1} and wave height 4 V. Across all experiments, trap gas flow (2.0 mL min^{-1}), helium cell gas flow (180 mL min^{-1}), and ion mobility gas flow (90 mL min^{-1}) were kept constant.

Thermo Orbitrap Ascend and Eclipse: heated electrospray ionization (H-ESI) source operating in positive ion mode and negative ion mode. The spray voltage was set to 2.5 kV for negative mode and 3.5 kV for positive mode, with sheath, auxiliary, and sweep gas flows of 12, 2, and 2.8. The ion transfer tube temperature was maintained at 275 °C, and the vaporizer temperature was 30 °C. The instrument was operated in direct infusion mode with a total method duration of 1.2 min per acquisition. Mass spectrometric analysis was performed using a top-down multistage tandem MS (tMS^n) workflow in which sequential MS^2 experiments were acquired in 0.1-min time segments. Across each segment, a fixed precursor ion at m/z 275 (z = 1) was isolated using a quadrupole isolation window of 150 m/z. Activation times were progressively increased from 0.5 ms to 1000 ms throughout the experiment in either the ion trap or ion-routing multipole. Spectra were acquired over an m/z range of 150–400.

Bruker TIMS-TOF Flex

Infusions of EDTA and peptide P1 (same concentrations as for the Orbitrap) were collected using a standard Apollo ESI source with a flow rate of 10uL/min. Source settings were: dry gas (12), heater (350 °C), nebulizer gas flow (2), Sheath gas flow (4), 1.5kV capillary voltage (negative mode) or 3.6 kV (positive mode). For all experiments, D2O was first infused at a flow rate of 20 µL for 5 minutes to clear any H2O from the source lines (never faster than 40uL/min, to avoid ‘flooding’ the TIMS region with D2O). TIMS settings were adjusted to achieve a range of residence times for each

analyte; specifically, the 1/ko range was set to 0.55 to 1.9, with ramp times of 0 (TIMS off), 10, 20, 40, 80, 160, 320, 640, 1068, and 1380 ms. Data were processed for m/z and mobility information in Bruker Compass Data Analysis and exported to HX-Express v3. The complete residence time in the TIMS region for each ion was calculated as the accumulation time (equal to the ramp time, using a 100% duty cycle), plus the mobility time calculated as a fraction of the ramp time from the apex of the 1/ko of the mobility peak relative to the 1/ko range used for the analysis.

4.3.3 Post-ionization BEX Workflow

Before reporter measurements, each instrument was equilibrated by direct infusion of D_2O to minimize residual H_2O associated with the source and ion pathway. After equilibration, reporter solutions prepared in D_2O were infused directly under the instrument-specific conditions described above. Infusion flow rate ranged from 5 µL/min to 20 µL/min depending on the instrument platform. Reporter ions were isolated and maintained within the designated instrument region for controlled residence times. Mass spectra were acquired across the experimental residence-time window, and changes in deuterium content were used to construct deuterium uptake profiles representing post-ionization deuterium loss.

4.3.4 Environmental Enclosure Studies

Environmental enclosures were constructed around the Thermo LTQ and Waters Synapt G2-Si to evaluate how environmental conditions affect post-ionization back-exchange (BEX). The LTQ enclosure was constructed using PVC pipe, 10 × 20 in. plastic canvas, and Gorilla Tape (Home Depot). Temperature and relative humidity were continuously monitored using SensorPush HT.w

sensors (SensorPush, USA) positioned on the instrument computer, on top of the LTQ, and inside the instrument. Environmental conditions were monitored for 143 days.

For the Synapt G2-Si, temperature and relative humidity were monitored for 77 days using SensorPush HT.w sensors positioned on top of the instrument and within the full-instrument enclosure. Dry air supplied from the University of Washington laboratory in-house air line was continuously introduced into the enclosure with the line fully opened. Baseline BEX measurements were collected before installation of the enclosure.

A localized enclosure was subsequently constructed around the O-ring ion-gauge interfaces of the Synapt G2-Si TriWave region using aluminum foil and HVAC tape. Dry laboratory air was supplied through an inline moisture trap on the right side of the enclosure, while the environmental sensor was positioned on the left side. The TriWave enclosure was installed on day 21 of the 77-day Synapt monitoring period. Sensor data from all enclosure studies were continuously recorded, exported as CSV files, and averaged hourly for analysis.

Post-ionization BEX measurements were performed using the same Synapt G2-Si experimental method described in Section 4.3.2

4.3.5 TriWave O-Ring Replacement Study

The O-rings associated with the trap, helium, ion mobility, and transfer regions of the Synapt G2-Si TriWave were replaced to evaluate the influence of sealing material on post-ionization back-exchange. The original Waters-installed O-rings, in use for approximately six years, served as the experimental baseline. Replacement materials included Edwards Vacuum Viton,

polytetrafluoroethylene (PTFE), EPDM-90 (ethylene propylene diene monomer), AFLAS (tetrafluoroethylene-propylene copolymer), and silicone.

For each material, the TriWave O-rings were replaced as a complete set. After installation, the instrument was pumped down and allowed to equilibrate for approximately three days before measurements began. Each O-ring material was evaluated over approximately one month. The same experimental workflow and instrument conditions were maintained across materials to allow comparison relative to the original Waters-installed O-rings.

Post-ionization BEX measurements were performed using the same Synapt G2-Si experimental method described in Section 4.3.2

4.3.6 Data Analysis

Spectra for each time point were manually extracted from MassLynx and Thermo Xcalibur Qual Browsers. The spectra of the compounds were processed and analyzed using HX-Express[5]. The experimental error of measured deuterium values was estimated from the standard deviation of triplicate measurements (n=3) unless stated otherwise.

4.4 Summary

This chapter investigated post-ionization back-exchange (BEX) as a source of deuterium loss in HDX. A reporter-based workflow was developed to monitor deuterium loss across multiple instrument platforms. It showed that post-ionization BEX occurs in both positive- and negative-ion modes, with differences in loss magnitude and initial deuterium content among instruments. Environmental enclosure studies demonstrated that targeted reduction of ambient humidity

surrounding the Synapt G2-Si TriWave region reduced deuterium loss. Replacement of the TriWave O-rings with alternative sealing materials further reduced deuterium loss relative to the original Waters-installed O-rings. Together, these findings identify the post-ionization environment as a contributor to deuterium loss and demonstrate that post-ionization BEX can be mitigated.

4.5 Chapter Figures

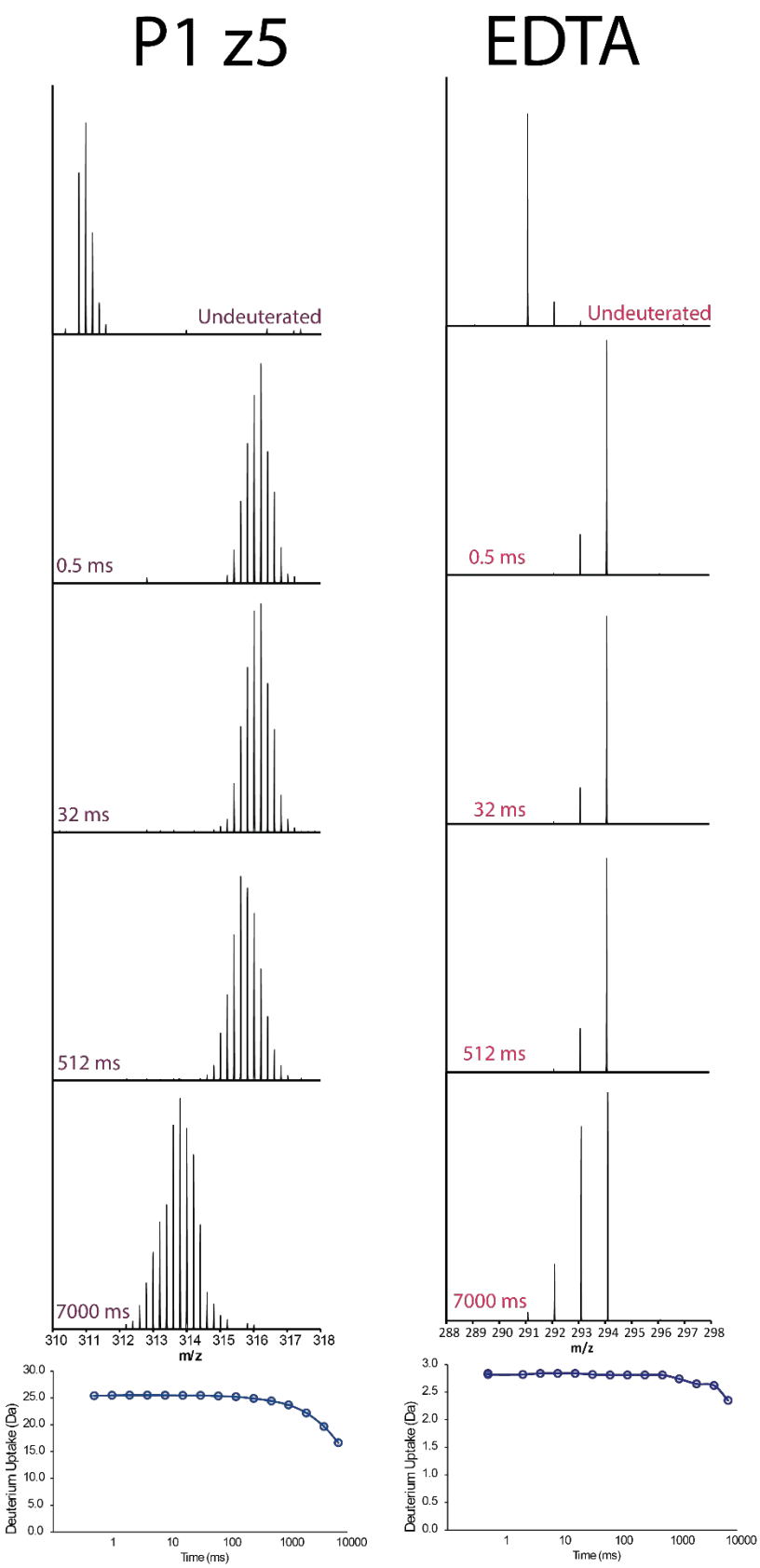
P1 z5
EDTA
Undeuterated
0.5 ms
32 ms
512 ms
7000 ms
310 311 312 313 314 315 316 317 318
m/z
288 289 290 291 292 293 294 295 296 297 298
m/z
Deuterium Uptake (Da)
Time (ms)
1 10 100 1000 10000

Figure 4.1: Representative post-ionization deuterium loss for P1 peptide and EDTA on the Orbitrap Ascend. Representative mass spectra are shown for A) P1 peptide charge state +5 in positive-ion mode and B) EDTA in negative-ion mode. We collected spectra for the undeuterated analytes and after deuteration at ion residence times of 0.5, 32, 512, and 7000 ms. Increasing residence time progressively shifted the isotope distributions toward lower *m/z*, consistent with post-ionization loss of incorporated deuterium. Corresponding deuterium uptake profiles show the deuterium loss over time for P1 and EDTA.

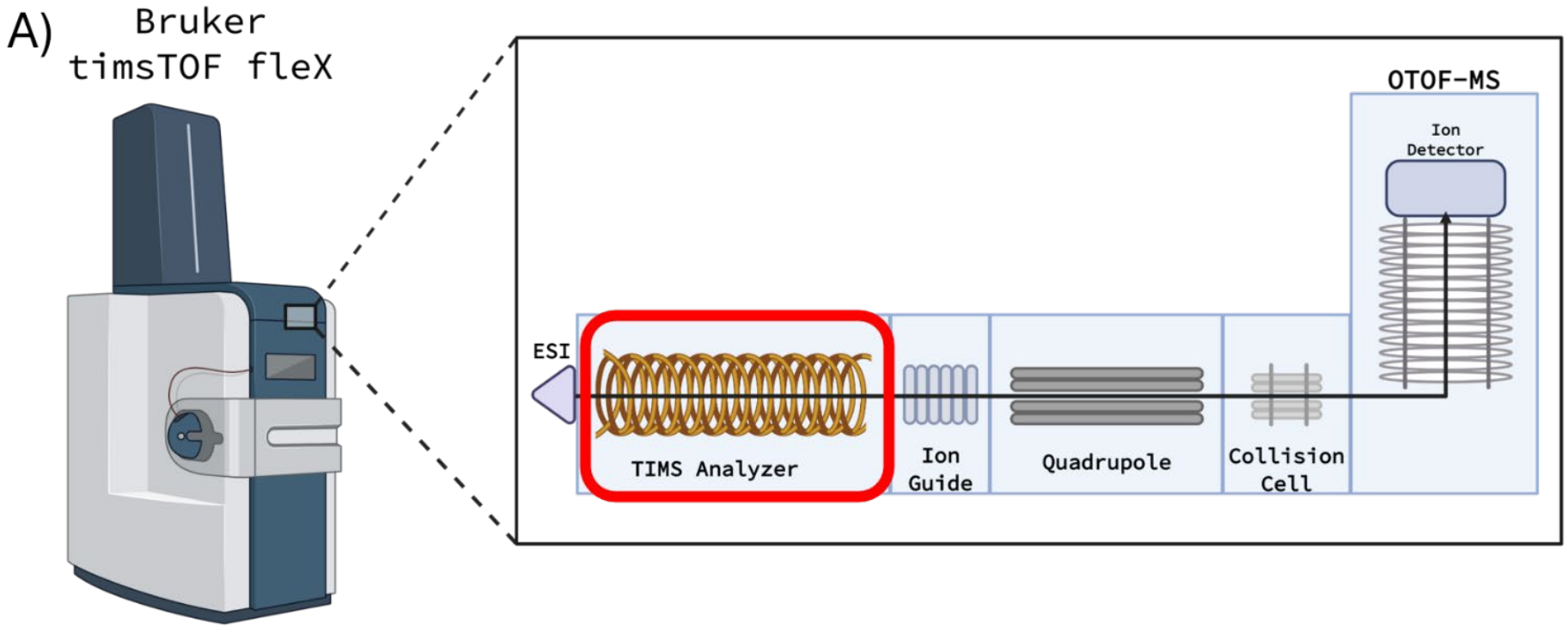
A)
Bruker
timsTOF fleX
OTOF-MS
Ion
Detector
ESI
TIMS Analyzer
Ion
Guide
Quadrupole
Collision
Cell

B)

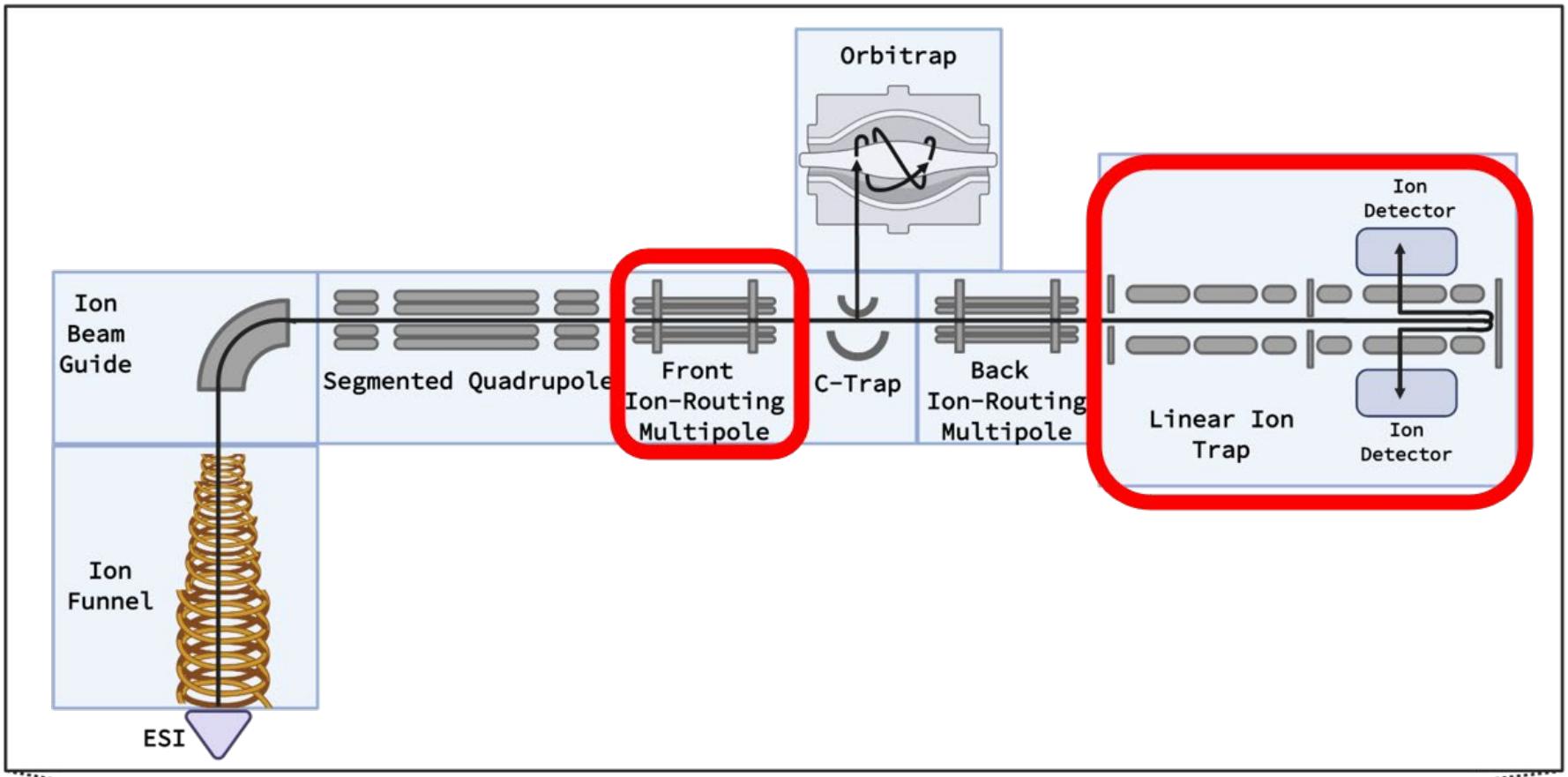

Thermo Ascend

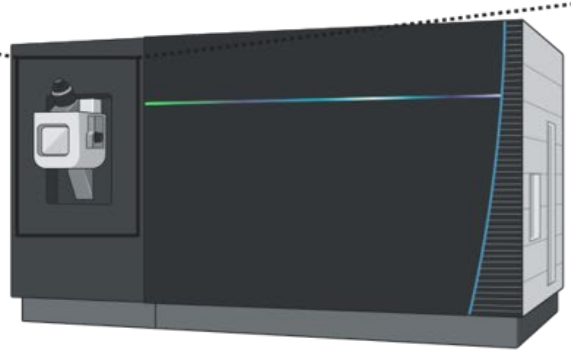

C)

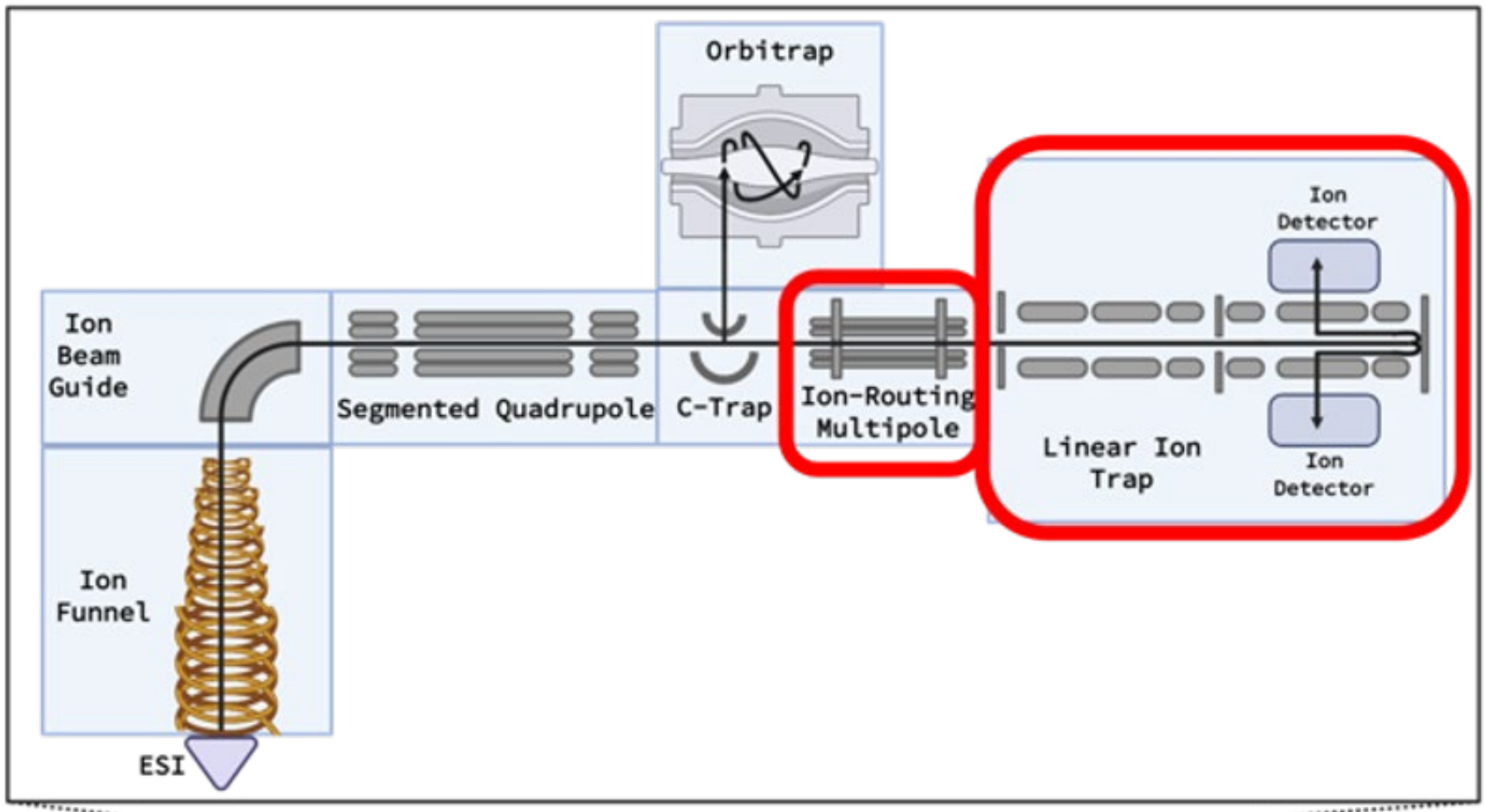

Thermo Eclipse

D) Waters Synapt G2-Si

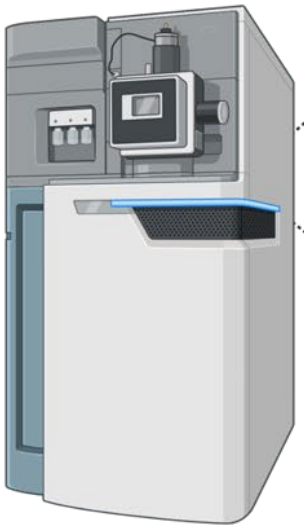

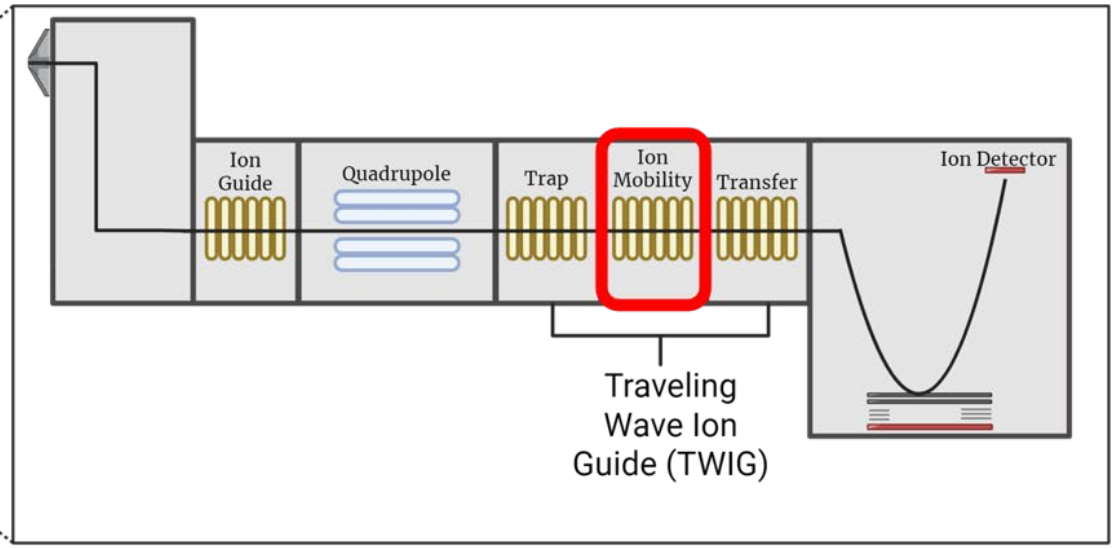

E) Thermo LTQ

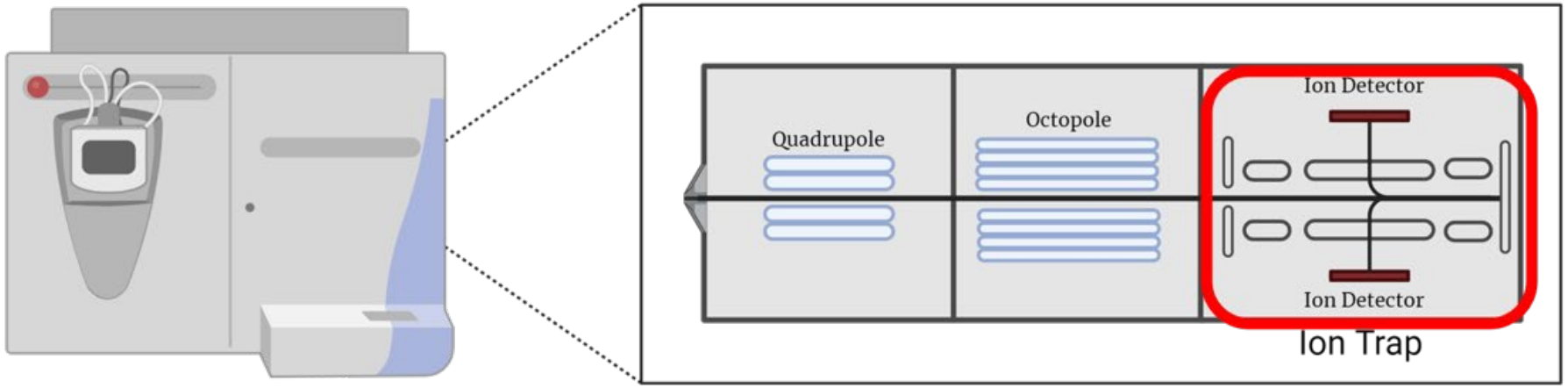

Figure 4.2: Schematics for each instrument. Experiments were performed by varying ion residence time within the post-ionization trapping or ion transport region of each instrument. Highlighted regions in red indicate where ions were retained before mass analysis. A) Bruker TIMS-TOF, B) Thermo Orbitrap Ascend, C) Thermo Orbitrap Eclipse, D) Waters Synapt G2-Si, and E) Thermo LTQ.

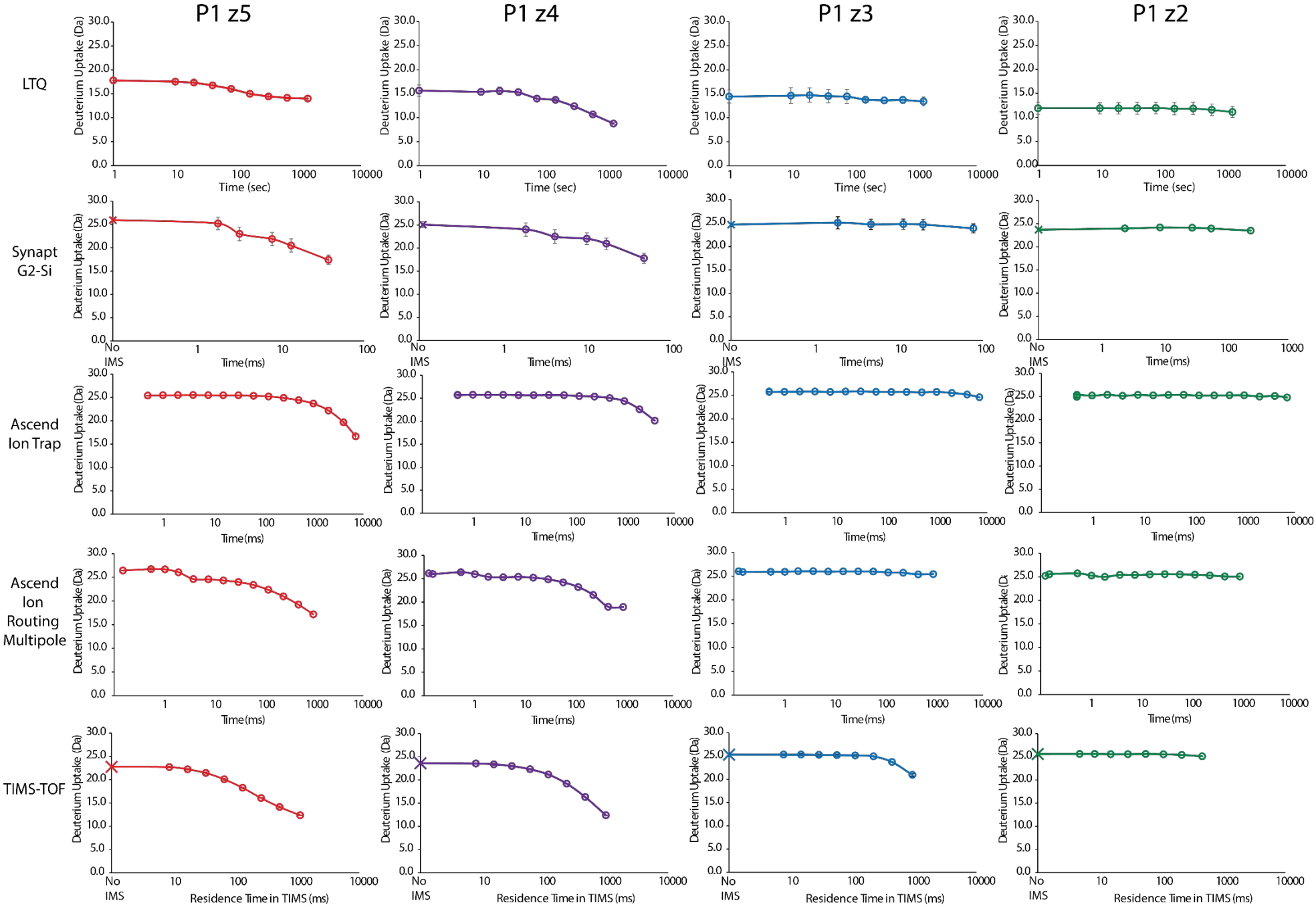
P1 z5
P1 z4
P1 z3
P1 z2
LTQ
Synapt G2-Si
Ascend Ion Trap
Ascend Ion Routing Multipole
TIMS-TOF
Deuterium Uptake (Da)
Time (sec)
Time (ms)
No IMS
Residence Time in TIMS (ms)

Figure 4.3: Instrument- and charge-state-dependent post-ionization deuterium loss of P1 peptide across five instruments. Post-ionization deuterium uptake profiles are shown for the P1 peptide charge states +5, +4, +3, and +2. Columns correspond to peptide charge state, while rows correspond to the instrument platform in the following order: Thermo LTQ, Waters Synapt G2-Si, Thermo Orbitrap Ascend ion trap (IT), Thermo Orbitrap Ascend ion routing multipole (IRM), and Bruker TIMS-TOF. Data points represent the average of replicate measurements (n = 3), with error bars indicating standard deviation. Solid lines are included as visual guides and do not represent kinetic model fits. All panels use identical y-axis scaling to facilitate direct comparison of the magnitude and time dependence of post-ionization back-exchange across instruments and charge states.

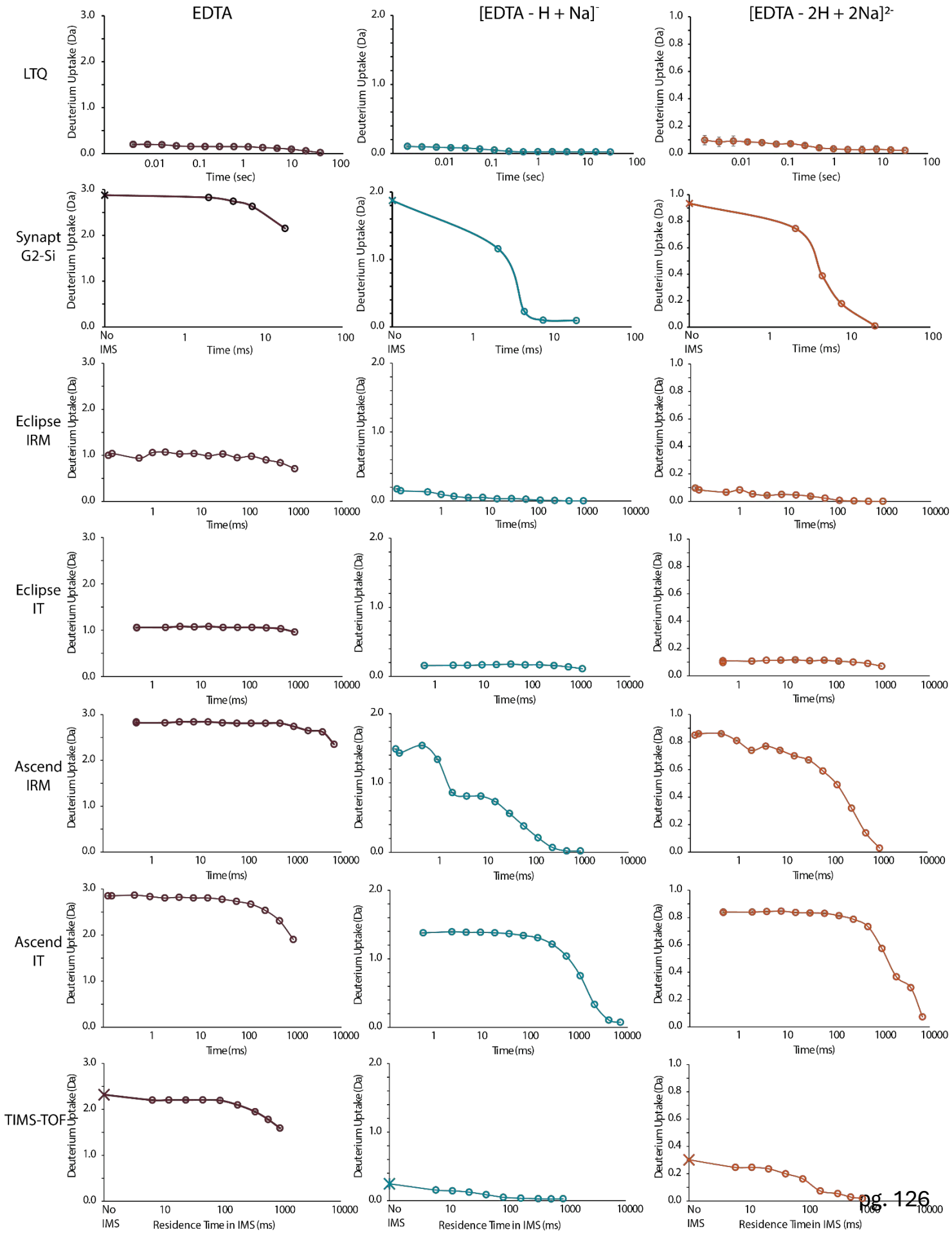
EDTA
[EDTA - H + Na]⁻
[EDTA - 2H + 2Na]²⁻
LTQ
Synapt G2-Si
Eclipse IRM
Eclipse IT
Ascend IRM
Ascend IT
TIMS-TOF
Deuterium Uptake (Da)
Time (sec)
Time (ms)
No IMS
Residence Time in IMS (ms)

Figure 4.4: Instrument-dependent initial deuterium content and post-ionization back-exchange of EDTA and sodium adducts. Negative-ion deuterium uptake profiles are shown for EDTA and its two sodium adducts across the Thermo LTQ, Waters Synapt G2-Si, Thermo Orbitrap Eclipse ion routing multipole (IRM) and ion trap (IT), Thermo Orbitrap Ascend IRM and IT, and Bruker TIMS-TOF. Columns correspond to ion identity, and rows correspond to the instrument and post-ionization region examined. All samples were prepared in D_2O under identical solution conditions before infusion. The earliest measured deuterium uptake varied among instruments. Data points represent the average of replicate measurements (n = 3), with error bars indicating standard deviation. Solid lines are included as visual guides and do not represent kinetic model fits. The y-axis is scaled according to ion identity and the extent of deuterium incorporation to facilitate comparison within each column.

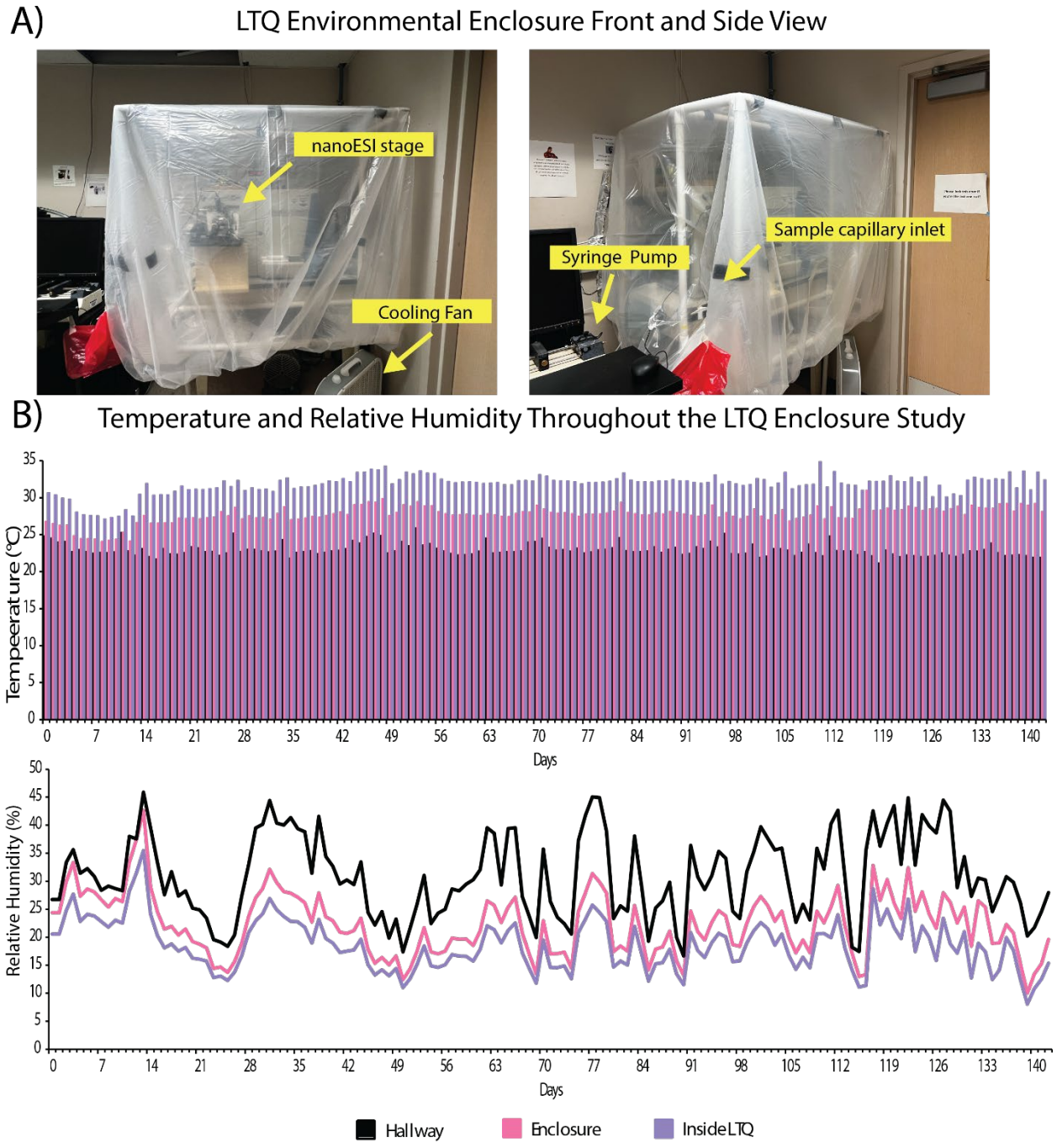

Figure 4.5: Environmental enclosure and long-term monitoring of laboratory conditions surrounding the Thermo LTQ. An environmental enclosure was constructed around the LTQ to reduce exposure to ambient laboratory conditions and evaluate the potential contribution of environmental humidity to post-ionization back-exchange. A) Photographs of the completed

enclosure showing the nanoESI stage, cooling fan, sample capillary inlet, and syringe pump used for sample infusion. B) Temperature and relative humidity were continuously monitored over the 143-day enclosure study using sensors positioned in the laboratory environment (hallway), within the enclosure, and inside the LTQ. Sensor measurements were averaged and presented across the study duration to compare environmental conditions.

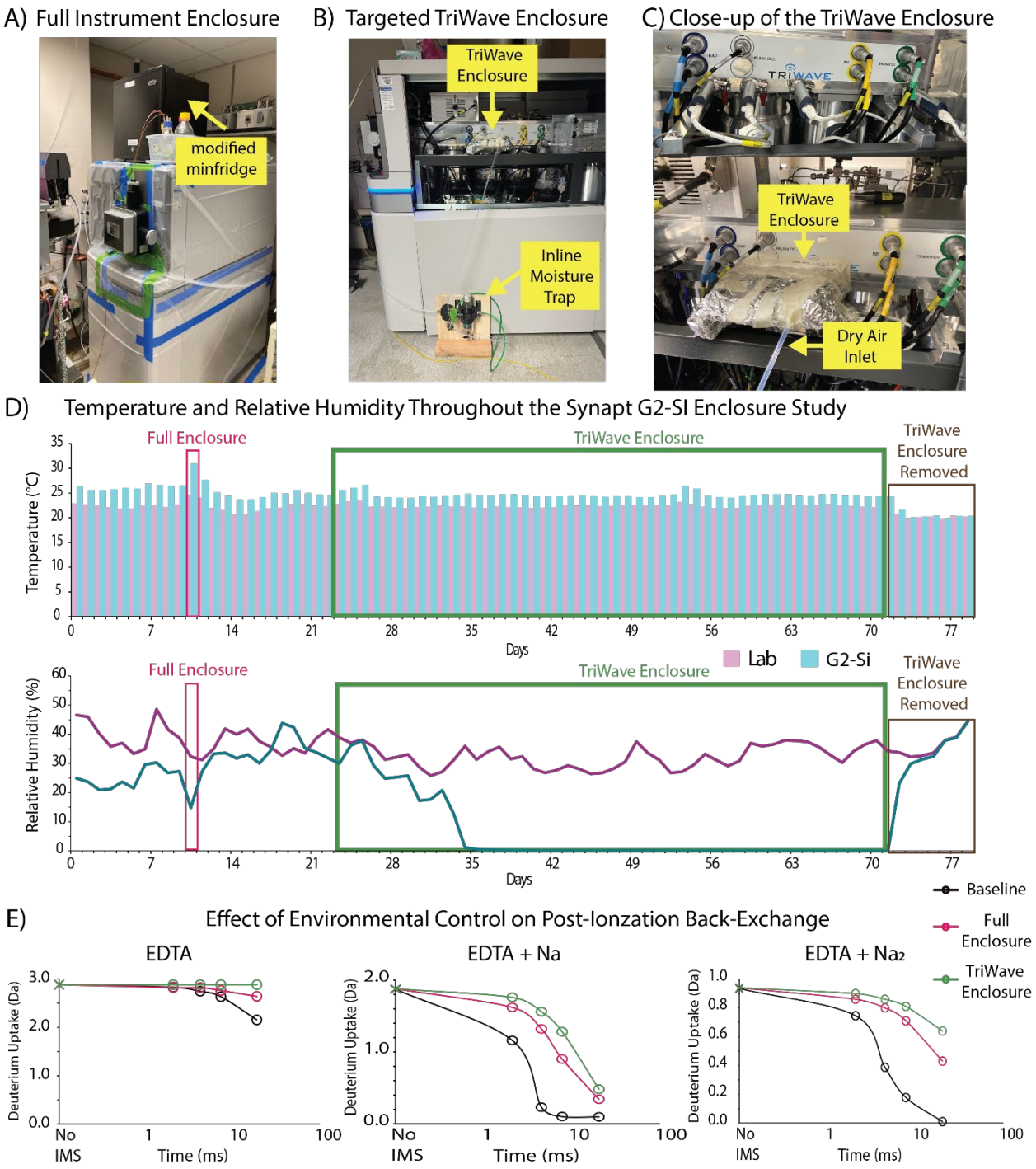

Figure 4.5: Targeted environmental control of the TriWave region reduces post-ionization back-exchange. Engineering modifications and environmental monitoring were used to evaluate the influence of ambient humidity on post-ionization back-exchange within the Waters Synapt G2-

Si. A) Photograph of the full-instrument enclosure and modified cooling system. Dry laboratory air was passed through a metal cooling line housed within a modified mini-refrigerator before entering the enclosure to reduce humidity while dissipating heat generated during full-enclosure operation. B) Photograph of the targeted TriWave enclosure and inline moisture trap used to reduce further water vapor in the supplied dry air. C) Close-up view of the TriWave region before and after installation of the localized enclosure surrounding the O-ring and ion-gauge, with the dry-air inlet indicated. D) Temperature (upper) and relative humidity (lower) monitored over the 77-day study period. Measurements from the laboratory environment and within the Synapt G2-Si enclosure are shown, with boxed regions indicating the periods corresponding to the full-instrument enclosure and targeted TriWave enclosure; the period following removal of the TriWave enclosure is also indicated. E) Post-ionization deuterium uptake profiles for EDTA and its two sodium adducts collected under baseline, full-instrument enclosure, and targeted TriWave enclosure conditions. Measurements were acquired using identical ion-residence-time conditions to enable direct comparison among environmental conditions. Solid lines are included as visual guides and do not represent kinetic model fits.

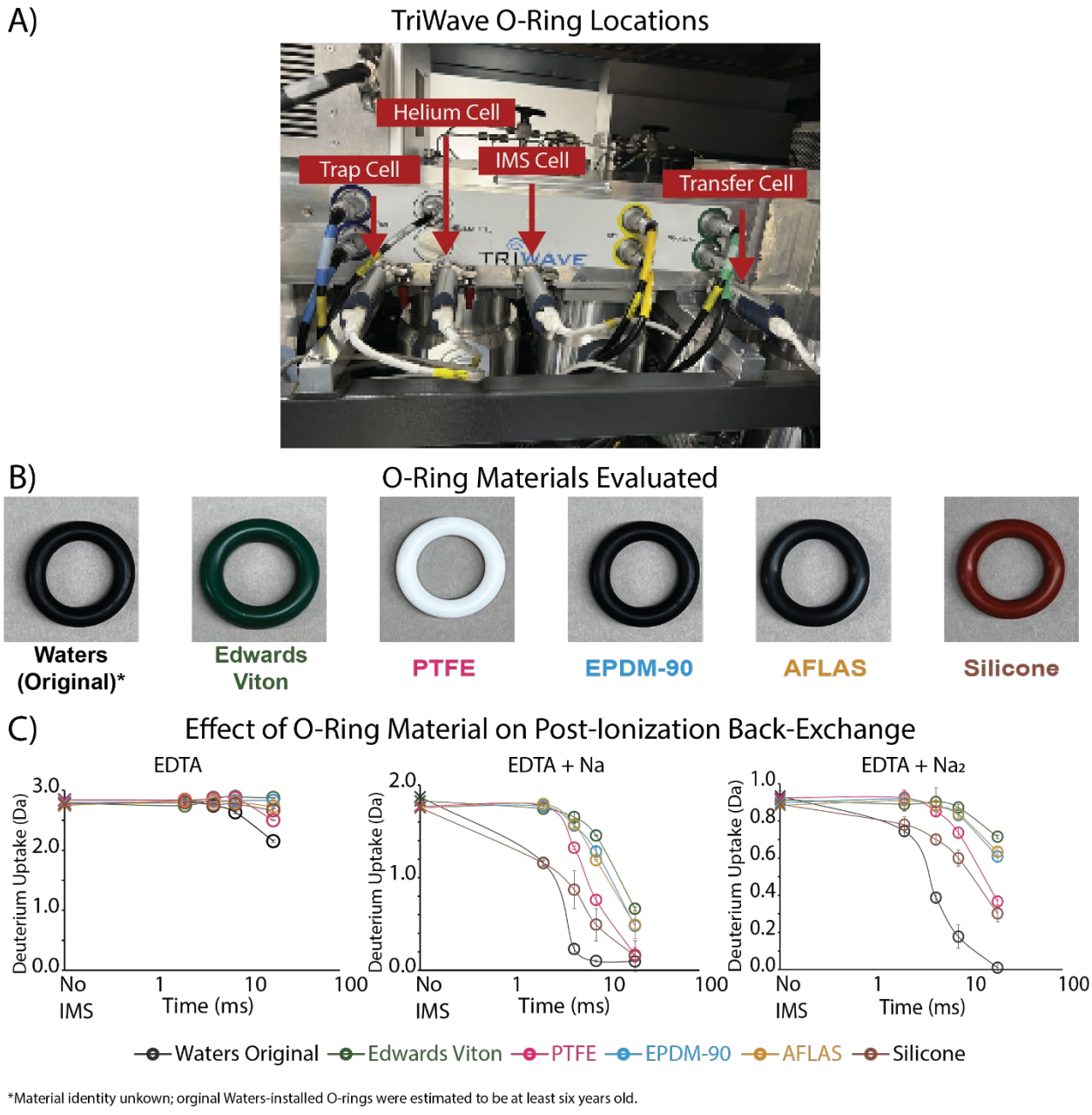

Figure 4.7: TriWave O-ring material reduces post-ionization back-exchange on the Synapt G2-Si. The TriWave O-ring sealing material was evaluated for post-ionization deuterium back-exchange. A) Photograph of the TriWave region identifying the four O-ring locations evaluated: the trap cell, helium cell, ion mobility spectrometry (IMS) cell, and transfer cell. B) O-ring materials evaluated, including the original Waters-installed O-rings (material composition unknown),

Edwards Viton, PTFE, EPDM-90, AFLAS, and silicone. C) Comparison of post-ionization back-exchange profiles for EDTA and its two sodium adducts obtained with each O-ring material. Error bars represent standard deviation. Solid lines are included as visual guides and do not represent kinetic model fits.

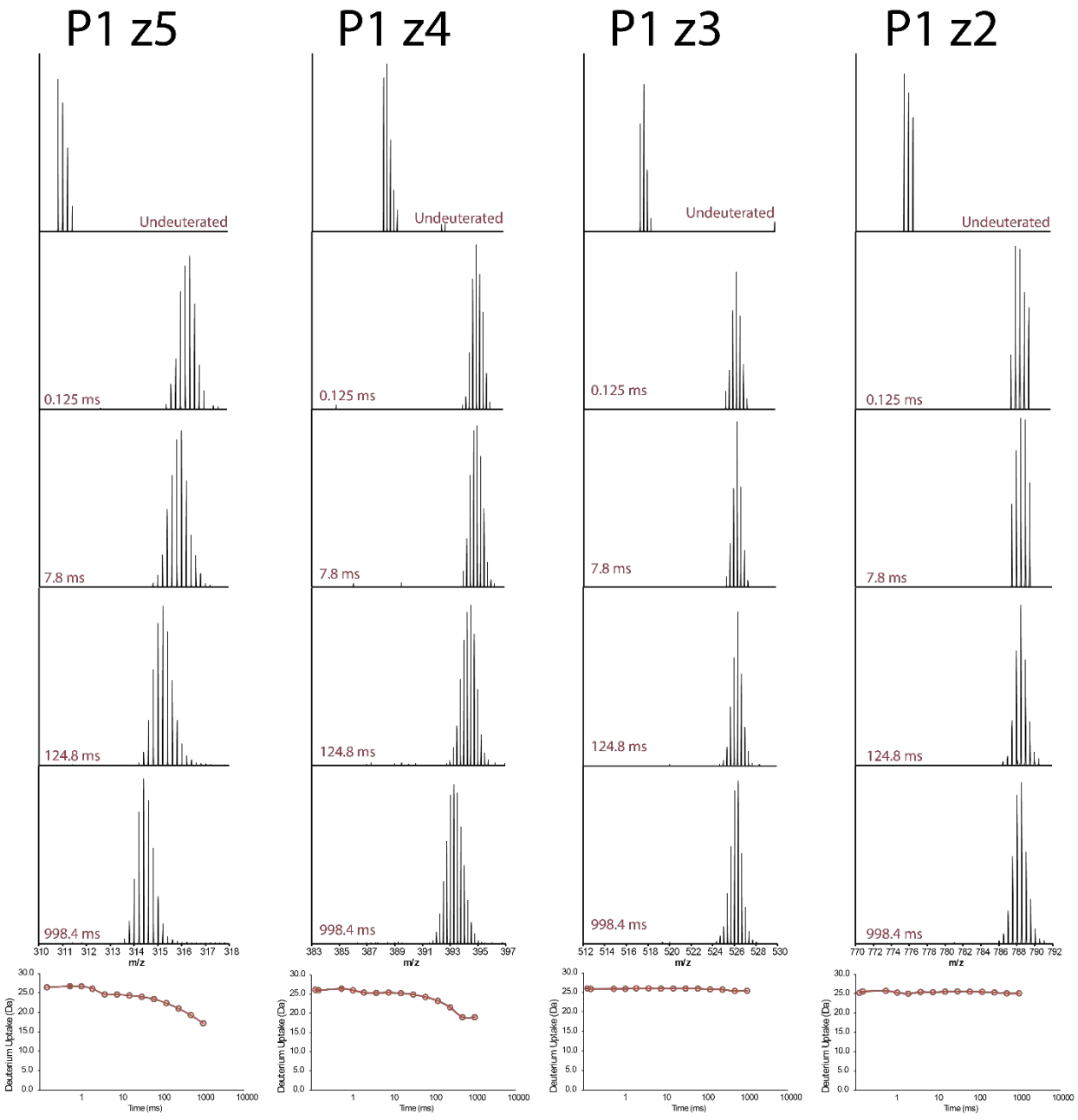

Supporting Figure 4.1: Time-resolved isotope distributions and back-exchange curves on the Thermo Ascend in Ion Routing Multipole.

Representative isotope distributions for the P1 peptide acquired in the Thermo Ascend ion-routing multipole are shown for charge states +5, +4, +3, and +2. Each column includes the undeuterated

isotope distribution and spectra collected at successive ion-holding times (0.125 ms, 7.8 ms, 124.7 ms, and 998.4 ms) following solution-phase deuterium labeling. Corresponding back-exchange curves derived from these measurements are shown below each charge-state spectrum.

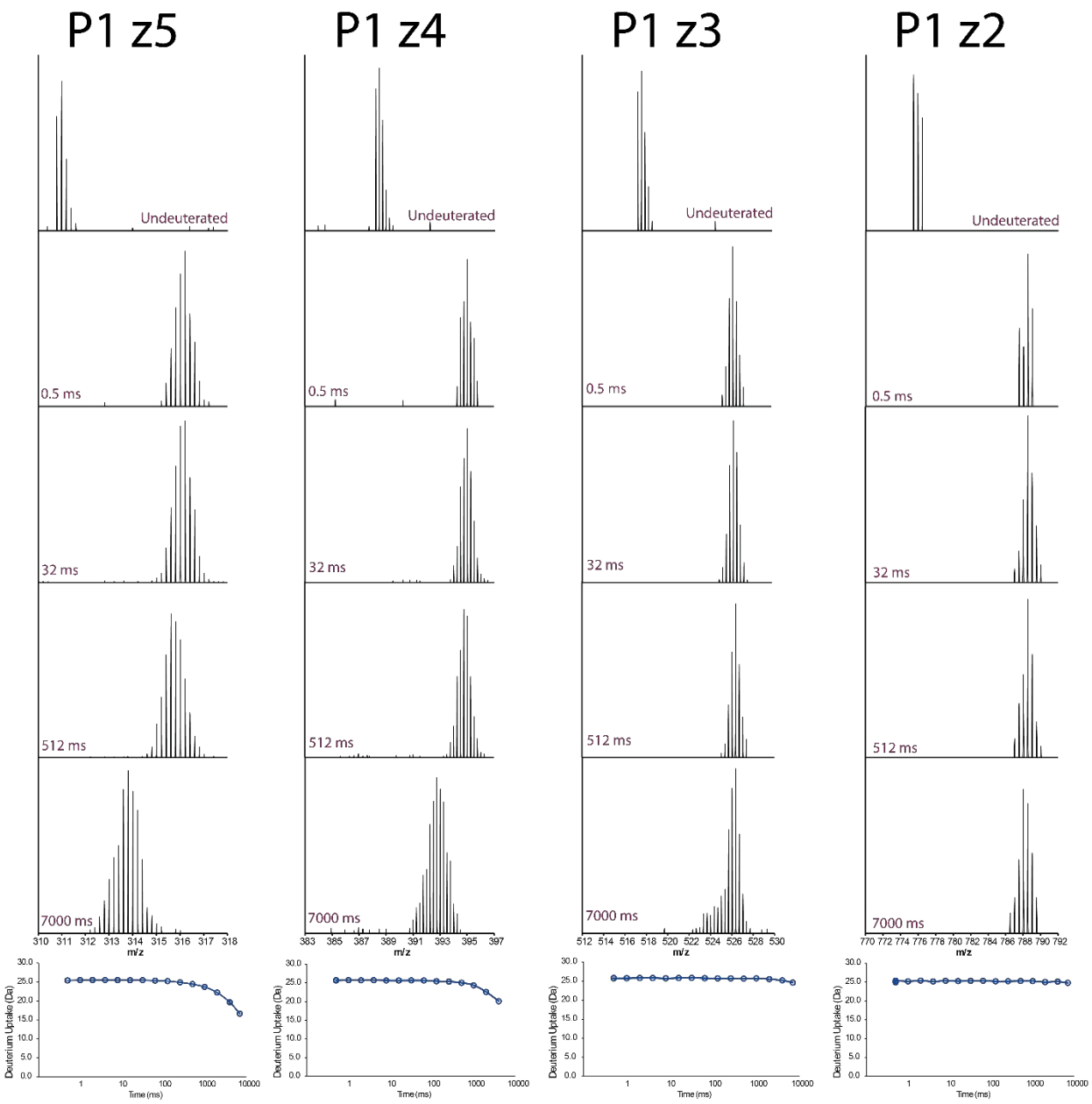

Supporting Figure 4.2: Time-resolved isotope distributions and back-exchange curves on the Thermo Ascend in the Ion Trap.

Representative isotope distributions for the P1 peptide acquired on the Thermo Ascend ion trap are shown for charge states +5, +4, +3, and +2. Each column includes the undeuterated isotope distribution, along with spectra collected at successive ion-holding times (0.5 ms, 32 ms, 512 ms,

and 7000 ms) following solution-phase deuterium labeling. Corresponding back-exchange curves derived from these measurements are shown below each charge-state spectrum.

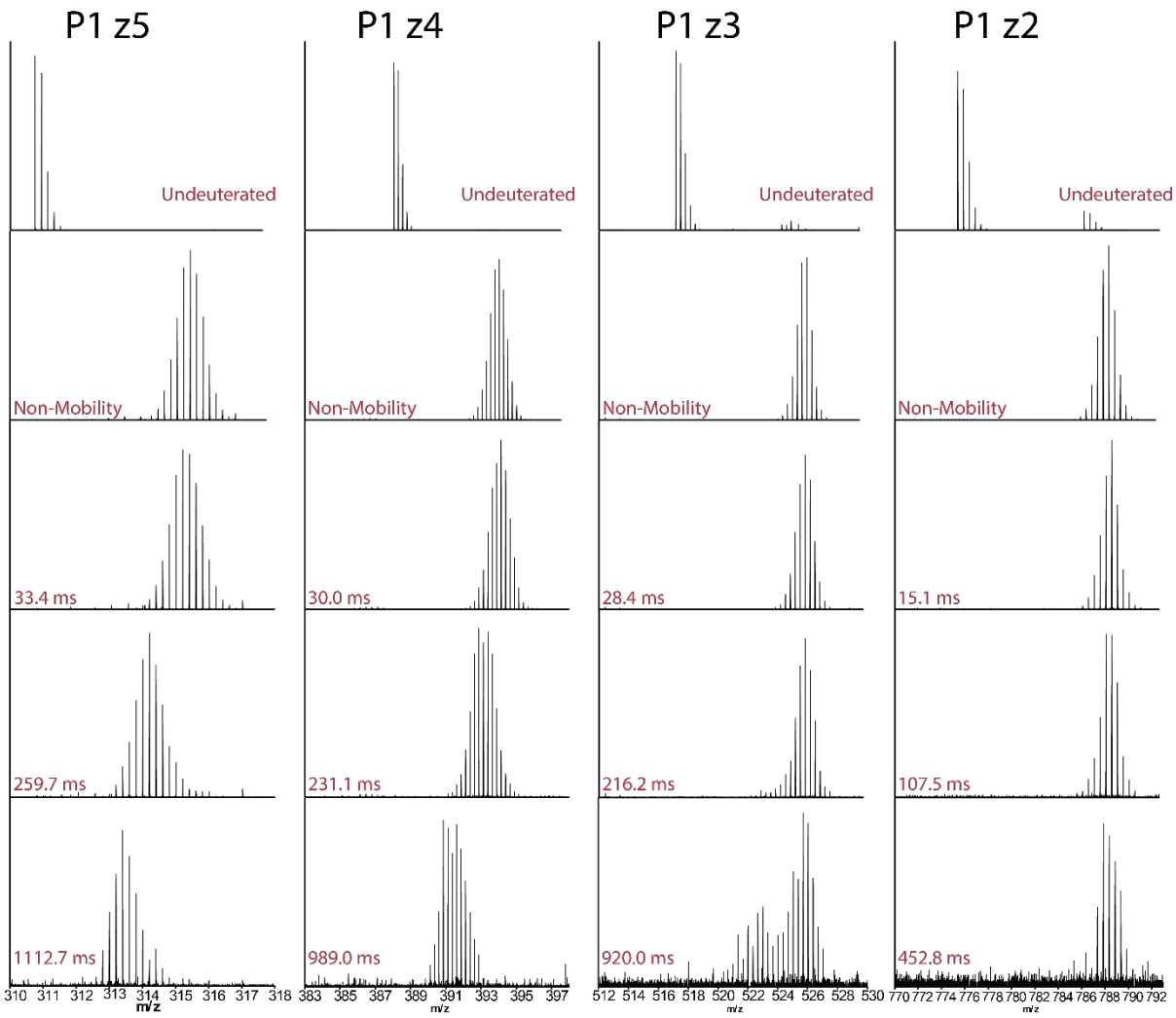

Supporting Figure 4.3: Time-resolved isotope distributions demonstrate progressive post-ionization deuterium loss on the Bruker TIMS-TOF.

Representative isotope distributions for the P1 peptide acquired on the Bruker TIMS-TOF are shown for the charge states +5, +4, +3, and +2. Each column contains the undeuterated isotope distribution, spectra collected immediately following solution-phase deuterium labeling (non-mobility), and successive mobility times illustrating the progressive leftward shift of the isotope envelope resulting from post-ionization deuterium loss.

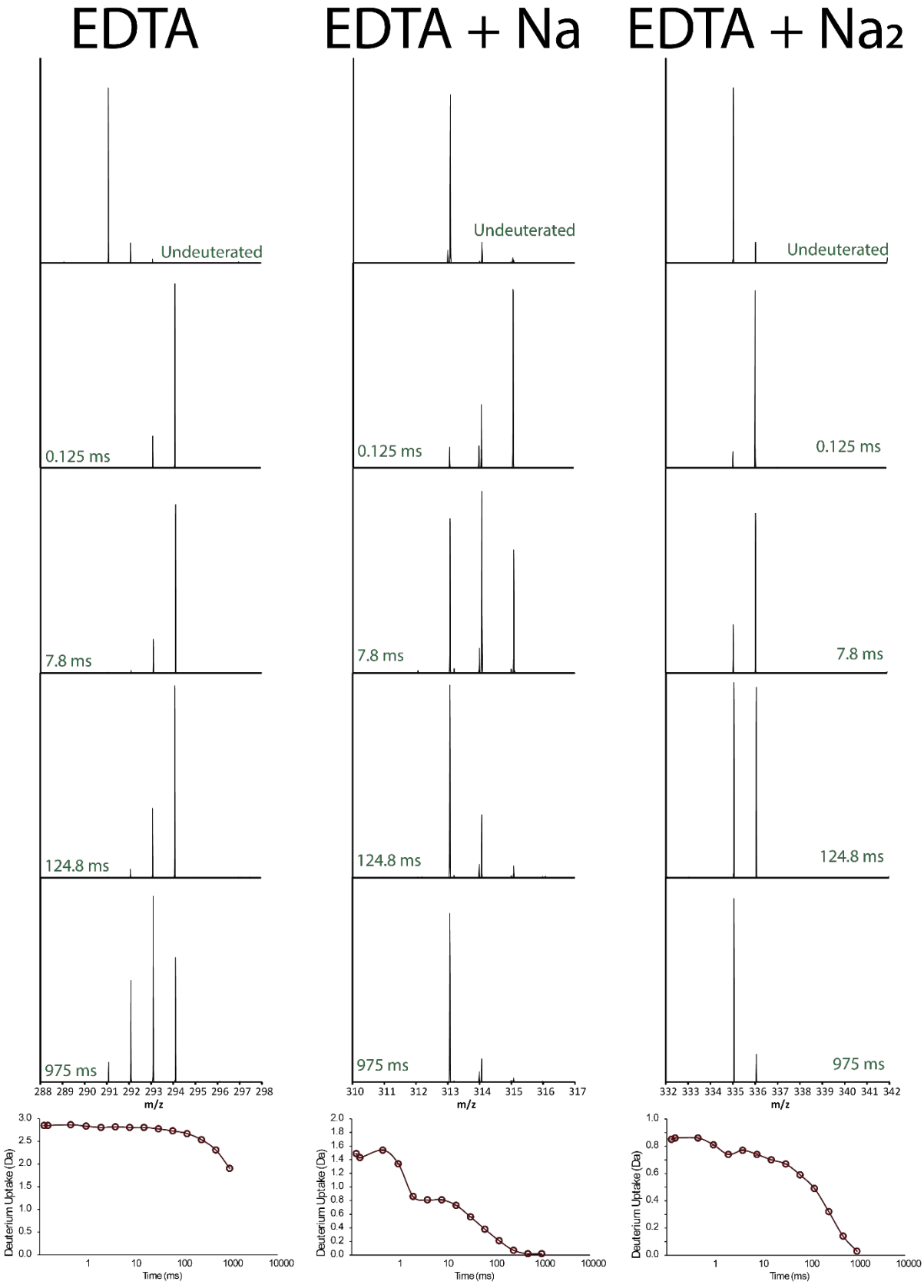
EDTA
EDTA + Na
EDTA + Na2
Undeuterated
0.125 ms
7.8 ms
124.8 ms
975 ms
m/z
Deuterium Uptake (Da)
Time (ms)

Supporting Figure 4.4: Thermo Ascend in ion routing multipole: negative-ion HDX spectra and back-exchange profiles for EDTA and sodium adducts.

Representative negative-ion HDX isotope distributions for EDTA and sodium adducts acquired on the Thermo Ascend. Spectra corresponding to the undeuterated, 0.125 ms, 7.8 ms, 124.8 ms, and 975 ms are shown to illustrate the progression of post-ionization back-exchange. All samples were prepared in D_2O before infusion to generate deuterium-labeled ions. For each ion, we monitored the deuterated species across the experimentally defined exchange time course. Deuterium loss curves in the bottom panels show the loss of deuterium over time for EDTA- and sodium-adducted species.

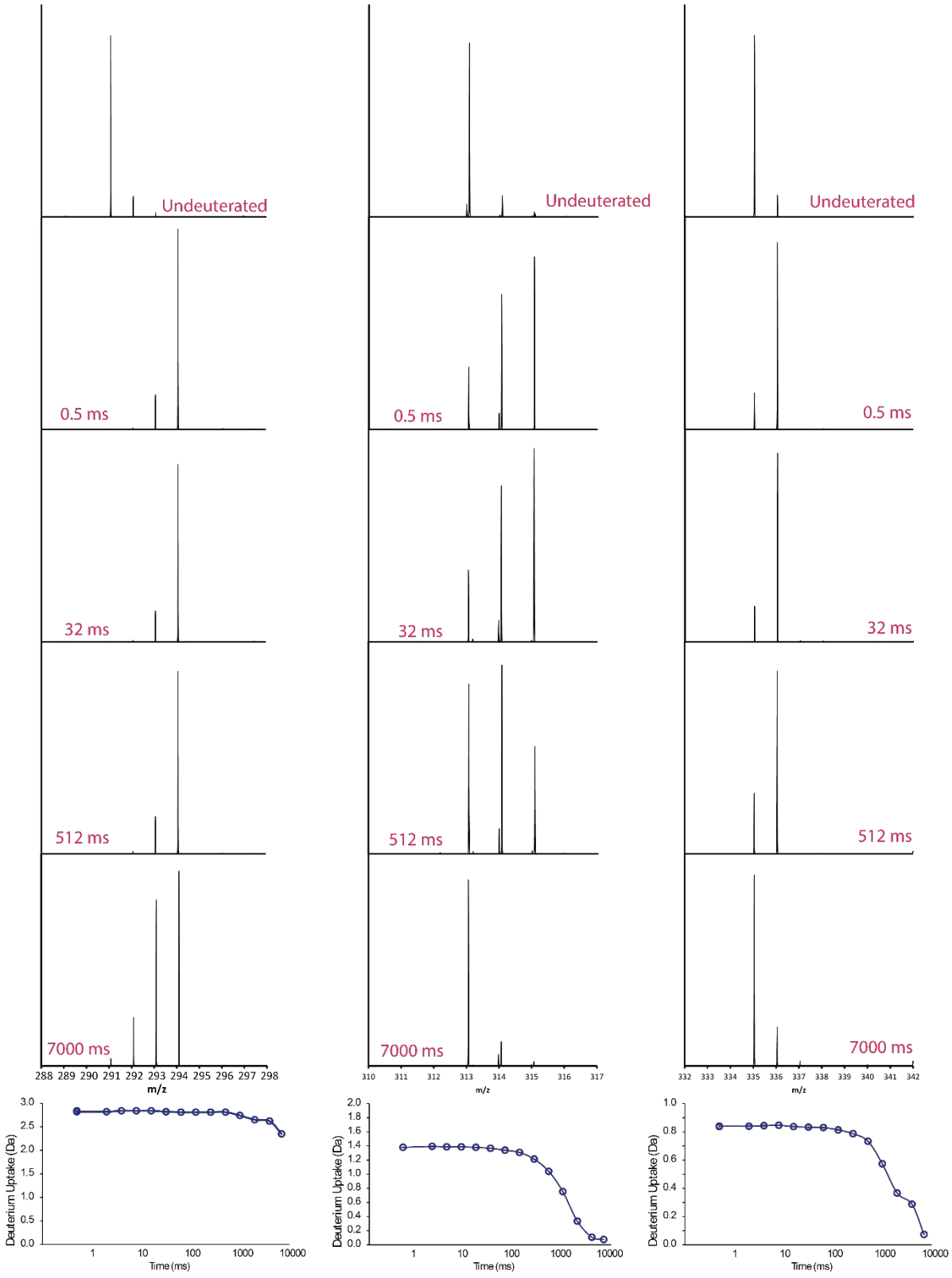
EDTA
EDTA + Na
EDTA + Na2
Undeuterated
0.5 ms
32 ms
512 ms
7000 ms
m/z
Deuterium Uptake (Da)
Time (ms)

Supporting Figure 4.5: Thermo Ascend in ion trap: negative-ion HDX spectra and back-exchange profiles for EDTA and sodium adducts.

Representative negative-ion HDX isotope distributions for EDTA and sodium adducts acquired on the Thermo Ascend. Spectra corresponding to the undeuterated, 0.5 ms, 32 ms, 512 ms, and 7000 ms are shown to illustrate the progression of post-ionization back-exchange. We prepared all samples in D2O before infusion to generate deuterium-labeled ions. For each ion, we monitored the deuterated species across the experimentally defined exchange time course. Curves in the bottom panels show the loss of deuterium over time for EDTA- and sodium-adducted species.

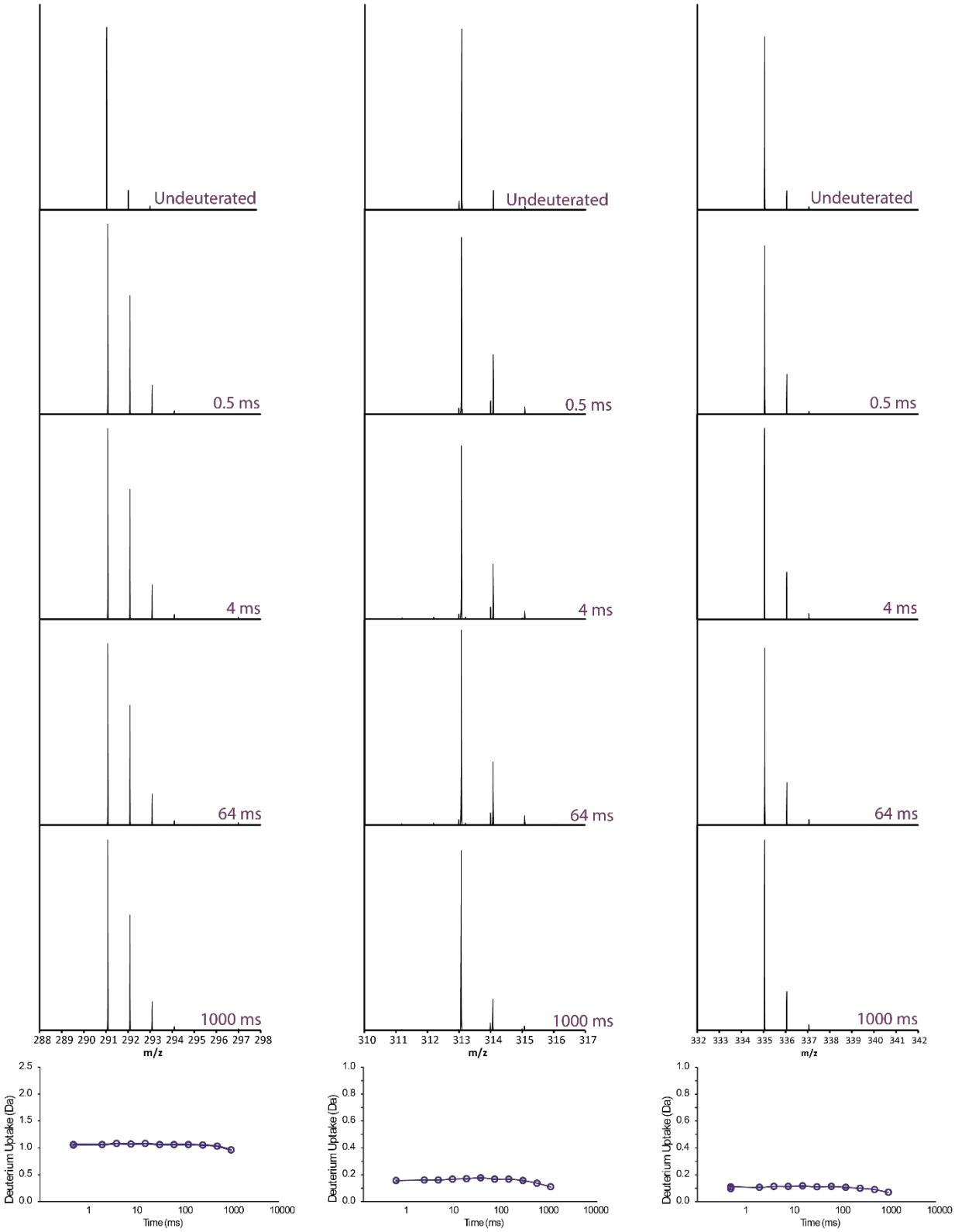
EDTA
EDTA + Na
EDTA + Na2
Undeuterated
0.5 ms
4 ms
64 ms
1000 ms
m/z
Deuterium Uptake (Da)
Time (ms)

Supporting Figure 4.6: Thermo Eclipse in ion trap: negative-ion HDX spectra and back-exchange profiles for EDTA and sodium adducts.

Representative negative-ion HDX isotope distributions for EDTA and sodium adducts acquired on the Thermo Eclipse. Spectra corresponding to the undeuterated, 0.5 ms, 4 ms, 64 ms, and 1000 ms are shown to illustrate the progression of post-ionization back-exchange. All samples were prepared in D_2O before infusion to generate deuterium-labeled ions. For each ion, we monitored the deuterated species across the experimentally defined exchange time course. Curves in the bottom panels show the loss of deuterium over time for EDTA- and sodium-adducted species.

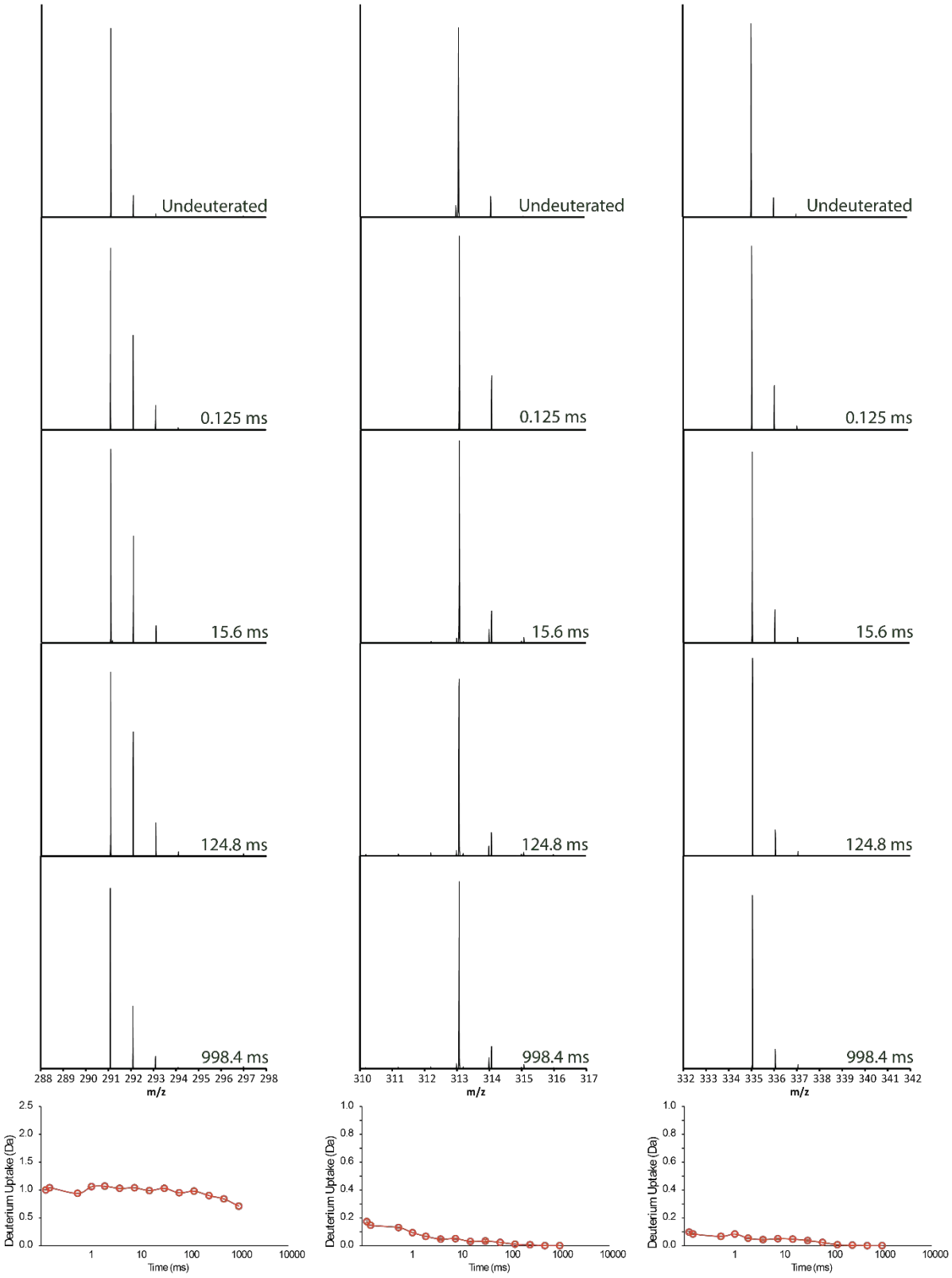
EDTA
EDTA + Na
EDTA + Na2
Undeuterated
0.125 ms
15.6 ms
124.8 ms
998.4 ms
m/z
Deuterium Uptake (Da)
Time (ms)

Supporting Figure 4.7: Thermo Eclipse in ion routing multipole: negative-ion HDX spectra and back-exchange profiles for EDTA and sodium adducts.

Representative negative-ion HDX isotope distributions for EDTA and sodium adducts acquired on the Thermo Eclipse. Spectra corresponding to the undeuterated, 0.125 ms, 15.6 ms, 124.8 ms, and 998.4 ms are shown to illustrate the progression of post-ionization back-exchange. We prepared all samples in D_2O before infusion to generate deuterium-labeled ions. For each ion, we monitored the deuterated species across the experimentally defined exchange time course. Curves in the bottom panels show the loss of deuterium over time for EDTA- and sodium-adducted species.

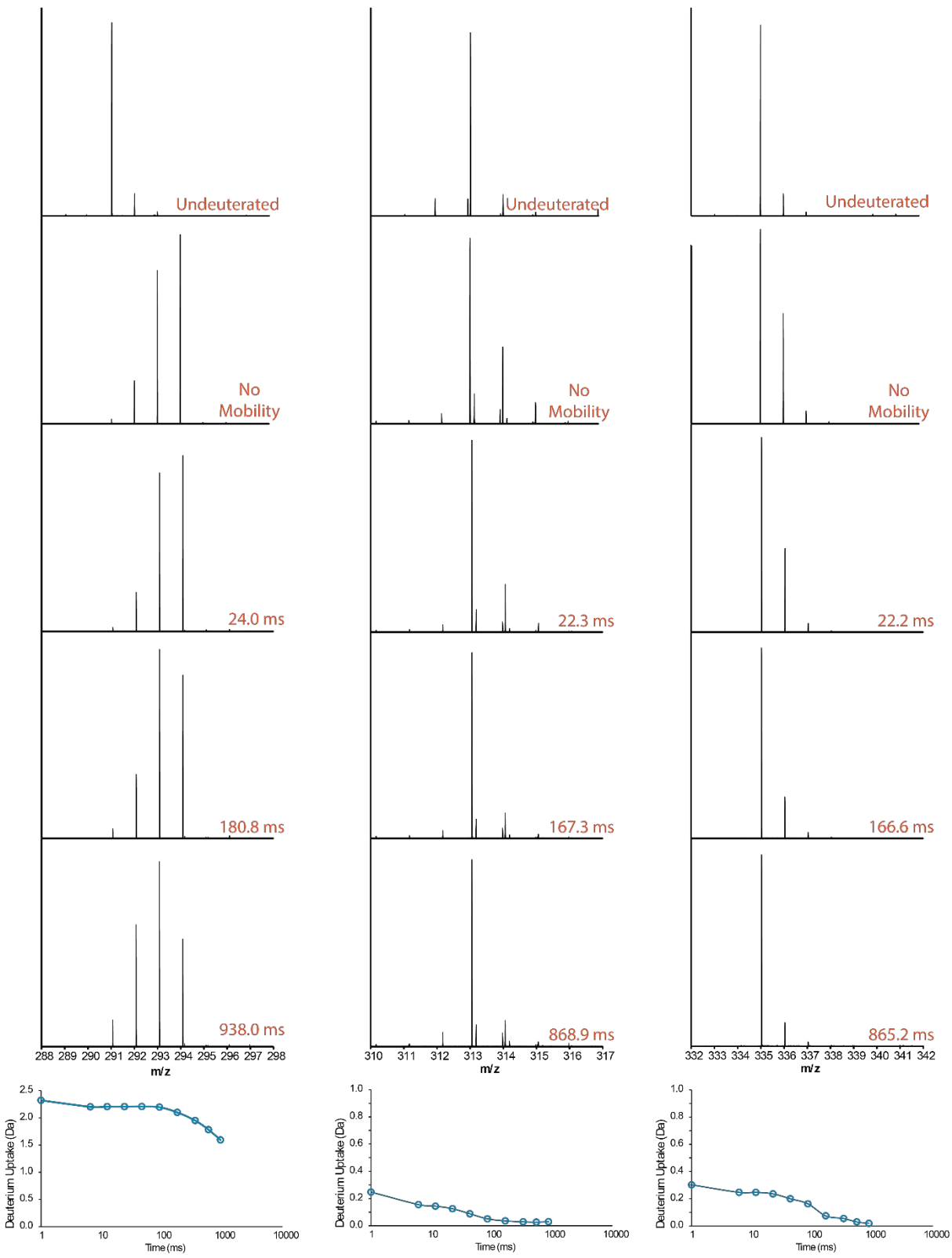
EDTA
EDTA + Na
EDTA + Na2
Undeuterated
No Mobility
24.0 ms
180.8 ms
938.0 ms
22.3 ms
167.3 ms
868.9 ms
22.2 ms
166.6 ms
865.2 ms
m/z
Deuterium Uptake (Da)
Time (ms)

Supporting Figure 4.8: Bruker TIMS-TOF in the TIMS cell: negative-ion HDX spectra and back-exchange profiles for EDTA and sodium adducts.

Representative negative-ion HDX isotope distributions for EDTA and sodium adducts acquired on the Bruker TIMS-TOF. Spectra corresponding to the undeuterated, non-mobility, and successive mobility times are shown to illustrate the progression of post-ionization back-exchange. All samples were prepared in D_2O before infusion to generate deuterium-labeled ions. For each ion, we monitored the deuterated species across the experimentally defined exchange time course. Curves in the bottom panels show the loss of deuterium over time for EDTA- and sodium-adducted species.

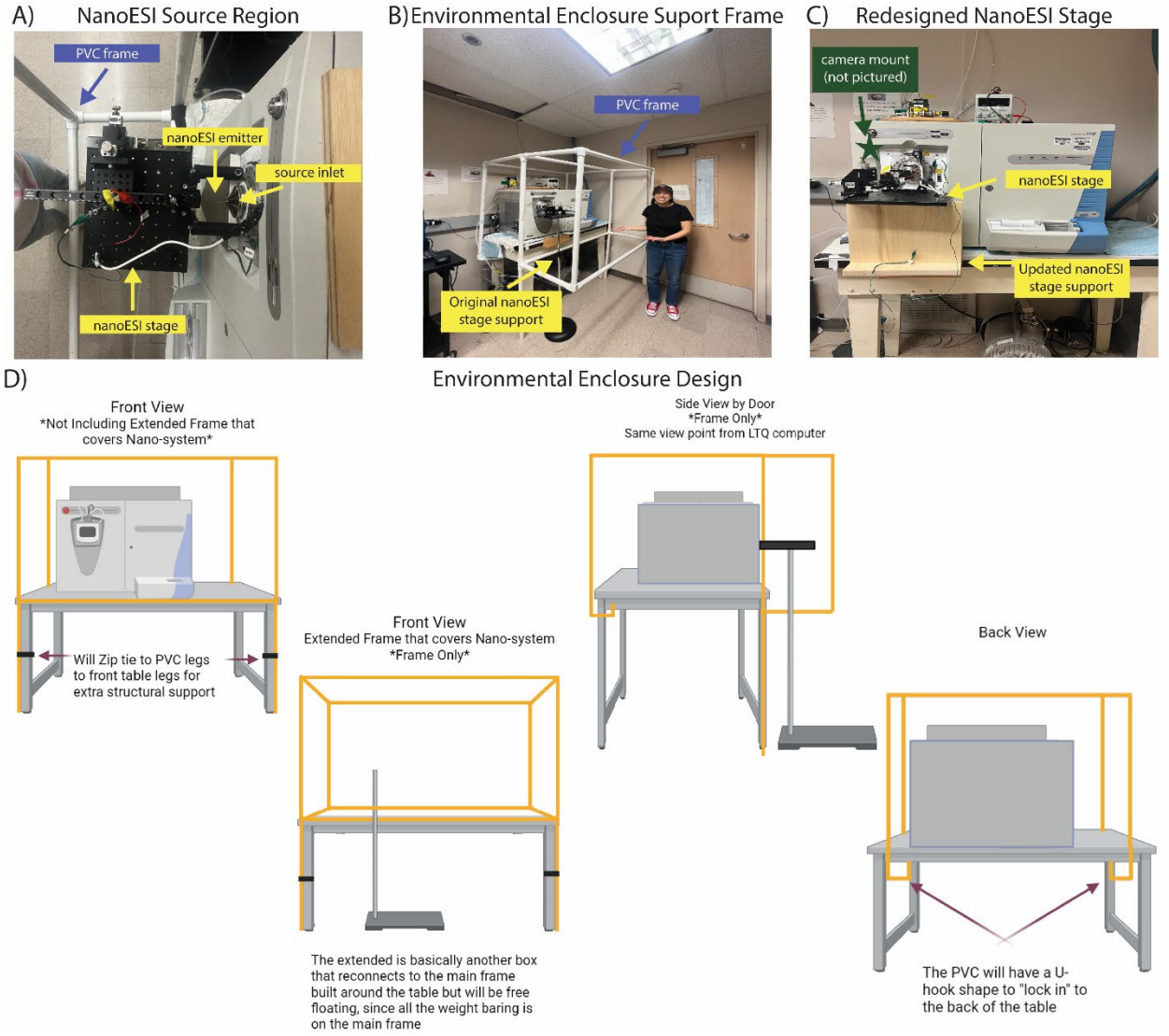

Supporting Figure 4.9: Engineering design and implementation of the LTQ environmental enclosure.

Photographs and engineering drawings illustrating the development and implementation of the environmental enclosure constructed for the LTQ. A) Top-view photograph of the nanoESI source region showing the nanoESI stage, emitter alignment, source inlet, and surrounding PVC enclosure frame. B) Photograph of the environmental enclosure support frame surrounding the LTQ, highlighting the PVC structural framework and the original microphone-stand support used

for the nanoESI stage before system redesign. C) Redesigned nanoESI stage incorporating a rigid wooden support platform secured to the laboratory bench and an integrated camera mount (denoted by a green star) for continuous monitoring of the nanoESI emitter during sample infusion. D) Engineering design drawings illustrating the enclosure geometry and structural frame from multiple view angles. Collectively, these modifications improved the stability of the nanoESI source assembly and enabled construction of the environmental enclosure, while maintaining unobstructed sample infusion and continuous visual monitoring during data acquisition.

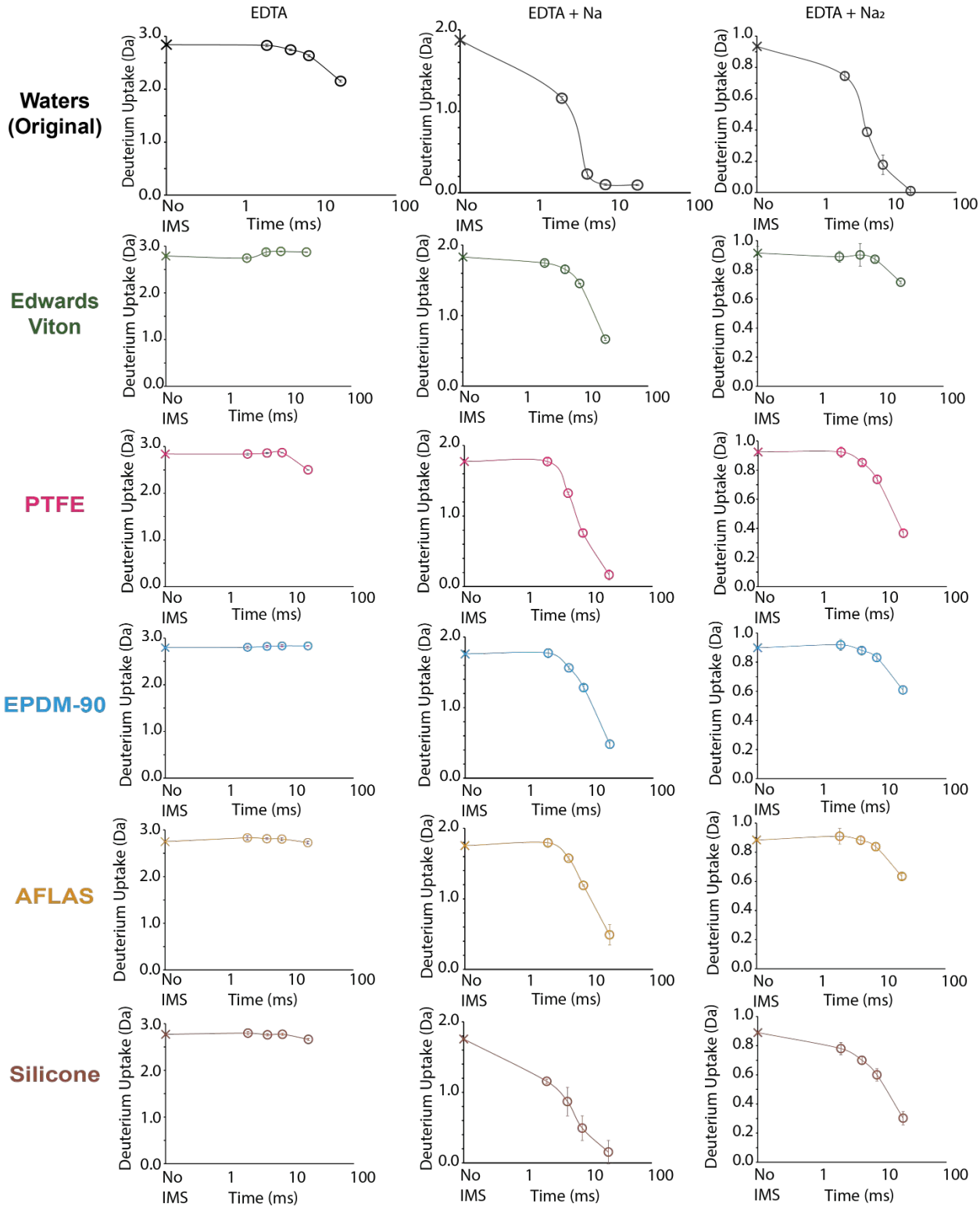

Supporting Figure 4.10: Individual post-ionization back-exchange profiles for each TriWave O-ring material.

Individual post-ionization back-exchange profiles for EDTA, EDTA + Na, and EDTA + Na_2 following replacement of the TriWave O-rings with each material evaluated in this study. Measurements were acquired after a three-day equilibrium period following venting and O-ring replacement. Data represent the average of four independent collection days (n=4) obtained over approximately one month for each O-ring material under identical preparation, experimental conditions, and experimentally defined exchange periods. Error bars represent standard deviation. Solid lines are included as visual guides and do not represent kinetic model fits.

4.6 References

1. Yoshimura, N., *Water vapor permeation through Viton O ring seals*. Journal of Vacuum Science & Technology A, 1989. **7**(1): p. 110–112.
2. Sefa, M. and J. Setina, *Comparison of permeation of atmospheric gases through Viton O-ring gaskets for different initial conditions*. Journal of Vacuum Science & Technology A, 2017. **35**(4).
3. de Csernatony, L., *The properties of Viton "A" elastomers II. The influence of permeation, diffusion and solubility of gases on the gas emission rate from an O-ring used as an atmospheric seal or high vacuum immersed*. Vacuum, 1966. **16**(3): p. 129–134.
4. Rand, K.D. and T.J. Jorgensen, *Development of a peptide probe for the occurrence of hydrogen (1H/2H) scrambling upon gas-phase fragmentation*. Anal Chem, 2007. **79**(22): p. 8686–93.
5. Guttman, M., et al., *Analysis of overlapped and noisy hydrogen/deuterium exchange mass spectra*. J Am Soc Mass Spectrom, 2013. **24**(12): p. 1906–12.

Chapter 5: Conclusion & Future Directions

5.1 Conclusion

Gas-phase hydrogen/deuterium exchange provides structural information through interactions between gas-phase ions and deuterated reagents. Still, the work presented throughout this dissertation shows that the resulting deuterium uptake cannot be understood from molecular structure alone. Across decades of gHDX studies, exchange has been shown to depend on the formation of productive ion–molecule interactions. Charge location, hydrogen bonding, the molecule's structural arrangement, and accessibility to hydrogens all contribute to whether a site participates in exchange and how rapidly that exchange occurs. At the same time, the literature in Chapter 1 demonstrated that the measured exchange response is strongly influenced by how the experiment is performed, creating an inherent connection between molecular behavior and instrumental conditions.

Chapter 2 expanded negative-mode gHDX studies by examining a chemically diverse panel of negatively charged compounds across two instrument platforms. The resulting behaviors ranged from no exchange to fast exchange, with a broad range of exchange behaviors among molecules sharing similar charge-bearing functional groups. Isomers and structurally related compounds further demonstrated that relatively small changes in functional-group arrangement could produce different exchange behavior. Together, these observations reinforced the ideas presented in Chapter 1 about protonated ions: negative-ion exchange also reflects the complete local environment surrounding the charge and exchangeable hydrogens, rather than simply the identity of the functional group. A key outcome of characterizing exchange behavior across a

broad panel of compounds was identifying compounds that could standardize gHDX measurements in negative mode. EDTA, 5-sulfosalicylic acid, benzene-1,3-disulfonic acid, and phytic acid underwent exchange representing the different categories (e.g, slow, intermediate, fast, and broad) and could serve as exchange reporters to monitor experimental variability.

Chapter 3 used the reporters to address one of the central practical challenges of gHDX: reproducibility. Because changes in experimental conditions can alter deuterium uptake, distinguishing a true structural difference from an experimentally induced shift becomes difficult when datasets are collected under different conditions. Rather than requiring the exchange environment to remain perfectly constant, the reporter strategy provided a way to measure how that environment had changed and determine whether the resulting differences could be corrected. Chondroitin sulfate disaccharides provided an important, biologically relevant analyte for this development because their closely related structures allowed evaluation of the structural sensitivity of negative-mode gHDX. Distinct exchange behavior was observed among the five disaccharides examined, demonstrating that negative-mode gHDX can distinguish relatively subtle structural differences. CSA was subsequently used as the representative analyte for evaluating reporter-based standardization. On the Synapt G2-Si, controlled changes in the concentration of ND_3 flow rate produced changes in the rate of exchange. This increased the exchange rate as ND_3 flow increased. The reporter 5-sulfosalicylic acid was used to quantify those changes, allowing correction factors to be derived and applied to measurements collected under the different conditions. When the same corrections were applied to CSA, uptake profiles that were initially separated due to differences in ND_3 flow rate collapsed into a single uptake profile after standardization. This demonstrated that a reporter can provide an internal measure of the

exchange environment that can then be used to improve comparison of analyte measurements. However, the behavior observed on the LTQ revealed that this standardization strategy was not universally transferable across instruments. Changes in ND_3 altered the amount of deuterium incorporated rather than producing the kinetic response observed on the Synapt. Because the reporter correction relied on changes in the rate of exchange, the same standardization strategy could not be applied to LTQ measurements. This result was initially a limitation of the standardization approach, but it ultimately became one of the most interesting observations of the dissertation. It indicated that the two instruments differed in more than their accessible reaction times and suggested that the exchange environment experienced by ions within the LTQ contained an additional component. Trace water provided a plausible explanation. If hydrogen-containing water molecules were present alongside ND_3, changing ND_3 delivery would alter the relative composition of the available exchange environment. This could change the final deuterium amount. The inability to standardize the LTQ therefore raised a broader question that extended beyond the original objective of developing negative-mode gHDX: does the deuterium labeling of an ion continue to change after the intended labeling process has ended (i.e., post-ionization)?

Chapter 4 directly examined this question. The resulting studies demonstrated progressive deuterium loss with increasing ion residence time. Importantly, this behavior was not confined to the LTQ, one molecule, or one ion polarity. It was observed using positive- and negative-ion reporters and across every mass spectrometry platform examined. The comparison across instruments also revealed that the initial deuterium content present before the experimentally controlled residence period was not equivalent among platforms. This observation is particularly

significant because it indicates that the earliest accessible measurement on an instrument does not necessarily represent the labeling state originally introduced into that instrument. This finding shifted the investigation from documenting post-ionization loss to identifying factors that could produce it. Vacuum sealing interfaces provided one potential connection between the surrounding laboratory and the nominally isolated mass spectrometer environment. Although elastomeric seals maintain the pressure differential required for instrument operation, their use does not imply complete exclusion of atmospheric gases. The known permeation of water vapor through vacuum sealing materials therefore provided a physical mechanism by which hydrogen-containing molecules could be continually introduced into regions encountered by deuterated ions. The environmental-control experiments provided experimental evidence supporting this relationship. Initial attempts to enclose entire instruments also revealed an important complication: changing humidity can simultaneously alter temperature, making environmental effects difficult to interpret without monitoring both variables. The targeted TriWave experiment resolved this issue by controlling the environment surrounding specific sealing interfaces while maintaining stable temperature. Under these conditions, lowering the humidity surrounding the TriWave region resulted in greater preservation of the deuterium label. Changing the sealing interfaces provided a second, independent test of the same hypothesis. Replacement of the original TriWave O-rings with newly installed alternative materials consistently improved deuterium retention, although the magnitude of that improvement depended on the material. Silicone, included as a relatively water-vapor-permeable comparison, provided the smallest improvement among the replacements. These results connect a physical component of

instrument construction to the isotopic measurement and demonstrate that post-ionization BEX can be influenced through engineering modifications to the mass spectrometer environment.

Ultimately, this dissertation advances gHDX in two interconnected ways. It establishes a framework for negative-ion gHDX, including exchange reporters and a strategy for improving measurement comparability, while also identifying post-ionization deuterium loss as an additional source of variability that extends beyond the intended exchange reaction. What began as an effort to understand and standardize negative-ion exchange therefore led to a broader understanding of the HDX measurement itself. The central conclusion of this work is that the deuterium content measured at the detector is not determined solely by the initial exchange reaction. It reflects the entire experimental pathway: from the molecular interactions that govern incorporation, through the conditions under which exchange is measured, to the degree to which that isotopic label is preserved as the ion travels through the mass spectrometer. Recognizing and controlling each of these contributions provides a path toward more reproducible, comparable, and ultimately more reliable HDX measurements.

5.2 Future Directions

The work presented in this dissertation advances negative-mode gHDX while also identifying several unresolved questions. Future studies should build upon these findings by further investigating the mechanism of negative-ion exchange, expanding the analytical scope of the technique, determining the broader applicability of reporter-based standardization, and more directly establishing the relationship between atmospheric water and post-ionization back-exchange.

A primary direction is to develop a more detailed mechanistic understanding of negative-mode gHDX. Although the relay mechanism is well established for protonated ions, an equivalent general mechanism has not been established for negatively charged species, and previous studies have proposed different pathways depending on the anion and reagent investigated. The compound survey performed in this dissertation further demonstrated that the identity of the charge-bearing functional group alone cannot predict exchange behavior. Instead, functional-group arrangement, hydrogen-bonding interactions, and accessibility of exchangeable hydrogens collectively influence whether exchange occurs. These relationships were developed primarily from experimental observations and provide a framework that can now be tested computationally. Density functional theory and molecular modeling could evaluate preferred deprotonation sites, possible ion–ND_3 complexes, intramolecular hydrogen-bonding networks, and the energetic barriers associated with individual exchange pathways. Comparing these calculations among compounds exhibiting no, slow, intermediate, and fast exchange could help determine why structurally similar anions produce markedly different kinetic behavior. Ultimately, a stronger mechanistic model could move negative-mode gHDX from describing observed exchange behavior toward predicting that behavior from molecular structure.

A second direction is to expand the structural applications of negative-mode gHDX, particularly for glycosaminoglycans. This dissertation demonstrated that five chondroitin sulfate disaccharides with differences in the number and position of sulfate groups produced distinguishable deuterium uptake profiles, including isomeric structures that cannot be differentiated by precursor mass alone. Heparan sulfate represents a particularly valuable next class because it would substantially increase the structural complexity being interrogated.

Extending these measurements to additional sulfation patterns and larger oligosaccharides would determine whether the structural sensitivity demonstrated for chondroitin sulfate is maintained as molecular complexity increases. This would move the technique beyond proof-of-concept differentiation of relatively small biomolecules and toward structurally challenging glycans for which conventional mass spectrometry measurements alone may provide limited differentiation.

The reporter-based standardization strategy should also be expanded beyond the conditions examined in this dissertation. The present approach successfully corrected ND_3-dependent changes in exchange kinetics on the Synapt G2-Si, demonstrating that an exchange reporter can characterize changes in the reaction environment and provide a correction that can be applied to an analyte. However, the literature reviewed in Chapter 1 indicates that reporter behavior can be reagent-dependent; standards that exchange effectively with ND_3 may exhibit little or no exchange with D_2O or MeOD. Future studies should therefore determine whether negative-mode reporters can be used for additional reagent gases and whether reporter-derived corrections remain applicable across chemically diverse analytes. Extending the approach to additional molecular classes, including peptides and small proteins, would further establish whether the reporter can correct experimental conditions for analytes with substantially different structures and exchange behaviors. These experiments would help define both the capabilities and boundaries of reporter-based gHDX standardization in negative mode.

A particularly important unresolved question is the unusual exchange environment of the Thermo LTQ**.** Increasing ND_3 on the LTQ increased the extent of deuterium incorporation while

leaving the exchange kinetics largely unchanged, preventing application of the kinetic scaling approach developed on the Synapt G2-Si. Trace water was proposed as an additional component of the LTQ exchange environment, but the environmental enclosure constructed in Chapter 4 did not sufficiently isolate the instrument from laboratory conditions; temperature and humidity inside the enclosure continued to follow the surrounding laboratory environment. Consequently, the original question remains unanswered: would true reduction of water vapor within the LTQ alter its ND_3-dependent exchange behavior? A redesigned enclosure incorporating improved sealing, continuous dry-air delivery, and effective moisture removal would allow this hypothesis to be tested directly. The ND_3-flow experiment from Chapter 3 could then be repeated under low-humidity conditions. If reducing water vapor changes the LTQ response from a change in deuterium content response toward the change in exchange rate response as observed on the Synapt, it would provide a basis for revisiting cross-platform reporter standardization under better-controlled exchange environments.

Finally, the relationship between atmospheric humidity and post-ionization BEX should be tested through controlled experiments in both directions. Chapter 4 demonstrated that reducing humidity surrounding the TriWave region decreased deuterium loss, while replacing the original O-rings with several alternative sealing materials also improved deuterium retention. These experiments support atmospheric water as a contributor to post-ionization BEX, but the strongest complementary experiment would be to intentionally introduce known levels of humidity and determine whether deuterium loss responds predictably. A relationship between increasing external humidity and increasing post-ionization deuterium loss would provide a more direct test of the proposed pathway connecting atmospheric water, vacuum seals, and the internal mass

spectrometer environment. This is particularly important given the observation that different instruments contained different amounts of deuterium at their earliest experimentally accessible time points, indicating that some label loss occurs before controlled ion-residence measurements even begin. Identifying where this early loss occurs could guide future instrument modifications toward the specific vacuum interfaces or ion-transfer regions that contribute most strongly to the process.